
**Acoustic-oceanographic data fusion for
prediction of oceanic acoustic fields**

MESTRE NELSON ESTÊVÃO MARTINS

Tese apresentada à Universidade do Algarve para a obtenção do grau de Doutor no ramo de Engenharia Electrónica e Telecomunicações, especialidade Processamento de Sinal.

2014

UNIVERSIDADE DO ALGARVE
FACULDADE DE CIÊNCIAS E TECNOLOGIA

**Acoustic-oceanographic data fusion for
prediction of oceanic acoustic fields**

Mestre Nelson Estêvão Martins

Orientador: Doutor Sérgio Manuel Machado Jesus, Professor Catedrático da
Faculdade de Ciências e Tecnologia, Universidade do Algarve

Tese apresentada à Universidade do Algarve para a obtenção do grau de Doutor no
ramo de Engenharia Electrónica e Telecomunicações, especialidade de Processamento de
Sinal.

2014

Acoustic-oceanographic data fusion for prediction of oceanic acoustic fields

Declaração de autoria do trabalho

Declaro ser o autor deste trabalho, que é original e inédito. Autores e trabalhos consultados estão devidamente citados no texto e constam da listagem de referências bibliográficas incluída.



Copyright ©Nelson Estêvão Martins

A Universidade do Algarve tem o direito, perpétuo e sem limites geográficos, de arquivar e publicitar este trabalho através de exemplares impressos reproduzidos em papel ou de forma digital, ou por qualquer outro meio conhecido ou que venha a ser inventado, de o divulgar através de repositórios científicos e de admitir a sua cópia e distribuição com objectivos educacionais ou de investigação, não comerciais, desde que seja dado crédito ao autor e editor.

Aos meus pais

๕

ที่รักของฉัน

Errata

Most entries are of the form: p. x, line y, change “A” to “B”. Line counts include chapter/section titles, but ignore figures, captions and equations. Negative line counts are from the bottom of the page.

- **p. iii, line -19**
Change “other, variable and with” to “other, with”
- **p. 22, line 2**
Change “forecasts for” to “forecasts, from an oceanographic model, for”
- **p. 23, line 1**
Change “with no horizontal dependence for physical properties.” to “each one with no horizontal dependence for physical properties.”
- **p. 23, line -4**
Change “The main argument when” to “The main statement, in the present work, when”
- **p. 24, line 1**
Change “The generic idea is materialized in Fig.” to “Let us consider the representation in Fig.”
- **p. 26, Eq. (2.3)**
Change the equals sign to \equiv
- **p. 32, Figure 3.1’s caption**
Change “(infinite) medium” to “(infinite) homogeneous medium”
- **p. 32, line 7**
Before the sentence “Thus, the field”, the following sentence should be inserted: “Equation (3.1) is valid for a single frequency (tone), and the signal time dependence is not shown, since the equation is expressed in the frequency domain.”
- **p. 34, Fig. 3.2**
Change “Cost” to $\mathcal{C}(r_e)$ in the y-labels
- **p. 35, line 3**
Change “black dots” to “black dots in Fig. 3.4”
- **p. 36, line 7**
Change “unbounded propagation” to “unbounded homogeneous propagation”
- **p. 37, line 1**
Change “a numerical distance” to “an Euclidean distance”
- **p. 39, line 3**
Change “where the meaning” to “according to the image method, where the meaning”
- **p. 40, Fig. 3.8**
Add “True” next to the dashed line at Receiver depth = 50 m

- **p. 42, Fig. 3.10**
Add “True” next to the dashed line at Receiver depth = 50 m
- **p. 43, Figure 3.12’s caption, line 2**
Change “in Fig. 3.9.” to “in Fig. 3.9 (red dots). The cost evaluated in the full interval $[0, 7000[$ m is shown by the black line.”
- **p. 44, Fig. 3.14**
Add “True” next to the dashed line at Frequency = 500 Hz
- **p. 45, Fig. 3.15**
The figure should have no title. In the caption, line 4, change “m for” to “m (white dot) for”
- **p. 46, line 1**
Change “obtain more accurate acoustic estimates” to “obtain acoustic estimates with less error”
- **p. 46, line -3**
Change “where the” to “where S_ω is the acoustic source strength, m is the index of the image source solution (Fig. 3.16), the”
- **p. 48, Fig. 3.17**
The ordinate axis label should be replaced by $\mathcal{C}(r_e)$. Add “True” next to the dashed line at Source-receive range = 1000 m
- **p. 48, line -5**
Change “irregular function” to “discontinuous function”
- **p. 48, line -4**
Change “the acoustic modeler includes the source-receiver range in” to “the source-receiver range is included in”
- **p. 49, Figure 3.19**
In the title, change “r-r_e” to “ $r - r_E$ ”. In the caption, line 1, change “Difference between” to “Difference in meters between”
- **p. 49, Figure 3.20**
In the title, change “zs-z_{se}” to $z_s - z_{se}$. In the caption, line 1, change “Difference between” to “Difference in meters between”
- **p. 57, chapter title**
Change all “m” to “M”, and “r” to “R”
- **p. 63, line -6**
Change “maximum of $\mathcal{C}_0(\theta_k)$ ” to “maximum of $\mathcal{C}_0(\theta_k)$ (in the interval $[0, 1]$, due to the triangle inequality)”
- **p. 64, line 6**
Replace c_{su} by s_u , and c_{sl} by s_l

- **p. 64, line 8**
Replace α_s by s_a , and α_b by b_a
- **p. 64, line -2**
After the sentence "... in Eq. (4.2).", the following sentence should be added: "For the EOF coefficients, the bounds are such that a value outside the bounds would imply a null acoustic field at every receiver".
- **p. 65, Figure 4.5's caption**
The following sentence should be appended: "Bounds chosen according to the explanation in pp. 63 and 64."
- **p. 67, line 7**
Change "at frequency f ... parameter value θ_k ." to "at frequency f , \mathbf{w} is a... parameter value θ_k , and tr is the trace operator."
- **p. 67, line -1**
After the sentence "... minimizes the cost.", the following sentence should be inserted: "As explained with Fig. 3.2, the parameter discretization has influence on the value of the compensating water depth."
- **p. 69, Figure 4.7's caption, line 1**
Change "depth that" to "depth (dots) that". The following sentence should be appended: "The points for which the acoustic error is below the threshold of 0.1 are connected by the yellow line."
- **p. 71, Figure 4.10's caption, line 1**
Change "optimal water depth that" to "optimal source-receiver range that"
- **p. 82, line -6**
Change "data produced" to "acoustic data produced"
- **p. 83, line 7**
Change "method assimilates acoustic" to "method includes acoustic"
- **p. 83, line -2**
Change "netween two" to "between two"
- **p. 87, line 2**
After the sentence "... EOF values stabilize.", the following sentence should be added: "This means that the first 10 days of water column CTD measurement are likely to be sufficient to solve the problem of acoustic nowcast for the whole month."
- **p. 89, Eq. (5.3) and below**
The equation should read $\mathcal{C}(\boldsymbol{\theta}) = 1 - \frac{1}{N_f} \sum_{k=1}^{N_f} \frac{\mathbf{w}^H(f_k, \boldsymbol{\theta}) \mathbf{C}_{RR}(f_k, \boldsymbol{\Theta}_T) \mathbf{w}(f_k, \boldsymbol{\theta})}{\|\mathbf{w}(f_k, \boldsymbol{\theta})\|^2 \text{tr} \mathbf{C}_{RR}(f_k, \boldsymbol{\Theta}_T)}$, and the text below should read "where $\mathbf{C}_{RR}(f_k, \boldsymbol{\Theta}_T)$ is an estimate of the receiver data correlation matrix at frequency f_k , $N_f = 10$..."
- **p. 89, line -3**
Change "the synchronous acoustic" to "the acoustic"

- **p. 91, Fig. 5.6 (b) and (c)**

The title should have the following appended text: “(inversion results)”

- **p. 96, Figure 5.10’s caption, line 5**

Change “see list above” to “see list on p. 95”

- **p. 96, Eq. (5.4)**

The equation should read $\mathcal{C}_B(\boldsymbol{\theta}_E, r, t) = 1 - \frac{1}{N_f} \sum_{k=1}^{N_f} \frac{\mathbf{w}^H(\boldsymbol{\theta}_{E,r,f_k,t}) \mathbf{C}_{RR}(\boldsymbol{\Theta}_{T,r,f_k,t}) \mathbf{w}(\boldsymbol{\theta}_{E,r,f_k,t})}{\|\mathbf{w}(\boldsymbol{\theta}_{E,r,f_k,t})\|^2 \text{tr}(\mathbf{C}_{RR}(\boldsymbol{\theta}_{0,r,f_k,t}))}$,

- **p. 98, Eq. (5.9)**

The equation should read $\mu_{Tr}(r) = \frac{1}{N_z N_f N_t} \sum_{k=1}^{N_z} \sum_{l=1}^{N_f} \sum_{m=1}^{N_t} \mathcal{C}_T(r, z_k, f_l, t_m)$,

- **p. 98, Eqs. (5.11)–(5.13)**

The lower bounds in the sums should be non-coincident integer indices, and the variables in the present text replaced by variables with the integer indices. For instance, in Eq. (5.12), the bounds should be k, l and m , and the related variables, z_k, f_l and t_m .

- **p. 103, Fig. 5.14**

Change “Baseline” to “Paramet. 1”, “RI 5 & 10 km” to “Paramet. 5”, “5 km” to “Paramet. 2”, “10 km” (cyan line) to “Paramet. 3”, and “RD 5 & 10 km” to “Paramet. 4”.

- **p. 106, Fig. 5.15’s caption**

The following sentence should be appended: “An acoustic receiver array is positioned at 5-km range from the source, to measure the acoustic field, with receivers at the same positions as for the nowcast example —see Fig. 5.3.”

- **p. 106, Remark 5.2**

The variables $\boldsymbol{\theta}_T$ and $\hat{\boldsymbol{\theta}}_T$ should be replaced by $\boldsymbol{\Theta}_T$ and $\hat{\boldsymbol{\Theta}}_T$, respectively.

- **p. 109, line -9**

Change “ \mathbf{x} , and d_i is the corresponding value of the model output d ” to “ \mathbf{x} , d_i is the corresponding value of the model output d , and N is the number of samples in the training set”

- **p. 109, line -4**

Change “obtained targets. The” to “obtained response. The”

- **p. 110, line 3**

Change “where ξ_i ” to “where C is a user-defined constant, and ξ_i ”

- **p. 110, Eq. (5.18) and below**

The equation should read $K(\mathbf{x}_i, \mathbf{x}_j) = \boldsymbol{\varphi}^T(\mathbf{x}_i) \boldsymbol{\varphi}(\mathbf{x}_j)$, and the text below should read “subject to appropriate constraints, in which $\boldsymbol{\varphi}$ is a vector containing the values of the m_1 basis functions. The...”

- **p. 114, Eq. (5.21)**

The equation should read $\nu_p = \frac{1}{(F-P)N_z} \sum_{f=P+1}^F \sum_{k=1}^{N_z} |c(z_k, t_p) - c(z_k, t_f)|$.

Acknowledgements

I acknowledge the whole SiPLAB crew, for humanly and technically having raised the lab temperature, such as António Silva, Cristiano Soares, Friedrich Zabel (system guru), Paulo Felisberto and Paulo Santos, to mention only a few. To my supervisor, Sérgio Jesus, I address special thanks, for having created all the necessary conditions for the execution of the thesis, and having trusted me as a student. Sérgio has created SiPLAB, at University of Algarve, in 1992, with a very simply expressible purpose: to increase wealth, by increasing *knowledge*. The potential of *knowledge* as a means of human development has been recognized about two decades ago, and *knowledge* is nowadays competing at a large pace with the material component of life^a. SiPLAB is a well-developed laboratory, in terms of underwater acoustic signal processing techniques, and has faced a significant technological development in the last years, in terms of acoustic emission and reception systems. Included in the latter is the Acoustic Oceanographic Buoy, a drifting system with data storage capabilities, whose feasibility in ocean acoustic sensing has been demonstrated, for example, in the MREA'03 and '04, and RADAR'07 sea trials. Special thanks are due to Emanuel Ferreira-Coelho. He gave me an important input on oceanography, and explanations regarding the oceanographic forecasts used in the present work, when accepting me as a visiting student. Last but not least, I address warm hugs to my parents and my friends, specially Helga Hampton, my graduation colleagues, Paula Coelho, Barbara Nicolas, Julien Huillery, Anna Zabel, Cláudio Lima, Ana Bela, Fernando Marin, and, last but not least, my beloved wife, Usa Vilaipornsawai, for continuous and unconditional encouragement. To all the above, an ocean-wide THANK YOU!!!

This work was partially funded by National Funds through FCT - Foundation for Science and Technology under scholarship SFRH/BD/9032/2002, and by LARSyS PEst-OE/EEI/LA0009/2014.

^a*Reclaiming Development Agendas: Knowledge, Power and International Policy Making*. Utting, Peter (ed.), UN Research Institute for Social Development (UNRISD), Palgrave, Basingstoke, 2006.

Name: Nelson Estêvão Martins
College: Faculdade de Ciências e Tecnologia
University: Universidade do Algarve
Supervisors: Doutor Sérgio Manuel Machado Jesus, Full Professor of Faculdade de Ciências e Tecnologia, Universidade do Algarve
Thesis title: Acoustic-oceanographic data fusion for prediction of oceanic acoustic fields

Abstract

Maritime rapid environmental assessment exercises became rather important. An underlying objective is to predict the evolution of the acoustic field due to an underwater target. Main contributions to this end have relied on accurate models of acoustic propagation, which receive baseline properties and ocean forecasts as input. Intuitively, the most accurate oceanographic forecast should imply the most accurate acoustic forecast. This can fail, due to at least two reasons: 1) the full set of (space-time-variant) environmental properties are rarely known with enough accuracy; 2) even the most sophisticated propagation model cannot handle the full environmental detail in solving propagation equations, forcing the experimenter to reduce complex environmental features to a simplified representation. Acoustic modeling errors appear then as inevitable. Little possibility of error minimization exists, if the propagation model is simply run in a ‘forward’ manner. The results presented in this work show that the acoustic error can be minimized, if the propagation model is fed with an environmental parameter vector containing two distinct sets: one, fixed and formed by the environmental parameters with uncontrolled errors; the other, variable and with errors determined in a controlled way, adapted to the errors in the first subset. Here, the second set is treated as a distinct quantity, labeled as “equivalent model”. It can be determined by acoustic inversion. The equivalent model is employed for two objectives: to estimate the acoustic field at a given present time (nowcast), and a given future time (forecast). Synthetic acoustic fields, and oceanographic measurements and predictions (with the Navy Coastal Ocean Model) obtained for the Maritime Rapid Environmental Assessment 2003 sea trial, drive the simulations. For the problem of nowcast, the equivalent model is determined at sparse transect points, and interpolated to points with no acoustic measurements. For the problem of forecast, the equivalent model is furthermore ‘extrapolated’ to future time. The ‘extrapolation’ consists of a mapping between sound speed profile and equivalent model. When providing an estimate of the future sound speed at the mapping input, the estimate of the future equivalent model is obtained. The proposed method led to a decrease of 3–5 dB in transmission loss estimation error, as compared to standard procedures.

Keywords: acoustic propagation model, environmental mismatch, matched-field processing, oceanographic forecast, support vector machine.

Nome: Nelson Estêvão Martins
Faculdade: Faculdade de Ciências e Tecnologia
Universidade: Universidade do Algarve
Orientador: Doutor Sérgio Manuel Machado Jesus, Professor Catedrático da Faculdade de Ciências e Tecnologia, Universidade do Algarve
Título da Tese: Fusão de dados acústico-oceanográficos para previsão de campos acústicos oceânicos

Resumo

Os exercícios de estimação ambiental rápida ganharam crescente importância. Um dos objetivos subjacentes é o de prever a evolução do campo acústico devido a um alvo submarino. Contributos importantes para este fim têm contado com modelos precisos de propagação acústica, que recebem propriedades ambientais nominais e previsões oceânicas, à entrada. Intuitivamente, a previsão oceanográfica mais precisa implicará a previsão acústica mais precisa. Este raciocínio é falível, devido a, no mínimo, duas razões: 1) o conjunto completo das propriedades ambientais (variantes no espaço-tempo) raramente são conhecidas com precisão suficiente; 2) mesmo o mais sofisticado dos modelos de propagação não consegue tratar todos os detalhes ambientais na resolução de equações de propagação, obrigando o experimentador a reduzir características ambientais complexas a uma representação simplificada. Deste modo, erros de modelação acústica são inevitáveis. A possibilidade de minimização do erro é diminuta, se o modelo de propagação for utilizado simplesmente na forma ‘direta’. Os resultados apresentados neste trabalho mostram que o erro acústico pode ser minimizado, se o modelo de propagação for alimentado com um vetor de parâmetros ambientais contendo dois conjuntos distintos: um, fixo e formado pelos parâmetros ambientais com erros incontroláveis; o outro, variável e com erros determinados de uma forma controlada, adaptados aos erros no primeiro sub-conjunto. No presente contexto, o segundo conjunto é tratado como uma quantidade distinta, rotulada de “modelo equivalente”. Este pode ser determinado por inversão acústica. O modelo equivalente é utilizado para dois objetivos: estimar o campo acústico num momento presente (*nowcast*), e num momento futuro (*forecast*). Campos acústicos sintéticos, medidas ambientais e previsões oceanográficas (obtidas com o modelo *Navy Coastal Ocean Model*), respeitantes à campanha de mar *Maritime Rapid Environmental Assessment 2003*, alimentam as simulações. No problema de *nowcast*, o modelo equivalente é determinado em pontos esparsos de um transecto, e interpolado para pontos sem medições acústicas. No problema de *forecast*, o modelo equivalente é também ‘extrapolado’ para o tempo futuro. A ‘extrapolação’ consiste num mapeamento entre perfil de velocidade do som e modelo equivalente. Ao fornecer uma estimativa da velocidade do som futura à entrada do mapeamento, é obtida a estimativa do modelo equivalente futuro. O método proposto conduziu a um decréscimo de 3–5 dB no erro de estimação da perda por transmissão, comparativamente a procedimentos padrão.

Palavras-chave: modelo de propagação acústica, desajuste ambiental, processamento por ajuste de campo, previsão oceanográfica, máquina de vetor suporte.

Contents

Acknowledgements	i
Abstract	iii
Resumo	v
List of Acronyms	ix
List of Figures	xi
List of Tables	xix
1 Introduction	1
1.1 Ocean Acoustics	2
1.1.1 Problematic of Acoustic Propagation	8
1.2 Motivation	11
1.2.1 State-of-the-art	12
1.2.2 Contribution	17
2 Problem Statement	21
2.1 Framework	21
2.2 Definition of Acoustically-equivalent Environmental Model	25
2.3 Proposed Approach	27
3 Equivalent Models in Idealized Media	31
3.1 Pedagogical Examples	31
3.1.1 Unbounded Medium	32
3.1.2 Homogeneous Halfspace	38
3.1.3 Ideal Waveguide	46
3.1.4 Equivalent Models on Wave Reflection	50
3.2 Summary	55
4 Equivalent models in realistic media	57
4.1 Real and forecast environmental data	58
4.2 Equivalent modeling	61
4.2.1 Environmental parameter hierarchy	62
4.2.2 Environmental mismatch compensation	66
4.3 Summary	78

5	Application of Equivalent Models in Acoustic Nowcast and Forecast	81
5.1	Acoustic Nowcast	82
5.1.1	Acoustic Nowcast Test Case	82
5.1.2	Solution to Acoustic Nowcast	87
5.1.3	Numerical Results	89
5.2	Acoustic Forecast	104
5.2.1	Acoustic Forecast Test Case	105
5.2.2	Solution to the Acoustic Forecast	106
5.2.3	Numerical Results	111
5.3	Summary	134
6	Conclusion	137
	References	142

List of Acronyms

2D two-dimensional

3D three-dimensional

ADCPs acoustic Doppler current profilers

AOB Acoustic Oceanographic Buoy

APM acoustic propagation model

COAMPS Coupled Ocean/Atmosphere Mesoscale Prediction System

CTD conductivity, temperature and depth

EOF empirical orthogonal function

EOFs empirical orthogonal functions

ESSE error subspace statistical estimation

HFS Harvard Forecast System

HOOM Harvard Open Ocean Model

HOPS Harvard Ocean Prediction System

MMSE minimum-mean-square-error

MODAS Modular Ocean Data Assimilation System

MREA'03 Maritime Rapid Environmental Assessment 2003

NCOM Navy Coastal Ocean Model

NRL Naval Research Laboratory

NRLPOM relocatable version of the Princeton Ocean Model, implemented at the Naval Research Laboratory

REA rapid environmental assessment

RMSE root mean square error

SEPTR shallow water environmental profiler in trawl-safe real-time configuration

SNAP SACLANTCEN Normal-Mode Acoustic Propagation Model

SSP sound speed profile

SSPs sound speed profiles

SVM support vector machine

SVMs support vector machines

TL transmission loss

XBT expendable bathythermograph

List of Figures

1.1	Some of the activities in which sound is used in the ocean, to convey information: oil/gas exploration, estimation of water column and geological properties, marine mammal communication/navigation, and monitoring of all of the above as well as of earthquake/plate dynamics and shipping noise. The arrows represent propagation of acoustic energy. . .	2
2.1	(a) Ocean volume in which to estimate the acoustic field produced by an acoustic source. All the environmental properties are space-dependent. (b) Limited representation of the environment in (a), in which the space-dependence of several environmental properties was simplified or removed, in order to be given as input to an acoustic propagation model.	22
2.2	Estimation timeline in the problem at hand: estimation of the acoustic field at any “present time” and any “future time”.	23
2.3	Idealized cost functions representing environmental and acoustic misfits. The environmental misfit is defined as the difference between a true and an estimated environment, and has a global minimum at Θ_T . The acoustic misfit compares a true and a modeled acoustic field, is a function of the environment, and has a global minimum at Θ_E . . .	24
2.4	Proposed approach to the problem to be solved in the present work: the estimation of the acoustic field in an oceanic area, at present (acoustic nowcast) and at future time (acoustic forecast), on particular space points. After calibration of a given acoustic propagation model, using acoustic inversion, which takes a subjective environmental representation of the oceanic area, and gives the equivalent model as the output, the latter is extrapolated to the required space-time points of interest. By feeding the extrapolation result to the acoustic propagation model, the final acoustic estimate is obtained. For the problem of acoustic forecast, environmental forecasts are necessary to extrapolate the equivalent model, and to compute the acoustic forecast outcome at the last step —left arrows.	29
3.1	Vibrating sphere in an unbounded (infinite) medium (adapted from Jensen et al.[JKPS93]).	32
3.2	(a) Acoustic cost as a function of distance. The approximate equivalent distance is 5.012 km, as seen in the detailed representation in (b). The cost corresponding to the true distance (5 km) is 2.8×10^{-3} , while the one corresponding to the equivalent distance is 1.1×10^{-3} , 2.5 times smaller.	34
3.3	True (X) and candidate (–) acoustic fields. The sound speed in mismatch is 1503 m/s (the true value is 1500 m/s). The candidate fields are computed with the sound speed in mismatch, for several candidate distances in the interval [4.98, 5.02] km, defining a contour in the complex plane which does not contain the true field.	34

3.4	Effect of compensation for a sound speed in mismatch, in the case of an unbounded medium, with the simulation parameters described in the Eq. system (3.5). The sound speed varied between 1490 and 1545 m/s. The true field is represented by the cross; the field computed with the sound speed in mismatch is represented in red, with all the points lying in a circle; the field computed after compensation (by optimizing for distance) for each value of sound speed in mismatch, is represented in the black cloud.	35
3.5	Acoustic cost as a function of sound speed. Three from the infinite number of approximate equivalent sound speeds correspond to the three minima lying in the dashed line. The cost corresponding to the true sound speed is 2.0×10^{-2} , while the one corresponding to the equivalent distance is 2.0×10^{-3} , 10 times smaller.	37
3.6	Transmission loss error as a function of relative mismatch in distance (in percentage).	38
3.7	Point source at S placed in a fluid with a perfectly reflecting surface on the top.	39
3.8	Cost function used to determine the equivalent receiver depth to compensate for the source depth mismatch (101 m, instead of the true 100 m). The function has a single global minimum at $z = 2868$ m, hence this value of depth is a global equivalent model. The cost for the true value of 50 m (dashed line) is 1.5×10^{-5} , while for the equivalent value, it is 5.2×10^{-7} , 29 times smaller.	40
3.9	Equivalent receiver depths defined as the values that globally minimize the cost in Eq. (3.16), as a function of true source-receiver range.	41
3.10	Detail of the cost function in Fig. 3.8, in the interval [48, 51] m. In this interval, the function has the single minimum of 8×10^{-6} , at $z_E = 48.8$ m.	42
3.11	Local equivalent receiver depths defined as the values that locally minimize the cost in Eq. (3.16). The optimization search interval is defined as $[z - 10, z + 5]$, where z is the true receiver depth. The equivalent depths are shown as a function of true source-receiver range.	42
3.12	Cost in Eq. (3.16) evaluated with the acoustic field generated with the parameters in Eq. (3.17) and the acoustic field corresponding to the global equivalent depths in Fig. 3.9.	43
3.13	Cost in Eq. (3.16) evaluated with the acoustic field generated with the parameters in Eq. (3.17) and the acoustic field corresponding to the local equivalent depths in Fig. 3.11.	43
3.14	Equivalent receiver depth as a function of frequency, for the simulation parameters in Eq. (3.17).	44
3.15	Cost function used to determine the equivalent (source-receiver range, receiver depth) pair to compensate for source depth mismatch (90 m, as compared to the true 100 m), in the fluid halfspace scenario. In the (source-receiver range, receiver depth) search space, the minimum is 7.0×10^{-6} , giving the equivalent values (986, 11) m for the equivalent source-receiver range and depth, respectively.	45
3.16	Point source in an ideal waveguide. The distances $R0n, n = 1, 2, \dots, 4$ are relative to the depth (z) axis.	46
3.17	Cost function to determine the equivalent source-receiver range to compensate for duct depth mismatch (202 m, against the true 200 m), in the ideal waveguide scenario. The minimum cost is 6.0×10^{-10} .	48
3.18	Equivalent source-receiver range as a function of duct depth in mismatch, to (approximately) model acoustic propagation in the ideal waveguide of Fig. 3.16.	48

3.19	Difference between the true and the equivalent source-receiver range, as a function of true source-receiver range and receiver depth. The true duct depth and the one in mismatch are 200 and 202 m, respectively.	49
3.20	Difference between the true and the equivalent source depth, as a function of true source-receiver range and receiver depth. The true duct depth and the one in mismatch are 200 and 202 m, respectively.	49
3.21	Reflection and transmission at a fluid-viscoelastic interface (adapted from Ref. [JKPS93]).	51
3.22	Family of top-bottom halfspace density pairs which lead to the same reflection coefficient, in the fluid-fluid reflection case.	53
3.23	Family of top-bottom halfspace sound speed pairs which lead to the same reflection coefficient, in the fluid-fluid reflection case.	54
4.1	Maritime Rapid Environmental Assessment 2003 area: Elba channel (blue) and Northern Elba (red) working boxes for the ocean prediction system MODAS-NCOM, and acoustic transmission box (green).	59
4.2	View of a (42.5–43.3 °N, 9.40–11.0 °E) area, showing the locations of the conductivity, temperature and depth (CTD) casts (circles) performed during the Maritime Rapid Environmental Assessment 2003 (MREA'03) sea trial.	59
4.3	(a) Sound speed profiles along time, and (b) average sound speed profile over all the casts from the MREA'03 sea trial.	60
4.4	Parameters that describe the realistic underwater scenario for which the concept of equivalent model is characterized in the present chapter. The meaning of the parameters is explained in Tab. 4.1.	63
4.5	Environmental sensitivity analysis for the realistic simulations of the present work. The consequence of introducing an offset in each parameter at a time (see Tab. 4.1) on the acoustic field, is represented in terms of an acoustic cost (eq. (4.2)).	65
4.6	Environmental mismatch compensation: the source-receiver range is taken as 50 m inferior to the true value of 5 km. This environmental mismatch is compensated by an offset in the water depth, which subtracts 60 cm to the true 200 m.	67
4.7	Contour plot of the acoustic cost, and optimal water depth that compensates for source-receiver range mismatch.	69
4.8	Contour plot of the acoustic cost (background), and optimal sediment compressional attenuation that compensates for source depth mismatch (circles). The optimal values minimize the cost computed for each value in mismatch. The case of no mismatch is indicated by the white cross. The points for which the acoustic error is below the threshold of 0.1 are connected by the yellow line.	69
4.9	Contour plot of the acoustic cost (background), and optimal source-receiver range that compensates for water depth mismatch (circles). The optimal values minimize the cost computed for each value in mismatch. The case of no mismatch is indicated by the white cross. The points for which the acoustic error is below the threshold of 0.1 are connected by the yellow line.	70
4.10	Contour plot of the acoustic cost (background), and optimal water depth that compensates for water column sound speed profile (SSP) mismatch (circles). The optimal values minimize the cost computed for each value in mismatch. The case of no mismatch is indicated by the white cross. The points for which the acoustic error is below the threshold of 0.1 are connected by the yellow line.	71

4.11	Contour plot of the acoustic cost (background), and optimal source-receiver range that compensates for sediment thickness mismatch (circles). The optimal values minimize the cost computed for each value in mismatch. The case of no mismatch is indicated by the white cross. The points for which the acoustic error is below the threshold of 0.1 are connected by the yellow line.	71
4.12	Contour plot of the acoustic cost (background), and optimal water depth that compensates for sediment density mismatch (circles). The optimal values minimize the cost computed for each value in mismatch. The case of no mismatch is indicated by the white cross. The points for which the acoustic error is below the threshold of 0.1 are connected by the yellow line.	72
4.13	Contour plot of the acoustic cost (background), and optimal water depth that compensates for sediment upper compressional speed mismatch (circles). The optimal values minimize the cost computed for each value in mismatch. The case of no mismatch is indicated by the white cross. The points for which the acoustic error is below the threshold of 0.1 are connected by the yellow line.	72
4.14	Contour plot of the acoustic cost (background), and optimal sediment thickness that compensates for sediment lower compressional speed mismatch (circles). The optimal values minimize the cost computed for each value in mismatch. The case of no mismatch is indicated by the white cross. The points for which the acoustic error is below the threshold of 0.1 are connected by the yellow line.	73
4.15	Contour plot of the acoustic cost (background), and optimal sediment density that compensates for sediment compressional attenuation mismatch (circles). The optimal values minimize the cost computed for each value in mismatch. The case of no mismatch is indicated by the white cross. The points for which the acoustic error is below the threshold of 0.1 are connected by the yellow line.	74
4.16	Contour plot of the acoustic cost (background), and optimal source depth that compensates for basement density mismatch (circles). The optimal values minimize the cost computed for each value in mismatch. The case of no mismatch is indicated by the white cross. The points for which the acoustic error is below the threshold of 0.1 are connected by the yellow line.	74
4.17	Contour plot of the acoustic cost (background), and optimal basement compressional attenuation that compensates for basement compressional speed mismatch (circles). The optimal values minimize the cost computed for each value in mismatch. The case of no mismatch is indicated by the white cross. The points for which the acoustic error is below the threshold of 0.1 are connected by the yellow line.	75
4.18	Contour plot of the acoustic cost (background), and optimal sediment compressional attenuation that compensates for receiver array depth shift mismatch (circles). The optimal values minimize the cost computed for each value in mismatch. The case of no mismatch is indicated by the white cross. The points for which the acoustic error is below the threshold of 0.1 are connected by the yellow line.	75
4.19	Contour plot of the acoustic cost (background), and optimal source-receiver range that compensates for basement compressional attenuation mismatch (circles). The optimal values minimize the cost computed for each value in mismatch. The case of no mismatch is indicated by the white cross. The points for which the acoustic error is below the threshold of 0.1 are connected by the yellow line.	76
5.1	Acoustic nowcast estimator.	82

- 5.2 Idealized ocean transect in which the acoustic field nowcast is to be computed: (a) true and (b) baseline environmental properties. The environmental components in mismatch are represented by the red values/lines in (b). At every time sample, the presumably known sound speed profile has smaller or equal values than the true sound speed profile, and deviates linearly from the surface to the bottom, starting at 2 m/s and finishing at 0. 83
- 5.3 Ocean transect in which to estimate the acoustic field, monitored with two acoustic receiver arrays. The acoustic data observed at these array locations is inter/extrapolated in space and time, which is the main idea behind the approach to acoustic nowcast presented in the present work. The true geoacoustic properties are also shown (refer to Fig. 5.2 (a)). 84
- 5.4 Idealized timeline for acoustic nowcast, bounded by times $t_0 = 0$ (initial time sample) and $t_E = 28$ days (final time sample) —recall Fig. 2.2. At time t_P , the past acquired (erroneous) CTD data, together with baseline geoacoustic and geometric properties, and acoustic measurements at t_P , enter an estimation block. This block has the acoustic nowcast as output. Several nowcast exercises are executed, hence the “present time” t_P runs from t_0 to t_E 84
- 5.5 Time series of the first empirical orthogonal function (EOF) at selected depths, for the complete timeline of the nowcast exercise. 87
- 5.6 Acoustic inversion results for the parameters in Tab. 5.2. The true sound speed profile time history is shown in (a), followed by its corresponding inversion results (computed from the empirical orthogonal function coefficients), at the 5- (b) and the 10-km acoustic receiver array (c). The bottom three graphs show the inversion results for basement compressional speed (d) and sediment compressional speed (upper (e) and lower (f)). Here, the black and the blue lines correspond to the 5- and the 10-km receiver array, respectively. 91
- 5.7 Sum of the difference between the true and the equivalent sound speed profile. The black and the blue lines correspond to the 5- and the 10-km receiver array, respectively. 92
- 5.8 Equivalent sediment speeds shown against each other, for the acoustic nowcast exercise. 93
- 5.9 Acoustic cost in Eq. (4.3) at the end of the inversion, for the arrays at 5 (black) and 10 km (blue). 94
- 5.10 Approaches 4 (a) and 5 (b) for estimating the equivalent model for acoustic nowcast, in the 10-km transect. The approaches differ only for ranges in the]5, 10]-km interval. In approach 4, the equivalent model is defined as a two-sector range-dependent environment, bounded at 5 km. The sectors coincide with the acoustic inversion outcomes at 5 and 10 km, respectively. In parameterization 5 (see list above), a range-independent environment is defined for each range in which to estimate the field. For ranges in the interval]5, 10] km, the equivalent model is computed from spline-interpolation of the 5- and 10-km inversion outcomes. 96
- 5.11 Interpolation of the acoustic inversion results to estimate an equivalent model component, using the sediment upper compressional speed as an example. For a range in the interval 0 to 5 km, the equivalent speed estimate coincides with the inversion outcome at 5 km. For a range between 5 and 10 km, the estimate is the result from a Hermite polynomial-spline interpolation, using the inversion outcomes at 5 and 10 km. The spline has zero derivative at 5 and 10 km. 97

5.12	Bartlett-based acoustic estimation error as a function of range, when using each of the five environmental parameterizations described in p. 95. Those parameterizations, from 1 to 5, correspond to the colors pink, blue, cyan, yellow and green, respectively. In (a), all the parameterizations using equivalent models (indices 2 to 5) are compared, in terms of the corresponding average acoustic error, defined in Eq. (5.8). In (b), the parameterization 5 is compared with the parameterization 1 (baseline environment). In this case, the acoustic error is shown as an error band bounded by the average \pm one standard deviation (see Eq. (5.11)) (negative values clipped to zero).	99
5.13	Transmission loss estimation error as a function of range, when using each of the five environmental parameterizations explained in p. 95. Those parameterizations, from 1 to 5, correspond to the colors pink, blue, cyan, yellow and green, respectively. In (a), all the parameterizations using equivalent models (indices 2 to 5) are compared, in terms of the corresponding average acoustic error, defined in Eq. (5.8). In (b), the parameterization 5 is compared with the parameterization 1 (baseline environment). In this case, the acoustic error is shown as an error band bounded by the average \pm one standard deviation (see Eq. (5.11)) (negative values clipped to zero).	100
5.14	Transmission loss error corresponding to the baseline and the equivalent models, as a function of frequency. (a) Comparison for the usage of the baseline or the equivalent model defined as in "Approach 5" of Fig. 5.10; (b) comparison for the usage only of equivalent models.	103
5.15	Idealized ocean transect in which the acoustic field forecast is to be computed. (a) True and (b) baseline environment. The red values express the parameters that are in mismatch.	106
5.16	Hypothesis used for equivalent model forecast: the equivalent model is a function \mathcal{M} of the true environmental properties. The dots represent imaginary up-to-present-time (black) and future-time (white) data.	107
5.17	ϵ -insensitive loss function.	110
5.18	Acoustic inversion results for the forecast exercise. (a) Sediment upper compressional speed parameter estimate; (b) acoustic misfit corresponding to the previous estimate.	112
5.19	Timeline for acoustic forecast, using a support vector machine to estimate the mapping between oceanographic forecast and equivalent model. The support vector machine is trained with data acquired/produced during a "training window" (bounded by t_0 and t_P (present time)), with a time step of Δt , to estimate the future equivalent model corresponding to any time sample in the "prediction window". The superior bound for the prediction window is t_F (farthest future time). The notation t_p and t_f designates any time sample in the training or prediction window, respectively. The time sample t_P runs from t_0 to $t_F - \Delta t$	114
5.20	Prediction of the equivalent sediment upper compressional speed. (Green): equivalent speed for all times; (blue): estimated equivalent speed by support vector machine (SVM) regression. The bounds of the observed response during the training period are represented by horizontal dashed lines. Prediction made with data observed during a 8.6-h time window, with a sampling period of 1.4 h.	117
5.21	Sound speed profile information used in the training phase of the SVM, for regression, with a training time window of 8.6 h (7 data samples). The shaded area represents the minimum and maximum values of the sound speed, at each depth, of the profiles used to train the SVM. For reference, the sound speed profile at the farthest future time (day 28) is shown (dashed line).	117

5.22	Error (defined in Eq. (5.23)) of the prediction of the equivalent sediment upper compressional speed given by the SVM, for the case of ideal oceanographic modeling. For each present time $0 \leq t_P < 28$ [day] at which the forecast is issued, the error quantifies the quality of the estimates for times greater than t_P	118
5.23	Bartlett misfit as a function of range, in the problem of acoustic forecast, for the case of ideal oceanographic modeling, when using the baseline (pink) or the equivalent (green) environments.	120
5.24	Transmission loss error as a function of range, in the problem of acoustic forecast, for the case of ideal oceanographic modeling, when using the baseline (red and pink) or the equivalent (green) environments, as a function of frequency (a) and time (b). The errors are shown as average value \pm one standard deviation.	120
5.25	Prediction of the equivalent sediment upper compressional speed, in the problem of acoustic forecast, for the case of real oceanographic modeling.	122
5.26	Error (defined in Eq. (5.23)) of the prediction of the equivalent sediment upper compressional speed given by the SVM, for the case of real oceanographic modeling (with Navy Coastal Ocean Model (NCOM)). For each present time $3.4 \leq t_P < 28$ [day] at which the forecast is issued, the error quantifies the quality of the estimates for times greater than t_P	122
5.27	Bartlett misfit as a function of range, when using the baseline (pink) or the equivalent (green) environments. These errors correspond to acoustic forecast, in the case that the oceanographic model is the NCOM.	123
5.28	Transmission loss error as a function of frequency (a) and time (b), when using the baseline (red and pink) or the equivalent (green) environments. These errors correspond to acoustic forecast, in the case that the oceanographic model is the NCOM.	123
5.29	Root-mean-square-error of the synthetic oceanographic forecast as a function of the weighted average parameter ρ , as defined in Eq. (5.25).	125
5.30	Measure of improvement of equivalent modeling over baseline modeling, in terms of acoustic forecast error. The improvement is computed as the difference between the acoustic errors corresponding to the baseline and the equivalent model, respectively, and shown as a function of the synthetic oceanographic forecast root mean square error (RMSE) —see Fig. 5.29.	126
5.31	Sound speed estimation error of the forecast given by NCOM. Each point in the curve is the average absolute value of the difference between the true and the forecast sound speed, over depth.	128
5.32	Average measured (CTD) and forecast (NCOM) sound speed profiles.	129
5.33	Sound speed estimation error, for each present time with index P , t_P . The estimate is any of the Bayesian estimates which take the oceanographic forecast as the observation, to infer the CTD measurement at a future time.	130
5.34	Bartlett misfit as a function of range, when using the baseline (red and pink) or the equivalent (green) environments. These errors correspond to acoustic forecast, in the case that the water column is determined by Bayesian estimation using NCOM and CTD data, and the equivalent model is determined by an SVM trained with the CTD data and the acoustic inversion results up to present time, and responding to the Bayesian estimate as input.	132

-
- 5.35 Root-mean-square of transmission loss estimation error, as a function of present time. The curves represent four types of acoustic estimation: (red) water column fixed to the NCOM forecast, and remaining environmental parameters set to baseline values; (black) water column fixed to the NCOM forecast, and equivalent model determined by an SVM trained with the NCOM forecast and the equivalent model up to present time; (green) water column determined by Bayesian estimation using NCOM and CTD data, and equivalent model determined by an SVM trained with the CTD data and the equivalent model up to present time, and responding to the Bayesian estimate as input; (blue) SSP fixed to the ideal oceanographic forecast (coincident with the true SSP), and equivalent model computed as the response of the SVM to that SSP. 133

List of Tables

4.1	Environmental parameters.	64
4.2	Hierarchy of the parameters that define the acoustic field. The hierarchy was computed according to the maximum value of each of the costs in Fig. 4.5.	66
4.3	Pairwise environmental mismatch compensation. Each column represents one parameter in mismatch, and each row, one parameter which was given freedom to compensate the mismatch. The values filling the table are the maximum allowed mismatch such that the acoustic cost is ≤ 0.1 , after the mismatch compensation (expressed in percentage, except for α_1 and z_a (with a null true value), for which the absolute values are used). The values in bold are the maximum for each column. The notation is explained in Tab. 4.1.	77
5.1	Parameters to invert for.	87
5.2	Parameter search bounds and discretization for acoustic inversion, to solve the problem of acoustic nowcast.	90

Chapter 1

Introduction

“If you want to build a ship, don’t drum up people to collect wood and don’t assign them tasks and work, but rather teach them to long for the endless immensity of the sea.”

Antoine de Saint-Exupery

THE ocean covers 71% of our planet, overlying one-third of the continental crust. The ocean is used for fishing, transportation, ship craft docking in harbors, and also as a resource of renewable energy, touristic attraction and waste disposal. The ocean drives the global climate, transporting heat from the tropics to higher latitudes, absorbing large amounts of the carbon dioxide emitted by humankind, and also creating the conditions for the formation of systems such as hurricanes[MRS⁺10, SH11]. Oceanographic physical features such as currents, upwelling and eddies define habitats for fish[MH04]. A comprehensive understanding of oceanic processes allows to extend the accuracy and prediction window of weather systems (e.g. El Niño)[CWH06]. This requires an extensive observation, possible with measurements from ships, floats, moorings and satellites. Some boundaries between continental and oceanic crust are rich in oil, gas and mineral deposits of economic importance, with a continuously expanding exploitation[Ear90, Pag12]. As a resource of renewable energy, the ocean is a target for strong investments on wind and tidal current converters. From all the above,

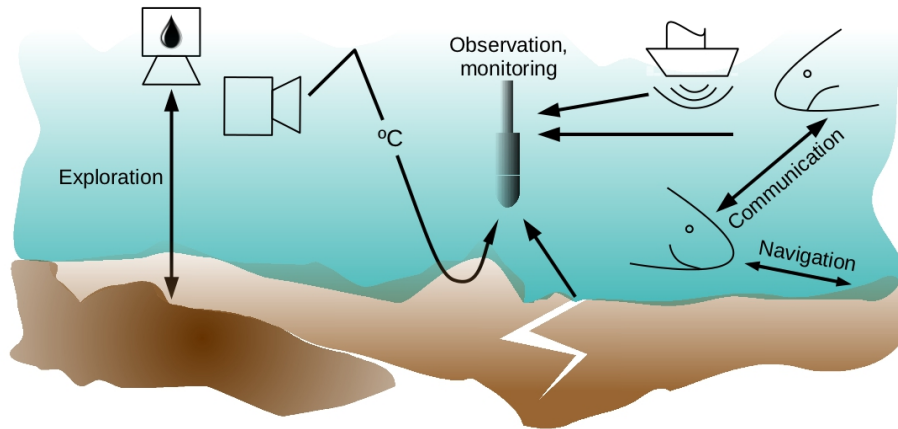


Figure 1.1: Some of the activities in which sound is used in the ocean, to convey information: oil/gas exploration, estimation of water column and geological properties, marine mammal communication/navigation, and monitoring of all of the above as well as of earthquake/plate dynamics and shipping noise. The arrows represent propagation of acoustic energy.

oceanic activities are of great socio-economic importance, representing a high percentage of the world GDP, and a source of employment opportunities[EFM⁺10, MHCO10].

1.1 Ocean Acoustics

Oceanic masses are immense and strongly permeable to sound. Natural evolution provided marine mammals with an enhanced sense of hearing, on which the animals heavily rely, in their routine behavior. Sound is one of the forms of energy that propagates farther in water, and is as important to marine mammal life as to human exploration of the ocean. The 20th century faced a significant development in ocean acoustical research, driven by needs such as submarine detection, undersea communications, mapping of the ocean's structure and topography, localization of mines or archaeological artifacts, and the study of ocean biology. The drawing in Fig. 1.1 represents some of the activities involving ocean acoustics, in which the role of the latter in the transmission of information is put in evidence. These activities are detailed in the following text.

Research recordings released in 1970 as “Songs of the humpback whale” served as a strong stimulus for further study of marine mammal life environments[Sto03]. In this context, sound (songs, calls and echolocating clicks) is important for orientation, communication, individual recognition, predator avoidance, hunting engagement, prey capture (with sound blasting), and mating[BC03, BV11]. Available evidence suggests that cetaceans adapt to the environment, in order to maximize range of transmission and detectability[Man00, TC00].

In a *Beyond Discovery* article, Victoria Kaharl wrote: “Had the world known how to harness the extraordinary ability of sound to travel through water in 1912, the Titanic might have had some warning of the iceberg (...) that took the lives of 1522 passengers and crew”[Kah99]. The tragic event motivated the development of tools using sound to locate underwater objects and ocean boundaries. Basically, these tools send acoustic pulses, whose return echoes carry information on their distance. Improved versions allow to find submarines, buried objects and mines, and are routinely used in oil and gas exploration, and fishing[BvVV12]. The knowledge of the shape of ocean basins is strictly a product of acoustics. Vessels typically employ some type of commercial hydroacoustic device (bottom profiler or side scan sonar, among others) for navigation, depth finding, seafloor mapping, or biological detection[Her65, Cou09]. In particular, fish stocks and marine organisms (e.g. Antarctic krill) are regularly surveyed with acoustic sounding[RIC05, RHT⁺12]. Fisheries research is supported by remotely operated vehicles, which carry cameras and sound transducers, allowing to image and continuously monitor populations in areas covering thousands of km²[DMD⁺07, JBS⁺09]. A recurrent problem in fishing activity is that marine mammals get trapped by fishing gears. This problem has been solved by using acoustic deterrent devices, ‘alerting’ marine mammals to the presence of fishing gears. The acoustic

alarms are used for at least three purposes: to avoid bycatch of, and harmful action from marine mammals (depredation on fish, and fishing net damage), and to minimize revenue losses[LFMN04, GGA08]. Devices such as low-frequency “clangers”, high-intensity acoustic “harassment” devices, and low-intensity (less intrusive) sound-generators called “pingers” are typically used to prevent marine mammals of getting entangled in fishing nets.

Researchers in behavioral biology also use acoustics to study marine animals. An intrusive technique known as acoustic tagging allows to locate a particular specimen. The specimen’s skin lodges an acoustic emitter, whose periodic pulses are broadcast. Non-intrusive techniques are used as well, in which the acoustic instrumentation is “passively” deployed, i.e. listening to animal sounds, which are supplied to a processing system able to detect and identify the sound source[MSMH06, Zim11]. Acoustic-based methods allow significantly more detections than visual surveys, and have the exclusive advantage that they can continue at night, in poor weather and other demanding conditions[CEB86, RNS⁺07].

Passive acoustic monitoring systems exist worldwide, and are able to locate earthquakes, volcanoes, and study geophysical phenomena, in some cases using an acoustic positioning system, by deploying acoustic emitters and receivers in concert, at strategic points in the ocean[AUfU09, KTNK10]. Sound is widely used in acoustical oceanography for the estimation of ocean properties, in different spatial scales. On a scale of tens of meters, sound is used for the estimation of currents, using acoustic Doppler current profilers[RY79]. The latter emit sound, which is reflected back by floating scatterers (small particles or plankton) which are moving at the speed of the water current. The reflected sound is modified (distorted) by the Doppler effect, according to the scatterer speed. By analyzing the characteristics of the reflected signal, it is possible to infer the speed of the scatterer, hence

the current speed. On a scale of hundreds of meters to thousands of kilometers, sound is used as a remote sensing tool to infer water temperature, seabed properties, and geometric variables such as topography and the position of underwater acoustic sources. A comprehensive analysis of acoustic propagation shows that the water column temperature and salinity (even pH), and the seabed density, topography, sound speed and attenuation to sound, determine acoustic energy paths and distortion. This defines the insonification of the medium. The sound sensed at a particular ocean point never equals the emitted sound, and this difference reflects the particular instantaneous ocean environmental “picture” at the time of transmission. In general, different environmental properties lead to different types of distortion. Thus, by comparing the emitted with the distorted received sound, it is seen that the received sound carries information of the medium, if it is possible to recover the medium characteristics responsible for the sound distortion. This idea was explored by Munk and Wunsch, who proposed a technique to infer physical properties by processing propagated signals: ocean acoustic tomography[MW79, MW82]. The evolution of this technique resulted in a multipurpose tool, used for estimation of water temperature and currents, sediment properties, acoustic source position, and ocean bottom stratification, among others[DWCH94, MC98]. Advantages such as accuracy, and applicability in oceanic basins (difficult with point measurements) and problematic regions (for example, with strong currents), makes ocean acoustic tomography very attractive. Well-known tomography experiments include the Heard Island Feasibility Test[BM92] and the Acoustic Thermometry of Ocean Climate[Con98, DAH⁺07], on scales of $O(10^4 \text{ km})$ and $O(10^3 \text{ km})$, respectively.

A byproduct of anthropogenic activities in the marine environment is the extensive and increasing production of noise[HW07]. Major high-level human sound sources include seis-

mic surveys for oil and gas exploration, commercial shipping, scientific research, fishing, and sonar systems for military purposes. Anthropogenic noise covers the full frequency bandwidth (1 Hz–200 kHz) that marine animals use to sense their surroundings and to communicate[Sto03, MW08]. The effect of human-generated noise on marine mammals is a sensitive subject. On the one hand, the latter have evolved to use sound as a primary sense, and if deprived of this sense, can be expected to perish; on the other hand, commercial shipping is injecting increased levels of noise in the ocean, which can “disperse” over wide areas[SDW03, Sou05]. Cetaceans have been observed changing their behavior close to powerful, low-frequency sound sources (including drill rigs[Sch00] and seismic operations[MMS⁺99]), wind farms, and omnidirectional sources such as acoustic deterrent devices and military echo-sounders, sometimes with injury[ONSF02, SBE⁺07]. Current knowledge confirms that increased anthropogenic noise levels can induce prey evasion, strandings, reduce the quality and transmission range of sounds, and cause stress or hearing loss to marine mammals[MMS⁺99, AL04]. New regulatory initiatives have placed additional restrictions on the use of sound in the ocean, and mitigation of marine mammal endangerment is now a consideration in the design and operation of acoustic systems[Ett12]. For instance, restrictions were imposed that require tankers traveling to deepwater gas terminals in Massachusetts Bay to slow down to 10 knots or less, when notified with real-time acoustic buoy detection of the presence of right whales[BBC⁺11, SB12]. In the context of environmental monitoring, some long-range transmissions use broadband low-power signals with energy spread over a large transmission time, in order to not harm marine life[MWW95, Rod02].

Maritime security has been a concern since early times, when important ocean routes were established. Nowadays, though surface targets can be detected using e.g. radars and thermal

imaging, sonar remains the only technology able to provide a large coverage for surface and subsurface threat detection (in the most complex setting, with a network of sources and receivers)[Yak08, vVBvdS11]. High-frequency sonars can be used for detection of threats like mines[Com01, RR02]. The international exchange of goods through maritime transportation requires ship craft docking in ports and harbors, the latter becoming sensitive in terms of security. Current tendencies are to increase the use of inshore acoustic surveillance systems, in integrated marine security models for harbor protection. An example of a small-scale and silent threat is a diver or a swimmer. Swimmer detection has been tackled through the use of Doppler sonars, installed at several Navy sites worldwide[RR02, BSRB08]. Response measures can be taken from boats, using acoustic, explosive or less-lethal diver recall devices (e.g. low-frequency sounds likely to cause discomfort).

One of the ultimate developments in underwater acoustics was the development of digital communication systems. These are used to link moored oceanographic instruments to surface platforms, with real-time data delivery and a continuous monitoring of the instrumentation. Several sampling platforms can be acoustically connected, integrated in an ocean observation network[APM05]. In such a system, data collection is supported by fixed instruments and by vehicles, the latter equipped with oceanographic, acoustic and video sensory, playing an important role in exploration, surveillance and patrolling[LHZ⁺09, VSJ11]. Computer networks find their homologs in ocean observation networks, which use acoustic modems, gateways and rerouting schemes. Some of the network nodes are interfaced to shore through cabled or aerial links. Two examples of on-going projects relying on observation networks are LIDO (Listening to the Deep Ocean Environment)[AvdSZ⁺11] and OOI (Ocean Observatories Initiative)[Ack12]. The LIDO system contains modules which process real-

time acoustic streams for assessment, classification and localization of acoustic events (e.g. presence of cetaceans). This project includes partnerships with multidisciplinary networks such as the European ESONET, the Canadian NEPTUNE, and the Japanese JAMSTEC observatories[dCM11]. The OOI is a program to provide 25–30 years of expandable-network measurements to study climate, ocean circulation and acidification, ecosystem dynamics and seafloor processes, across a range of scales.

1.1.1 Problematic of Acoustic Propagation

The transmission of sound in the ocean is affected by its bottom topography and the distribution of the physical variables (such as temperature, salinity and pressure) due to various ocean phenomena including turbulence, internal waves, fronts, currents, vortices, eddies and filaments. The ocean offers a significant distortion to sound, including diffraction, reflection, scattering at rough boundaries, attenuation of compressional and shear waves by the bottom, and in which the sound speed acts as a refraction index, determining the amount of interaction of sound with any particular ocean physical/geometric feature[MC98, Med05]. For example, sound is trapped in zones of minimum sound speed[TC87]. The physical properties responsible for sound distortion vary on space scales of millimeters to planetary, and on time scales from seconds to geological. Summarily, the complex multi-scale space-time variability of the properties affecting acoustic propagation induce an equally complex variability on the phenomenon of sound propagation.

Modeling sound propagation has become as important as the phenomenon itself, mainly during the Cold War, which required a better understanding of underwater acoustics. As a result, great advances in sound propagation modeling were made[McC04]. Going back in

history, Newton is normally credited with the first theoretical attempt to describe sound propagation in a fluid[JKPS11]. More recently, in 1919, soon after the end of World War I, Lichte published the first scientific paper on underwater sound[Lic19]. In this paper, the author describes theoretically the bending of sound rays produced by slight temperature and salinity gradients in the sea, and recognizes their importance in determining sound ranges. Sound paths can be understood from Snell's law, which relates the ray angle with respect to the horizontal, to the local sound speed. Ray theory has historically proved to be an indispensable tool for understanding and studying sound propagation. At the best approximation, sound propagation in the ocean is mathematically described by the wave equation, whose parameters and boundary conditions are descriptive of the ocean environment. Over the 80s, a number of ocean-acoustic propagation models (computer solutions to the wave equation) have been developed, with the objective of modeling the acoustic field in various ocean channels[Buc92]. There are essentially five approximations to describe sound propagation in the sea: spectral or "fast field program"[Pek48b], normal mode[Pek48a, KP60], ray[Lic19, PB87], parabolic equation[HT73, Ros99], and direct finite-difference[Ste88, Fri93] or finite-element[Bur87, Hua88] methods. All these approximations allow for the ocean environment to vary with depth, representing the water column sound speed as an SSP. A model that also permits horizontal variations in the environment, in the bottom or the water column properties, is termed range-dependent. Furthermore, some models tackle three-dimensional (3D) propagation, modeling horizontal refraction of acoustic energy, when presented with a 3D environmental field. They either divide the full 3D space into N range-dependent vertical sectors and solve a range-dependent problem for each of them ($N \times 2D$ models[CBGE⁺86]), or solve the wave equation in 3D coordinates (e.g. HARPO (Hamil-

tonian ray-tracing) model[JRG87], KRAKEN (normal mode) model[Por91], and parabolic equation models such as FOR3D[LBS92] and the models mentioned in the review papers by Tolstoy[Tol96] and Sturm [Stu05]). An accurate simulation of acoustic propagation demands for a precise environmental description (e.g. three-dimensional distribution of SSP and bathymetry variations) on the order of fractions of a wavelength. Nevertheless, the accuracy of the available geophysical databases is much lower than the accuracy of the acoustic models. The lack of detailed environmental knowledge leads inevitably to a series of approximations regarding the ocean-acoustic environment. A common approach is to assume a horizontal stratification for most of the water column and bottom layer properties. Furthermore, the insufficient spatial density of measurements of water column and bottom properties frequently requires extrapolation. The latter might use old, inaccurate archival data as additional data sources. At last, several approximations deviate further from reality, in the presence of currents, tides, turbulence, and internal waves[POC63, Sku63], which are forever disturbing whatever idealized, average picture one assumes for the medium. In summary, the amount of environmental uncertainty imposed by the complexity of the medium itself is the primary limiting factor to the accurate modeling of sound transmission in the ocean[Zak10]. Additionally, current propagation models have limitations regarding the admissible complexity of the environmental input (for instance, regarding the description of the bottom structure), and modeling phenomena such as backscattering, or propagation with an extremely rough ocean surface or irregular bathymetry, with a higher impact towards the high-frequency end[Hua12, Mar13]. Though each model specializes in (a) particular aspect(s) of acoustic propagation, it is virtually impossible to find the model that can account for the full environmental detail, and handle all the peculiarities of propagation at all

frequencies of interest. Finally, the ocean is a dynamic medium, in which the environment and the acoustic/oceanographic instrumentation position (for acoustic sources and receivers, temperature sensors, etc.) fluctuates with time, representing an additional level of difficulty in modeling acoustic propagation.

1.2 Motivation

In the preceding text, it was evidenced that: 1) ocean science is diverse and serves multiple interests; 2) acoustic propagation is an important way of conveying information, for both natural and anthropogenic activities; 3) modeling acoustic propagation represents a tremendous task, with inevitable errors, when regarding the collection or use of detailed environmental information for the relevant space-time scales, in acoustic propagation codes with limited admissible environmental input structure.

The accomplishment of many technical/scientific operations at sea relies on the physics of acoustic propagation, in order to understand natural phenomena, use the ocean in an efficient and responsible way, or transmit information between observing platforms. As a general rule, societal and economic benefits are not maximized until some sort of prediction of asset/payoff is involved. This is clearly visible on the importance of having at hand accurate forecasts of e.g. weather and evolution of natural hazards (such as hurricanes, cyclones, oil spills and volcanic eruptions), possible to obtain with accurate ocean/atmosphere circulation models. In the context of ocean acoustics, most of the activities involving sound can be optimized, if an accurate prediction of sound levels at present and at future time is available. In view of the immensity of the ocean, this allows, for instance, for an optimized (in space and time) positioning of acoustic emitters/receivers to perform acoustic monitoring, ocean surveillance,

autonomous vehicle navigation, ship route planning, prediction of sonar performance, global warming studies, and observation and risk mitigation for cetaceans.

1.2.1 State-of-the-art

Acoustic prediction is the estimation of the acoustic field in a specific space-time domain, which requires information concerning environmental properties (from measurements or estimates). The environmental properties are usually provided to an acoustic propagation model, and their accuracy directly impacts in the acoustic accuracy. As mentioned in Sec. 1.1.1, current acoustic propagation modeling reflects a well grounded understanding of acoustic propagation. With some exceptions towards the high-frequency end[Hua12, Mar13], low and medium frequency propagation can be acceptably modeled with the more than 100 acoustic propagation models available nowadays[Lic19, Pek48a, Pek48b, KP60, HT73, Bur87, PB87, Hua88, LM88, Ste88, Buc92, Fri93, LB98, Ros99, McC04, JKPS11, Ett13]. In their majority, these models predict the sound field in range and depth, and some give a prediction in the 3D space[CBGE⁺86, BLK87, Por91, Stu05]. In order to have at hand accurate environmental information to provide to the propagation model, a tremendous effort has been made in the last three decades to develop means of sampling the ocean complexity, by using ship- and aerial-operated instrumentation, and moored and drifting sensors. Often, the concern in an oceanic sampling exercise is to gather most of the information about the medium, as is the example of “Rapid Environmental Assessment”[Aka08]. The aim of this type of exercises is twofold: 1) to gather the maximum possible information of the ocean state, to use as input to circulation models; 2) to use the environmental information together with estimates from the circulation models, to predict sonar performance.

The ocean is a turbulent fluid that is driven mainly by mechanical wind forcing and the net effect on density of surface exchanges of heat and moisture. It responds according to conservation of mass, momentum, energy, and other properties. The resulting 3D flows are influenced by Earth's rotation and are regulated by internal mixing and boundary friction. Since the early eighties, the Harvard University Physical Oceanography Group has been involved in the research and development of practical ocean nowcasting and forecasting in real time[LRA⁺96b]. Some systems have emerged, having application to various open and partially open domains from hundreds to thousands of kilometers in extent. Some of such systems are the former quasi-geostrophic Harvard Open Ocean Model (HOOM)[RW87], later on, the Harvard Forecast System (HFS)[RCG94], and finally, the Harvard Ocean Prediction System (HOPS)[LRA⁺96b]. Common to many forecast systems/models is the numerical solution of the primitive equation model[LPA⁺94] and the quasi-geostrophic equation model[OLR92]. From the innumerable models available today, other examples are the NCOM[RBSR02], used in the present work (see Ch. 5), the Princeton Ocean Model[BM87], the Regional Ocean Modeling System[SH94], the MITgcm[Mar97], the Hybrid Coordinate Ocean Model[SB06] and the Modular Ocean Model[Gri12]. The main output of these models is the *oceanographic forecast*, consisting of estimates of the water column temperature, salinity and current fields, at a time posterior to a measurement and estimation period. In the present work, the term *oceanographic forecast* designates also any estimate of a future SSP (derived from the temperature and salinity forecast).

One of the main problems to tackle in the present work is the estimation of acoustic pressure or transmission loss at a future time. The estimate to be obtained is termed here an *acoustic forecast*, and is computed from the oceanographic forecast issued for the same

time sample of the acoustic forecast. An intuitive approach to obtain an acoustic forecast consists of coupling a circulation model with an acoustic propagation model (APM), through a coupling scheme. The set formed by the models and the coupling scheme is known as a “coupled ocean-acoustic model” [RL94]. The first reported coupling is the Harvard Open Ocean Model with the implicit finite difference parabolic approximation model [Rob87]. The coupling scheme determines if the circulation model outputs are used directly or through derived quantities by statistical models [LAL00], objective analysis [CR87], structured data models [LRA⁺96a], or melding of fields [Rob97], to obtain gridded fields appropriate for direct input to the acoustic model. Several works on coupled ocean-acoustic modeling can be found in the literature (see [RL94], for an overview), some of which are mentioned below. In [HSM91], a 3D ocean model provided data for input to a ray-tracing acoustic model, to study the effect of frontal eddy features on sound propagation characteristics. One of the main conclusions was that the propagation characteristics were comparable to those predicted from environmental measurements and from theoretical considerations. However, the acoustic prediction was sensitive to ocean model parameters, in particular the horizontal eddy viscosity coefficient. In [FES02], a coupled ocean-acoustic model was introduced, for a continental shelf/slope environment. The oceanographic component, starting from a profile obtained from the SWARM95 data set [FOT⁺00], allowed for the generation and propagation of sub-mesoscale phenomena such as internal tides and solitary waves. The results of this component were mapped into the corresponding sound speed distribution, used as input to a wide-angle, split-step parabolic equation which computed 400-Hz transmission loss (TL), over 30-km range. In [LCR02], the uncertainties in the predicted low-frequency acoustic field from a transmission from the continental slope to the shelf, in the Middle Atlantic Bight,

are studied. Based on oceanographic data from the 1996 Shelfbreak Primer Experiment, at New England, HOPS was initialized with 80 realizations of physical fields, and integrated to produce 80 realizations of a 5-day sound speed forecast. The forecasts were fed into a Naval Postgraduate School coupled-mode propagation model, to produce 80 Monte-Carlo realizations of the TL. In [LC02, RL04, Ler06], error subspace statistical estimation (ESSE) was employed to the estimation of 3D environmental and two-dimensional (2D) acoustical fields, as a single coupled data assimilation problem. Both acoustic and oceanic variables were included in a coupled state vector, and their measurements assimilated according to their uncertainties. The goal of the assimilation was to minimize the trace of the data-forecast error covariance[Ler99]. References [Sch02, WX06] present adaptive rapid environmental assessment, a measurement procedure to improve the ocean estimation relevant for acoustics, illustrated with FAF-05 exercise data. The sound speed fields and uncertainties predicted by HOPS/ESSE were used to compute TL uncertainties (by RAM)[JKPS11], via Monte Carlo runs. The weighted sum of those uncertainties was minimized, to guide autonomous underwater vehicles sampling plans. In [RGH⁺09], the acoustic field was computed from the sound speed predicted by super-ensemble forecast techniques, in the framework of the BP07 experiment. These techniques find ocean model output combinations which minimize data-model errors. Pressure fields were computed with the RAM acoustic model, for frequencies up to 1800 Hz[Col89]. In Ref. [LHJ⁺09], the coupling of a data-assimilative ocean modeling system with an acoustic propagation model was carried out at sea, in real-time, for the first time, within the BP07 exercise. A chain of operational oceanographic-acoustic forecasting, involving in situ and external data, provided high-resolution oceanographic forecasts, the latter used as inputs to the TNO performance prediction toolbox, ALMOST[Sch95]. To

carry out acoustic prediction, the ocean model sound-speed forecasts were interpolated onto a suitable grid for acoustic modeling, and the coupled system provided high-resolution sonar performance nowcasts and predictions up to several days.

In the context of acoustical inverse problems, the situation of environmental mismatch has been referred to in the literature as a factor precluding the successful estimation of the ocean environment by ocean acoustic tomography. In practical setups, the environment is divided into two components, one is fixed, and the other is variable. The former is supposedly known from measurements, archival data, etc. The latter is unknown, and is to be estimated from the ‘knowledge’ of the former, combined with measurements of propagated sound. In the event that the ‘knowledge’ of the fixed component is not exact —situation of environmental mismatch—, the estimate of the variable environment is driven to incorrect values[CK91, Dos93, ZDF96]. In the work of D’Spain, it was observed that estimates of source range and depth remain surprisingly coherent in the presence of large mismatch in bathymetry, but are offset from the true position by as much as 100%[DMHB95]. Dosso and Zakarauskas described two methods of matched-field inversion for source localization with an inadequate knowledge of the bathymetry[DZD95]. These methods are based on determining an acoustically-equivalent bathymetry model as part of the localization procedure. The acoustically-equivalent bathymetry model is a bathymetric structure different from the true one, though leading to an acoustic field very similar to the true field. In other works, equivalent geoacoustic models were proposed and studied for different purposes, such as parabolic equation modeling[Buc83] or the study of the effects of shear waves[LH97]. Garlan and Démoulin considered equivalent geoacoustic models for sonar applications[DPSS00]. By using simpler (equivalent) environmental models than their real homologs, it was possible

to model the acoustic reflection coefficient and the data-derived impulse response with acceptable accuracy. The authors named the obtained geoacoustic model as “sonar truth” (from the French “vérité sonar”), as opposed to “ground truth”.

Acoustic propagation can be seen as a multivariate transformation of the full set of environmental properties (and points of acoustic emission and reception) into the acoustic field. Within this dependence with multiple degrees of freedom, it is a priori not impossible that different environments/geometries can induce a similar distortion on a propagating wave. For instance, it should not be surprising that a tone signal from a far acoustic source, propagating in a medium with a highly reflective bottom, will be received at a particular point, with similar characteristics as compared to one propagated from a close source, in a medium with a highly absorbent bottom. In this example, two parameters (source distance and bottom material) are simultaneously different between the two propagation scenarios. This is a key point, when using an acoustic propagation model: if there is imprecise knowledge in one parameter (for example, the source is thought of being located closer than it is in reality) —situation of mismatch—, the acoustic effect of this error can still be compensated, provided that an error is purposely introduced in other parameters (for example, by using a more absorbent bottom material). In summary, in a situation of environmental mismatch, the modeled acoustic field can be closer to the actual field, if the propagation model is parameterized with properties shifted from the measurements[MJ09].

1.2.2 Contribution

The present work approaches the problem of acoustical estimation in the underwater context, in a situation of environmental mismatch. In practice, it is intended to estimate the acoustic

field produced by a hypothetical acoustic source. It is assumed that an acoustic propagation model is used as the link between the available knowledge of the oceanic physical properties and the acoustic estimate (acoustic pressure, transmission loss, etc.). Importantly, the question of dealing with incorrect environmental representations of the ocean for acoustic propagation modeling is worked out. Incorrect representations arise due to environmental uncertainty and to limitations in the environmental structure admissible by any propagation model. From the literature and empirical knowledge, it is well known that dealing with incorrect environmental models can lead to deviations from actual measured acoustic signals[POC63, Sku63, Zak10, Hua12, Mar13]. Nevertheless, apparently no work has been done so far in the direction of overcoming this problem. The typical procedure in acoustic estimation is to concentrate on the estimation of the environment. The true value of each environmental parameter is sought individually, minimizing an environmental error. At the end, the ensemble of minimum-error environmental parameters is provided to the propagation model, whose output is expected to produce a minimum-error acoustic estimate. The present work proves two related aspects: 1) the acoustic estimate thus obtained is not a minimum-error estimate; 2) the substitution of a minimum environmental error by a minimum acoustical error as the estimation criterion leads naturally to a minimum-acoustic-error solution. Here, the methodology consists in: 1) measuring the acoustic field at sparse ocean locations; 2) infer environmental parameters by inversion of the acoustical measurements; 3) use the obtained environmental parameters in a propagation model forward run, which produces the acoustic estimate. In the second step, the environmental parameters form the termed “equivalent model”. In the third step, a preprocessing step is needed, when the acoustic estimate respects to a time sample ahead in time with respect to a time window in

which several acoustic and oceanographic measurements have been made in the area in which to estimate the acoustic field. The preprocessing step consists in estimating the relationship between true environment and equivalent model, and using this estimate to deduce a future value for the equivalent model from an estimate of the future true environment. In this case, an “acoustic forecast” is obtained, as opposed to an “acoustic nowcast”, in the previous case. The environmental parameters to invert for can include or not properties which have incorrect values, as long as the former are optimized (by acoustic inversion) to compensate for the environmental mismatch. Those environmental parameters, after realized by acoustic inversion, giving rise to the “equivalent model”, are seen here as the most valuable information concerning the acoustic field (apart from the fixed environmental properties, either in mismatch or not). The ground of the contribution of this work is to treat the “equivalent model” as a quantity distinct from reality, whose values are allowed to differ from reality with unbounded shifts, and are used directly in a propagation model, for acoustical estimation.

The proposed methods exhibit advantages with respect to conventional acoustic estimation approaches, in the test cases considered. Specifically, for the problem of acoustic nowcast, a scenario with a systematic error in the water column and in some geoacoustic parameters was considered. A conventional method using the propagation model parameterized with some zero-error environmental parameters and the incorrect parameters was compared with the proposed method, which included acoustic measurements. The proposed method not only made explicit the optimal values of the parameters in the acoustic inversion, for acoustical estimation, as also lowered the acoustic estimate error by ≈ 5 dB, as compared to the conventional method. For the problem of acoustic forecast, a scenario with a systematic error in some geoacoustic and geometric parameters was considered. A similar

comparison was made between a conventional and the proposed method. In the problem of forecast, the addition is that a forecast of the water column is required. This forecast, with its own errors, was used, combined with the incorrect environmental properties, and other properties with zero error. The proposed method lowered the acoustic forecast error by ≈ 1.4 dB, as compared to a conventional method of direct ocean-acoustic model coupling. In the case that the oceanographic forecast exhibits zero error, the improvement in the acoustic estimation error can increase to ≈ 2.5 dB.

The motivation and preliminary building results for the present work are published elsewhere [MSJ08, MJ09, MJ10, PJ10, MFJ11, CWC⁺11, CCM⁺12]. In Ref. [MSJ08], it is pointed out the advantage of using environmental parameters inferred from acoustic inversion, in the process of estimating the acoustic field. Ref. [MJ09] presents a Bayesian scheme to compute the acoustic forecast, in a scenario with minimal environmental mismatch, and using several approximations for the involved probability density functions. The references [MJ10, PJ10, MFJ11, CWC⁺11, CCM⁺12] illustrate the concept of using acoustic inversion for the problem of acoustic estimation in the context of acoustic nowcast or forecast, with application to data sets not considered in the present report. Finally, a publication is in preparation, which summarizes the present report [Mar14].

Report Structure

The present report is structured as follows. Ch. 2 formalizes the problem at hand; Ch. 3 defines the concept of equivalent model and illustrates its application in simple scenarios; Ch. 4 illustrates the properties of equivalent models in a realistic scenario; Ch. 5 presents results of acoustic nowcast and forecast in the above scenario; Ch. 6 concludes the study.

Chapter 2

Problem Statement

*“Life is not a problem to be solved, but a reality to
be experienced.”*

Søren Kierkegaard

THIS chapter explains the acoustic estimation problem to be solved in the present work. After describing the context in real oceanic applications, it defines the concept of equivalent model, and finally outlines the steps towards accomplishing the problem at hand.

2.1 Framework

Consider Fig. 2.1 (a), which represents an oceanic volume with a point source producing an acoustic field $u(\Theta_T, r, z, f)$, of interest to a hypothetical *user*. Here, Θ_T is a vector containing all the properties (environmental/geometric) influencing acoustic propagation, and r , z and f designate *range*, *depth* and *frequency*, respectively. Consider now the time samples $t_0 \leq t_P < t_F \leq t_E$, where t_0 designates past *initial time*, t_P designates *present time*, t_F is a *future time*, and t_E is the final time sample. Finally, consider the problem of estimating the acoustic field at a space-frequency *estimation set* \mathcal{E} , for times $t = t_P$ (acoustic nowcast) and $t = t_F$ (acoustic forecast), using a numerical acoustic propagation model. Environmental information characterizing the oceanic volume is available, including water

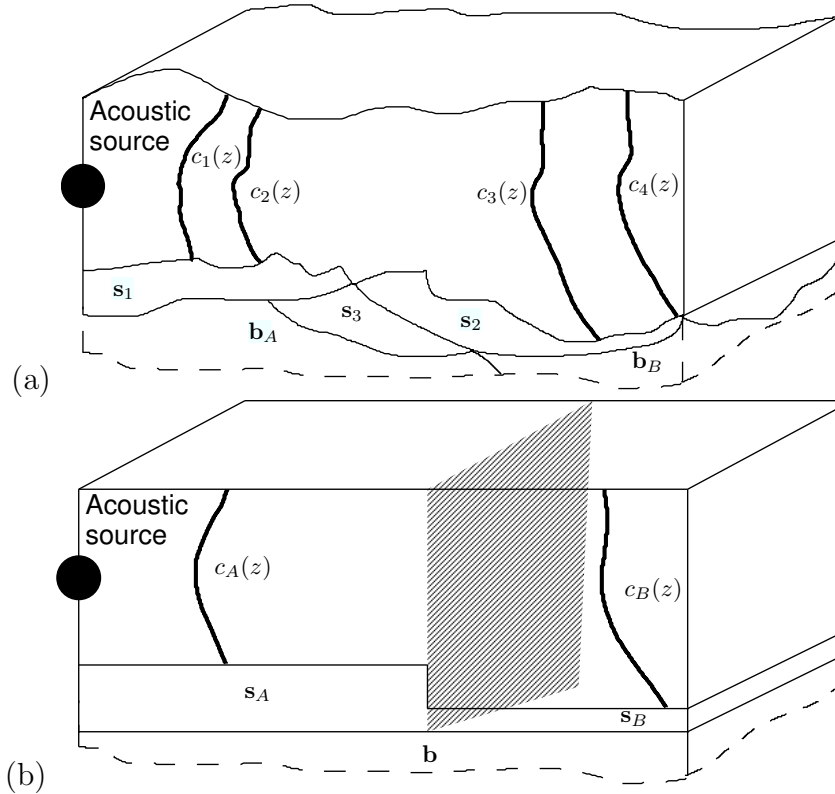


Figure 2.1: (a) Ocean volume in which to estimate the acoustic field produced by an acoustic source. All the environmental properties are space-dependent. (b) Limited representation of the environment in (a), in which the space-dependence of several environmental properties was simplified or removed, in order to be given as input to an acoustic propagation model.

column temperature and salinity measurements for times in the interval $[t_0, t_P]$, as well as ocean bottom data, and water column forecasts for all the times in the interval $[t_0, t_E]$. The timeline of the estimation exercise is shown in Fig. 2.2. Taking into account the lack of environmental knowledge in full detail, and the environmental structure admissible by the particular acoustic propagation model of choice, or any other reason mentioned in Sec. 1.2, the environmental properties in Fig. 2.1 (a) have to be represented in a simplified way. This leads to a representation such as the one in Fig. 2.1 (b). Notice that there are several differences between the properties in Fig. 2.1 (a) and the box-like representation in Fig. 2.1 (b). The horizontal dependence is rather simplified in the modeled environment in (b), where the true environment was transformed into an ocean volume divided into two sub-volumes,

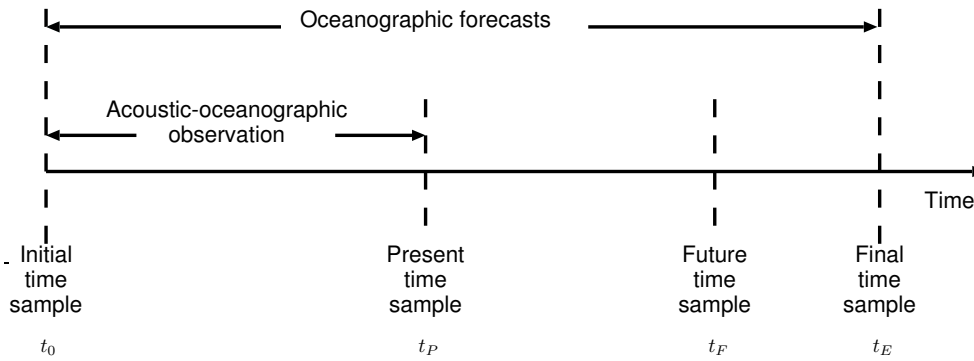


Figure 2.2: Estimation timeline in the problem at hand: estimation of the acoustic field at any “present time” and any “future time”.

with no horizontal dependence for physical properties. The four sound speed profiles in the true environment were reduced to two profiles, the three sediment layers were reduced to two layers, and the space-dependent basement was replaced by a space-independent one. In this simplified representation, where a homogeneous sediment is used in each ocean sub-volume, the reason for considering homogeneous materials can be a lack of geological information or a limitation of the propagation model (which might allow for no more than one sediment layer in each sub-volume). Thus, the user has to intuitively choose single-layer sediment properties that describe the influence of the true multilayer sediment (at worst, the true number of layers may be unknown) on the propagation of the frequencies of interest to the space points of interest. In summary, environmental structures such as that of Fig. 2.1 (b) are often subjective, turning the problem of acoustic estimation into one with a solution that is unpredictably away from the true value.

The main argument when dealing with no better than approximate environmental descriptions is that many of the environmental parameters in the simplified environmental model have to be offset from real values, if the problem at hand is to model the ocean acoustic field. In the above example, this is translated by differences between the parameters in

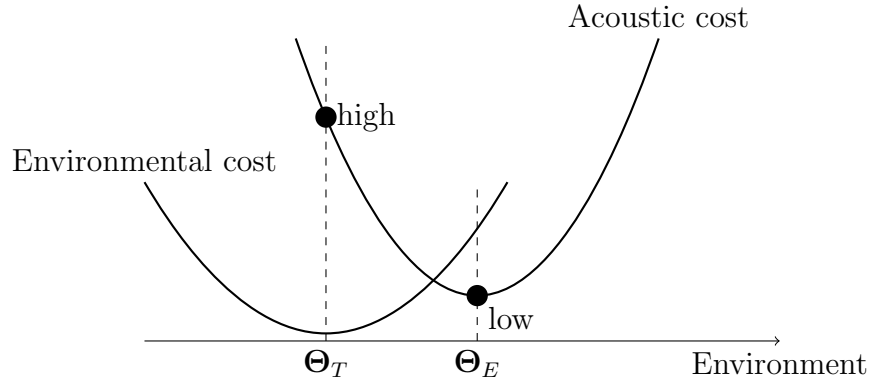


Figure 2.3: Idealized cost functions representing environmental and acoustic misfits. The environmental misfit is defined as the difference between a true and an estimated environment, and has a global minimum at Θ_T . The acoustic misfit compares a true and a modeled acoustic field, is a function of the environment, and has a global minimum at Θ_E .

Fig. 2.1 (b) and their homologs in Fig. 2.1 (a). The generic idea is materialized in Fig. 2.3, where the goals of acoustic estimation and environmental estimation are distinguished. It is illustrated that the modeled acoustic field corresponding to a maximum ‘match’ to the real acoustic field should be computed with an ‘optimum’ environment Θ_E which is different from the true environment Θ_T (the latter minimizes the environmental cost). As a consequence of the present reasoning, only in a situation of no environmental mismatch the values that minimize the functions in Fig. 2.3 would coincide, thus the true environment would coincide with the one that leads to a minimum acoustic error. The latter environment, Θ_E , is thus seen to produce an effect on acoustic propagation similar to the true environment. It can be considered as an environmental model which is ‘equivalent’ to the true environment, from the point of view of acoustics.

The present work claims that it is possible to cope with erroneous environmental descriptions such as the one in Fig. 2.1 (b), provided that the true acoustic field is observed at a spatial domain in the oceanic area in which to estimate the field. By using a subjective environmental structure parameterized from an objective measurement and inference approach,

optimal environmental values are obtained for modeling the acoustic field. Furthermore, the optimum (from the ‘acoustic point of view’) environment can be extrapolated to future times. The next section formalizes the concept of ‘acoustically-equivalent’ environmental model.

2.2 Definition of Acoustically-equivalent Environmental Model

Let us consider an acoustic field u , which represents a real field, and can be seen as a function \mathcal{P} of range r , depth z , frequency f and true environmental properties Θ_T :

$$u = \mathcal{P}(r, z, f, \Theta_T), \quad (2.1)$$

in which \mathcal{P} stands for the real propagation phenomenon, i.e., the natural transformation from true environmental properties and signal frequency to the field observed at a spatial point (r, z) . The field u is to be estimated by running an acoustic propagation model. Since the acoustic propagation model approximates the real propagation phenomenon, it is noted as $\hat{\mathcal{P}}$, and the associated acoustic field estimate is noted as \hat{u} , which is a function of the modeled environment Θ :

$$\hat{u} = \hat{\mathcal{P}}(r, z, f, \Theta). \quad (2.2)$$

Consider now the objective of adjusting \hat{u} to u , i.e., making $\hat{\mathcal{P}}(r, z, f, \Theta)$ to coincide with $\mathcal{P}(r, z, f, \Theta_T)$. In order to meet this objective, it is almost unavoidable that the model $\hat{\mathcal{P}}$ has to be fed with an environment Θ_E different from the true Θ_T , due to the previously mentioned limitations of operational acoustic modeling. Formally, the *exact equivalent model*

Θ_E would satisfy the following equation:

$$\mathcal{P}(r, z, f, \Theta_T) = \hat{\mathcal{P}}(r, z, f, \Theta_E). \quad (2.3)$$

Equation (2.3) defines the exact equivalent model as a parameter vector which leads the modeled acoustic field to coincide with the real field. The situation of equality may be difficult to be verified in practice, hence an approximate solution has also to be considered, defined as:

$$\begin{aligned} \hat{\Theta}_E(r, z, f, \Theta_T, \mathcal{C}, \mathcal{P}, \hat{\mathcal{P}}) &= \arg \min_{\Theta} \mathcal{C}(u, \hat{u}) \\ &= \arg \min_{\Theta} \mathcal{C}(\mathcal{P}(r, z, f, \Theta_T), \hat{\mathcal{P}}(r, z, f, \Theta)). \end{aligned} \quad (2.4)$$

The ‘acoustic cost function’ $\mathcal{C}(u, \hat{u})$ measures the dissimilarity between u and \hat{u} , and is parameterized by the environment Θ , while fixing all the remaining parameters. The value $\hat{\Theta}_E(r, z, f, \Theta_T, \mathcal{C}, \mathcal{P}, \hat{\mathcal{P}})$, which minimizes the cost, is defined as the *approximate acoustically-equivalent environmental model*, or *equivalent model*, in short. The term “model” stands for “parameters of a physical model of reality”, in some or all the aspects that influence acoustic propagation, such as acoustic source depth, receiver position, water column and geoacoustic properties.

In Eq. (2.4), it is seen that the equivalent model depends on several quantities and functionals. An important dependence regards the real propagation phenomenon \mathcal{P} . The latter determines the characteristics of the real field u , which enters Eq. (2.3). The structure of \mathcal{P} determines the influence that each component of Θ_T has on the definition of the acoustic field u . Upon computing the expression (2.4), if a particular true property has weak or no influence, its equivalent counterpart can even be undetermined, or assume a value significantly far from the true one. Since \mathcal{P} acts differently for different values of r , z and f , the depen-

dence of the equivalent model on \mathcal{P} also changes with the particular acoustic receiver spatial point and frequency of interest. Importantly, there is a dependence on the cost function \mathcal{C} . This dependence exists when it is not possible to obtain an exact equivalent model, which is the current case. The dependence on frequency and space can be understood by taking into account the intrinsic space-frequency dependence of the propagation phenomenon, and the distance-accumulated effect of oceanographic errors when modeling acoustic propagation.

2.3 Proposed Approach

The present work aims at estimating the acoustic field in a given oceanic area, at a given present time —acoustic nowcast— or at a given future time —acoustic forecast. A subjective environmental model representing the true environment is taken as a starting point, together with environmental measurements and forecasts, and sparse acoustic measurements taken in the true environment, till present time. The overall procedure is outlined in Fig. 2.4, and consists of the following steps:

1. Solve an acoustic inversion problem, using information from the environmental and acoustic measurements, to estimate the equivalent model;
2. Extrapolate the equivalent model to every space and time point of interest;
3. Run an acoustic propagation model taking the extrapolated equivalent model as input, to obtain the required acoustic nowcast or forecast.

In the problem of acoustic forecast, for which a time extrapolation is required, the extrapolator takes as input both the equivalent model and the environmental measurement/forecast time histories, indicated by the left-top arrow in Fig. 2.4. Additionally, the output of the ex-

trapolator, which is an estimate of the equivalent model for a future time, enters the “acoustic propagation model run” block together with the environmental forecast for the same future time (apart from other measured static properties), as indicated with the left-bottom arrow in Fig. 2.4.

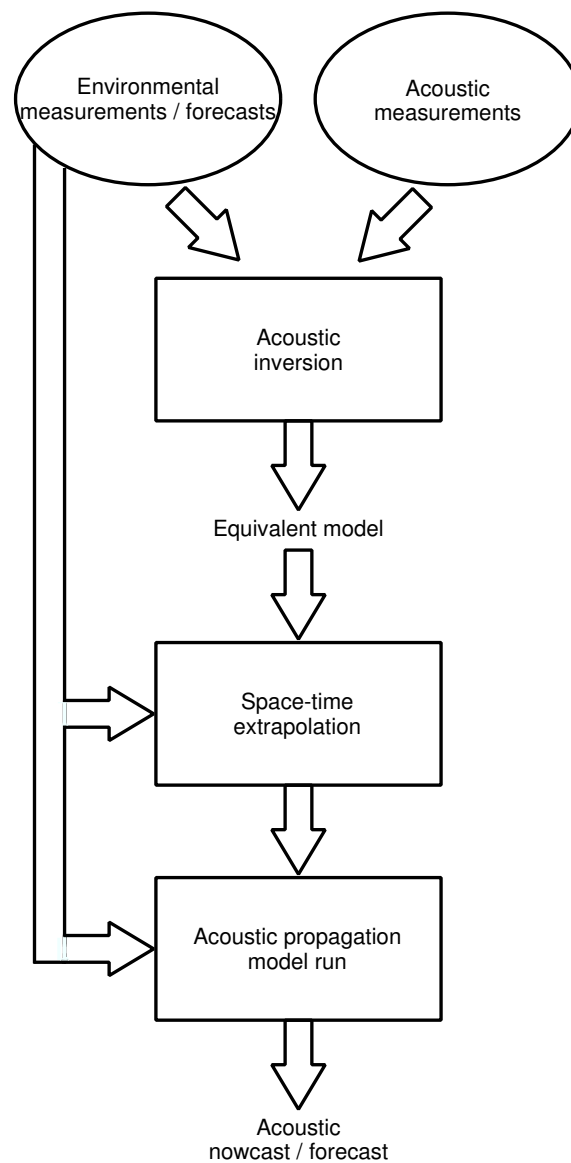


Figure 2.4: Proposed approach to the problem to be solved in the present work: the estimation of the acoustic field in an oceanic area, at present (acoustic nowcast) and at future time (acoustic forecast), on particular space points. After calibration of a given acoustic propagation model, using acoustic inversion, which takes a subjective environmental representation of the oceanic area, and gives the equivalent model as the output, the latter is extrapolated to the required space-time points of interest. By feeding the extrapolation result to the acoustic propagation model, the final acoustic estimate is obtained. For the problem of acoustic forecast, environmental forecasts are necessary to extrapolate the equivalent model, and to compute the acoustic forecast outcome at the last step —left arrows.

Chapter 3

Equivalent Models in Idealized Media

“Supply yourself with a mental equivalent, and the thing must come to you.”

Emmet Fox

THIS chapter demonstrates the use of equivalent models in idealized oceanic scenarios, to model the acoustic field. The intention is to show by examples the influence of physical laws on the interplay between the parameters that affect acoustic propagation. The examples, many of which with possible analytical descriptions, provide an insight into the generic properties and limitations of equivalent models.

3.1 Pedagogical Examples

The examples in the following sections are presented by increasing complexity. Though far from realistic, they allow to illustrate equivalent modeling possibilities for acoustic propagation in fluids with/out frontiers and acoustic reflection at different media interfaces, including viscoelastic media. In all the examples, the goal is to accurately model the acoustic field in a space-frequency domain. One or several properties have an offset —situation of environmental mismatch. There will be a search for values of (an)other property(ies) —the equivalent parameter(s)—, optimum(al) in the sense that the full environmental vector allows to obtain

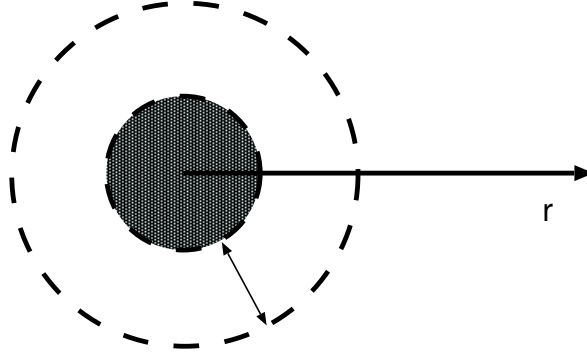


Figure 3.1: Vibrating sphere in an unbounded (infinite) medium (adapted from Jensen et al.[JKPS93]).

an acoustic field very similar (when not equal) to the true one.

3.1.1 Unbounded Medium

Let us consider a spherical sound source in an unbounded medium, as illustrated in Fig. 3.1.

The field $\Psi(f, r, c)$ produced by the source, proportional to the displacement potential, is given by[JKPS93]:

$$\Psi(f, r, c) = \frac{e^{i2\pi fr/c}}{r}, \quad (3.1)$$

where f is the wave frequency, r is the distance from the source, and c is the propagation speed. Thus, the field depends on three variables: f , r and c . For a fixed wave frequency, two cases will be shown: a sound speed mismatch compensated by an equivalent distance, and a distance mismatch compensated by an equivalent sound speed. In the notation, the subscript “ M ” is used for quantities in mismatch, while “ E ” is used for equivalent quantities.

Sound Speed Mismatch Compensation by Equivalent Distance In the case that the sound speed is erroneously taken to be $c_M \neq c$, the purpose is to find the equivalent distance r_E that guarantees that the true acoustic field $\Psi(f, r, c)$ is exactly equal to the field

$\Psi_E(f, r_E, c_M)$ produced with the sound speed in mismatch and the equivalent distance,

$$\Psi_E(f, r_E, c_M) = \frac{e^{i2\pi fr_E/c_M}}{r_E}. \quad (3.2)$$

This amounts to solve the following equation w.r.t. r_E :

$$\frac{e^{i2\pi fr/c}}{r} = \frac{e^{i2\pi fr_E/c_M}}{r_E}. \quad (3.3)$$

Equation (3.3) has no solution in r_E , if $c_M \neq c$, because any attempt to equate the phases in both sides of the equation will lead to different field magnitudes. In conclusion, there is no value of distance that can completely compensate for the sound speed mismatch, i.e., there is no *exact equivalent distance* following the definition in Eq. (2.3). It is thus legitimate to search for an *approximate equivalent distance* according to the definition in Eq. (2.4). In the search for an approximate equivalent distance, the acoustic cost is here defined as a simple Euclidean distance measure:

$$\mathcal{C}(r_e) = \left| \frac{e^{i2\pi fr/c}}{r} - \frac{e^{i2\pi fr_e/c_M}}{r_e} \right|, \quad (3.4)$$

where r_e represents a candidate approximate equivalent distance. The approximate equivalent distance r_E is defined as the value that minimizes $\mathcal{C}(r_e)$. Let us consider the following simulation parameters:

$$\begin{aligned} f &= 500 \text{ Hz}, \\ r &= 5 \text{ km}, \\ c &= 1500 \text{ m/s}, \end{aligned} \quad (3.5)$$

and the following value for the sound speed in mismatch:

$$c_M = 1503 \text{ m/s}. \quad (3.6)$$

In this case, the cost as a function of distance r_e is shown in Fig. 3.2. The cost never attains zero, and has the minimum value of 1.1×10^{-3} , for $r_E = 5.012$ km. As understood from

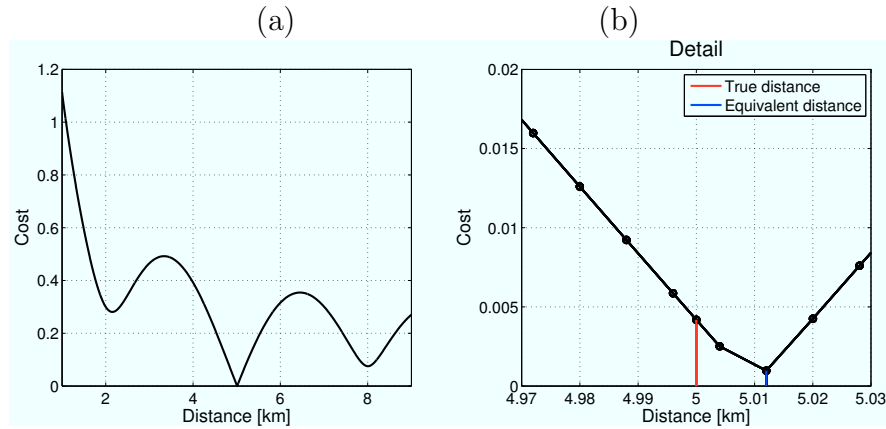


Figure 3.2: (a) Acoustic cost as a function of distance. The approximate equivalent distance is 5.012 km, as seen in the detailed representation in (b). The cost corresponding to the true distance (5 km) is 2.8×10^{-3} , while the one corresponding to the equivalent distance is 1.1×10^{-3} , 2.5 times smaller.

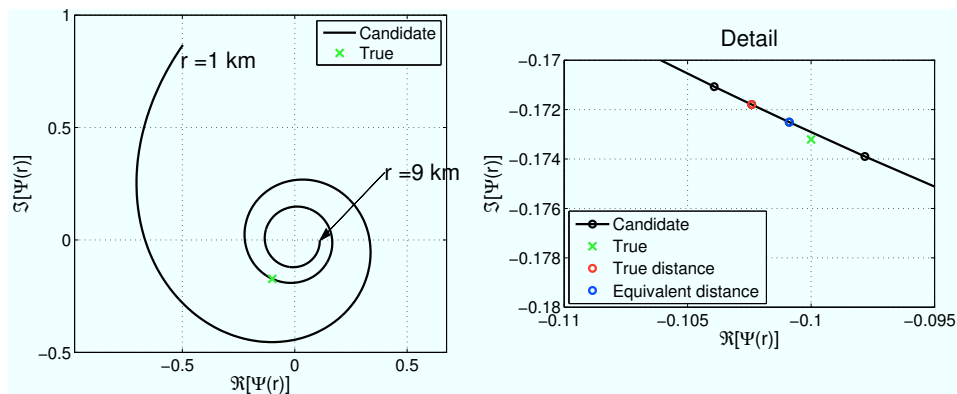


Figure 3.3: True (X) and candidate (-) acoustic fields. The sound speed in mismatch is 1503 m/s (the true value is 1500 m/s). The candidate fields are computed with the sound speed in mismatch, for several candidate distances in the interval [4.98, 5.02] km, defining a contour in the complex plane which does not contain the true field.

Fig. 3.2, the discretization of the search space will determine the value of the estimated equivalent distance. The true and candidate acoustic fields corresponding to the cost in Fig. 3.2 are shown in Fig. 3.3. It can be seen that the candidate field defines a contour in the complex plane which converges to the origin as the candidate distance tends to infinity, and that the candidate field never coincides with the true one.

It is interesting to quantify the difference between compensating or not for environmental mismatch. A test was done in which the acoustic field was computed, without compensating for the sound speed in mismatch, which varied between 1402 and 1550 m/s, and is shown

in red, in Fig. 3.4. The field thus obtained defines a circle in the complex plane with

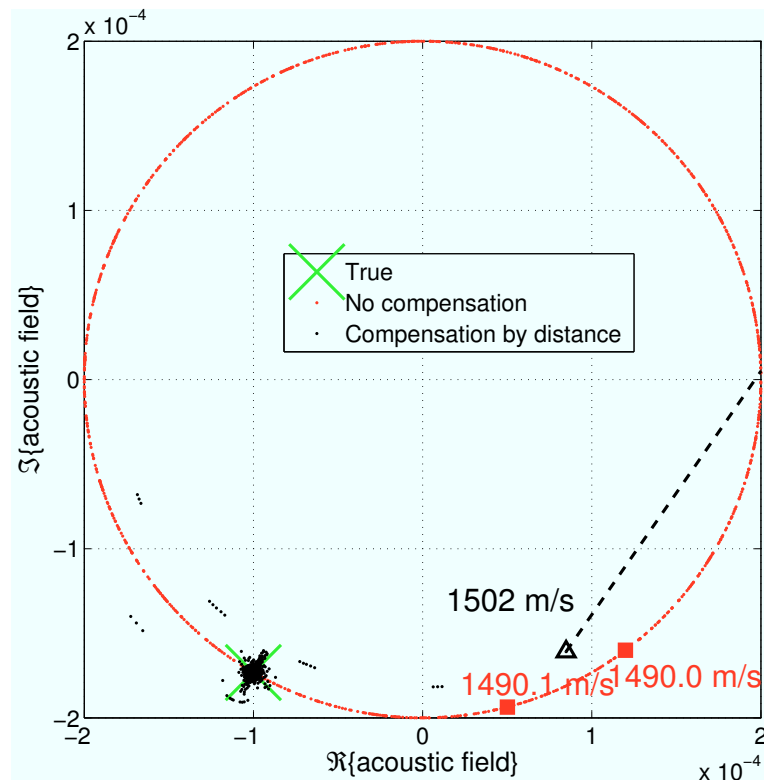


Figure 3.4: Effect of compensation for a sound speed in mismatch, in the case of an unbounded medium, with the simulation parameters described in the Eq. system (3.5). The sound speed varied between 1490 and 1545 m/s. The true field is represented by the cross; the field computed with the sound speed in mismatch is represented in red, with all the points lying in a circle; the field computed after compensation (by optimizing for distance) for each value of sound speed in mismatch, is represented in the black cloud.

radius $1/r = 2.0 \times 10^{-4}$, according to the definition in Eq. (3.1). The field obtained after compensating for the sound speed mismatch is shown by the black dots. It can be seen that, if no compensation is done, the resulting acoustic field can be far from the true value (cross). Two such points are shown on the squares in Fig. 3.4, which show that a small difference in the sound speed in mismatch can change the field to be significantly different, showing how unpredictable the field estimation can be, in the presence of mismatch. After compensation, most of the acoustic field estimates are located close to the true field. One of them, corresponding to the worst compensation in terms of the cost in Eq. (3.4), for the values tested, is the one corresponding to a sound speed of 1503 m/s (in mismatch). For

this case, the field obtained when no compensation is done is the intersection of the circle with the dashed line in Fig. 3.4, while the one obtained after compensation is represented by the triangle.

In certain applications, the elected acoustic quantity to be modeled is the transmission loss. In terms of the field $\Psi(f, r, c)$, it can be defined as:

$$\begin{aligned} \text{TL}(f, r, c) &= -20 \log_{10} |\Psi(f, r, c)| \\ &= 20 \log_{10} r, \end{aligned} \quad (3.7)$$

which, noticeably, is not a function of sound speed c . This allows to conclude that any transmission loss estimate, in an unbounded propagation medium, is insensitive to errors in sound speed, and sensitive exclusively to errors in distance.

Distance Mismatch Compensation by Equivalent Sound Speed In the case that an erroneous distance r_M is considered, the idea is to find an equivalent sound speed c_E that guarantees that the true acoustic field $\Psi(f, r, c)$ is exactly or approximately equal to the field $\Psi_E(f, r_M, c_E)$ produced with the distance in mismatch and the equivalent sound speed,

$$\Psi_E(f, r_M, c_E) = \frac{e^{i2\pi f r_M / c_E}}{r_M}. \quad (3.8)$$

The equivalence problem at hand amounts to solve the following equation w.r.t. c_E :

$$\frac{e^{i2\pi f r / c}}{r} = \frac{e^{i2\pi f r_M / c_E}}{r_M}. \quad (3.9)$$

This equation has no solution in c_E , if $r_M \neq r$, because this condition prevents the left- and right-hand sides of Eq. (3.9) from having the same magnitude. In conclusion, there is no exact equivalent sound speed that can completely compensate for the distance mismatch.

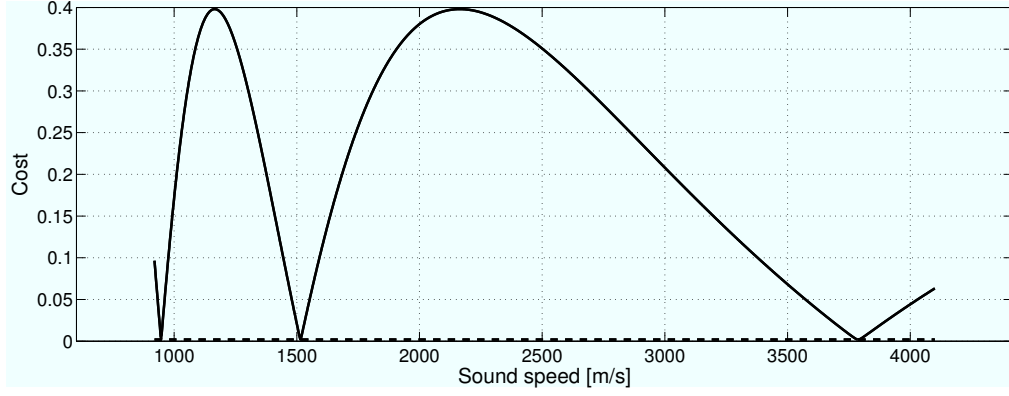


Figure 3.5: Acoustic cost as a function of sound speed. Three from the infinite number of approximate equivalent sound speeds correspond to the three minima lying in the dashed line. The cost corresponding to the true sound speed is 2.0×10^{-2} , while the one corresponding to the equivalent distance is 2.0×10^{-3} , 10 times smaller.

Let us define an acoustic cost function as a numerical distance measure, with the same structure as the one in Eq. (3.4), this time a function of the candidate equivalent sound speed c_e :

$$\mathcal{C}(c_e) = \left| \frac{e^{i2\pi fr/c}}{r} - \frac{e^{i2\pi fr_M/c_e}}{r_M} \right|. \quad (3.10)$$

The approximate equivalent sound speed(s) can be defined as the one(s) that minimize(s) this cost. Let us consider the simulation parameters in the Eq. system (3.5), and the following distance in mismatch:

$$r_M = 5.05 \text{ km}. \quad (3.11)$$

For the above parameter values, the cost function in Eq. (3.10) has an infinite number of global minima (with a cost value of 2.0×10^{-3}), due to the fact that the sound speed influences only the phase of the complex field, as seen in Eq. (3.1). Three of the global minima are shown in Fig. 3.5. In summary, there are an infinite number of equivalent sound speeds, situation which can be defined as multiple equivalent modeling. The infinite set of equivalent sound speeds is the *multiple equivalent model* for the considered scenario and particular distance mismatch.

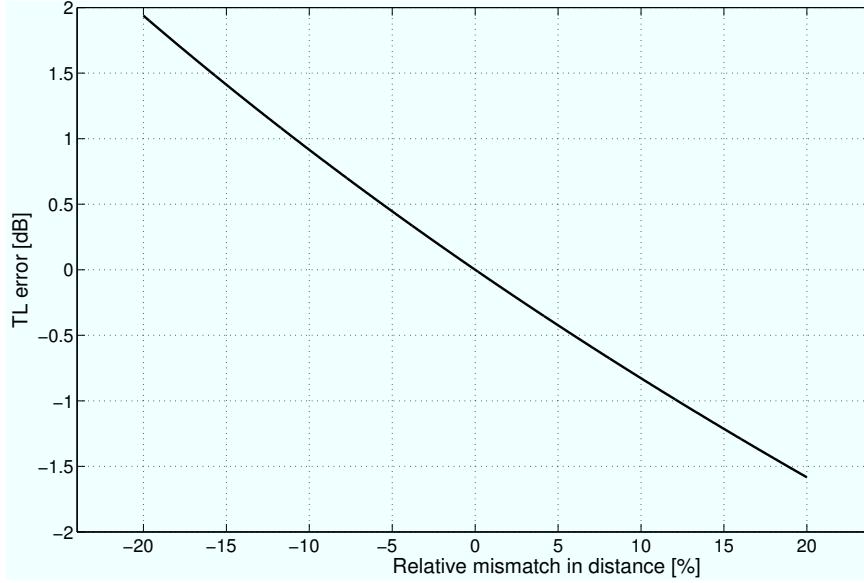


Figure 3.6: Transmission loss error as a function of relative mismatch in distance (in percentage).

Regarding the estimation of transmission loss in the presence of environmental mismatch, some notes are worth mentioning. According to Eq. (3.7), the transmission loss corresponding to a distance with a mismatch ϵ_r , $r_M = r + \epsilon_r$, is given by:

$$\begin{aligned} \text{TL}(r_M) &= 20 \log_{10} r_M \\ &= 20 \log_{10}(r + \epsilon_r). \end{aligned} \quad (3.12)$$

A transmission loss error measure can be defined by:

$$\text{TL}(r) - \text{TL}(r + \epsilon_r) = 20 \log_{10} \frac{1}{1 + \epsilon_r/r}, \quad (3.13)$$

hence completely characterized by the relative mismatch ϵ_r/r . For a relative mismatch expressed in percentage ranging from -20% to 20%, the error is shown in Fig. 3.6. Finally, the transmission loss is not a function of sound speed, which implies that the error induced by a distance mismatch cannot be compensated by any value of equivalent sound speed.

3.1.2 Homogeneous Halfspace

Let us consider an acoustic source in a homogeneous halfspace, as illustrated in Fig. 3.7. In

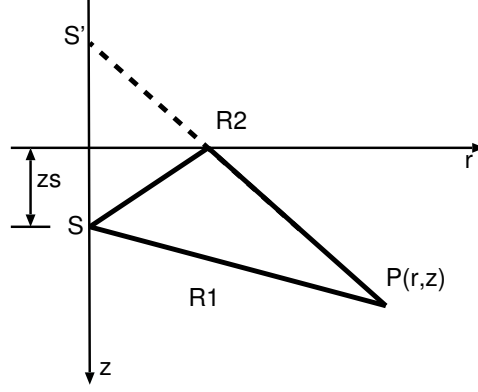


Figure 3.7: Point source at S placed in a fluid with a perfectly reflecting surface on the top.

this scenario, it is known that the acoustic pressure produced by the source is exactly given by [JKPS93]:

$$\begin{aligned}
 p(f, r, z, z_s, c) &= \frac{e^{ikR_1}}{R_1} - \frac{e^{ikR_2}}{R_2}, \\
 &= \frac{e^{i2\pi f \sqrt{r^2 + (z - z_s)^2} / c}}{\sqrt{r^2 + (z - z_s)^2}} - \frac{e^{i2\pi f \sqrt{r^2 + (z + z_s)^2} / c}}{\sqrt{r^2 + (z + z_s)^2}}, \quad (3.14)
 \end{aligned}$$

where the meaning of the variables can be understood from Fig. 3.7. The pressure depends thus on five variables: frequency f , source-receiver range r , receiver depth z , source depth z_s and sound speed c . Let us assume that an incorrect value of source depth z_{sM} is used to model the acoustic field. In the next paragraph, this source depth mismatch will be compensated by optimization for receiver depth; following that exercise, the optimization will be performed for both receiver depth and source-receiver range.

Source Depth Mismatch Compensation by Equivalent Receiver Depth

Let us consider the search for an equivalent receiver depth that compensates for a source depth mismatch. In order to find the equivalent value, it is required to solve the following equation w.r.t. equivalent receiver depth z_E :

$$\frac{e^{i2\pi f \sqrt{r^2 + (z - z_s)^2} / c}}{\sqrt{r^2 + (z - z_s)^2}} - \frac{e^{i2\pi f \sqrt{r^2 + (z + z_s)^2} / c}}{\sqrt{r^2 + (z + z_s)^2}} = \frac{e^{i2\pi f \sqrt{r^2 + (z_E - z_{sM})^2} / c}}{\sqrt{r^2 + (z_E - z_{sM})^2}} - \frac{e^{i2\pi f \sqrt{r^2 + (z_E + z_{sM})^2} / c}}{\sqrt{r^2 + (z_E + z_{sM})^2}}. \quad (3.15)$$

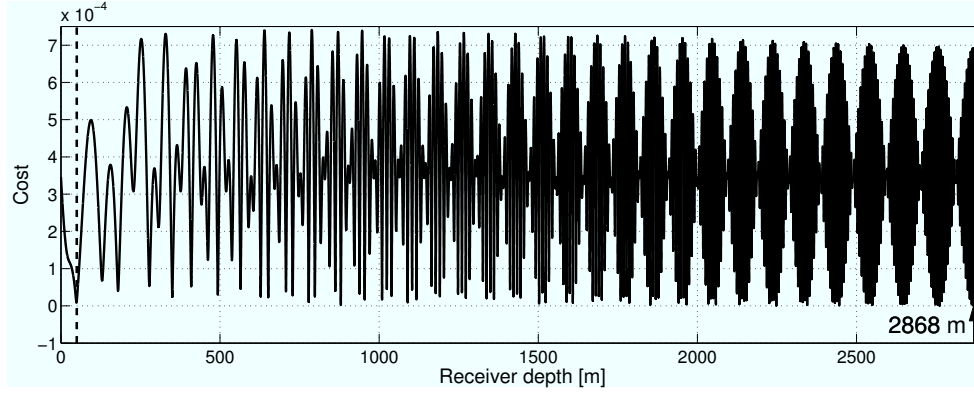


Figure 3.8: Cost function used to determine the equivalent receiver depth to compensate for the source depth mismatch (101 m, instead of the true 100 m). The function has a single global minimum at $z = 2868$ m, hence this value of depth is a global equivalent model. The cost for the true value of 50 m (dashed line) is 1.5×10^{-5} , while for the equivalent value, it is 5.2×10^{-7} , 29 times smaller.

Due to the impossibility of finding a solution to Eq. (3.15), an approximate equivalent receiver depth is searched for, such that it minimizes the cost expressed as:

$$\mathcal{C}(z_e) = \left| \frac{e^{i2\pi f \sqrt{r^2 + (z - z_s)^2}/c}}{\sqrt{r^2 + (z - z_s)^2}} - \frac{e^{i2\pi f \sqrt{r^2 + (z + z_s)^2}/c}}{\sqrt{r^2 + (z + z_s)^2}} - \frac{e^{i2\pi f \sqrt{r^2 + (z_e - z_{sM})^2}/c}}{\sqrt{r^2 + (z_e - z_{sM})^2}} + \frac{e^{i2\pi f \sqrt{r^2 + (z_e + z_{sM})^2}/c}}{\sqrt{r^2 + (z_e + z_{sM})^2}} \right|, \quad (3.16)$$

where z_e designates a candidate equivalent receiver depth. For illustration purposes, a simulation scenario was defined with the values below:

$$\begin{aligned} f &= 500 \text{ Hz}, \\ r &= 5 \text{ km}, \\ z &= 50 \text{ m}, \\ z_s &= 100 \text{ m}, \\ z_{sM} &= 101 \text{ m}, \\ c &= 1500 \text{ m/s}. \end{aligned} \quad (3.17)$$

Figure 3.8 represents the cost function defined in Eq. (3.16), with the parameters defined in the Eq. system (3.17). The global minimum cost is located at 2868 m, a value extremely far from the true value of 50 m.

An important question regarding the equivalent model is its generalization. In a problem of estimation of the acoustic field in an oceanic area, it is desirable to have at hand an

equivalent model parameterization sufficiently generic, such that the same parameter values can be used to model the acoustic field with an acceptable accuracy at any point in the area. Otherwise, it is demanded to deploy a high quantity of receivers, in order that each one gives the equivalent model value corresponding to its position or surrounding area. In the present example, the problem of equivalent model generalization was addressed by analyzing the values of the equivalent model as a function of (true) source-receiver range. The range varied between 4 and 6 km, and the remaining parameters were taken from the Eq. system (3.17). The obtained equivalent receiver depths are shown in Fig. 3.9. This figure shows

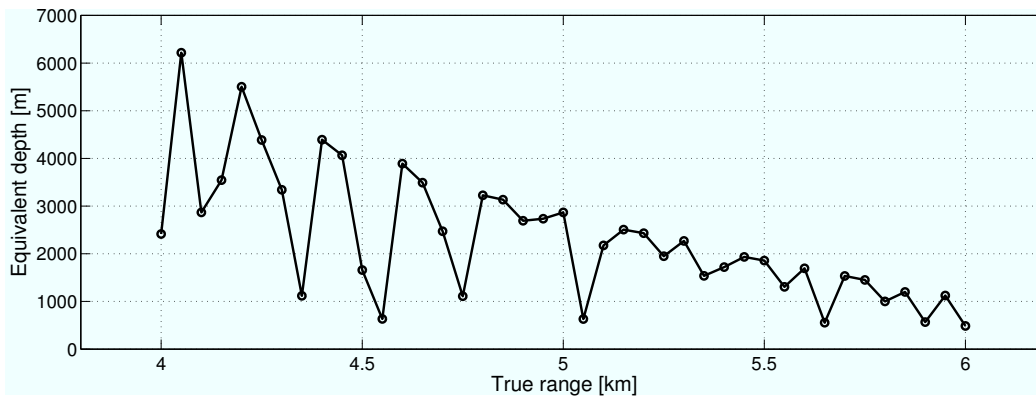


Figure 3.9: Equivalent receiver depths defined as the values that globally minimize the cost in Eq. (3.16), as a function of true source-receiver range.

that, in general, the equivalent receiver depth varies inversely with true source-receiver range. Additionally, the equivalent values present a large spread, covering the interval [490, 6200] m. After fixing again the true range at 5 km, let us analyze the cost function in the interval [48, 51] m, shown in Fig. 3.10. In this interval, the cost attains a minimum at 48.8 m. If the cost is computed exclusively for this interval, then the equivalent receiver depth becomes equal to 48.8 m, since this is the value that minimizes the cost in the analyzed interval. This idea leads to the concept of *local equivalent model*. It minimizes the cost function only locally, as opposed to the global minimizer defined in Eq. (2.4). In the case shown,

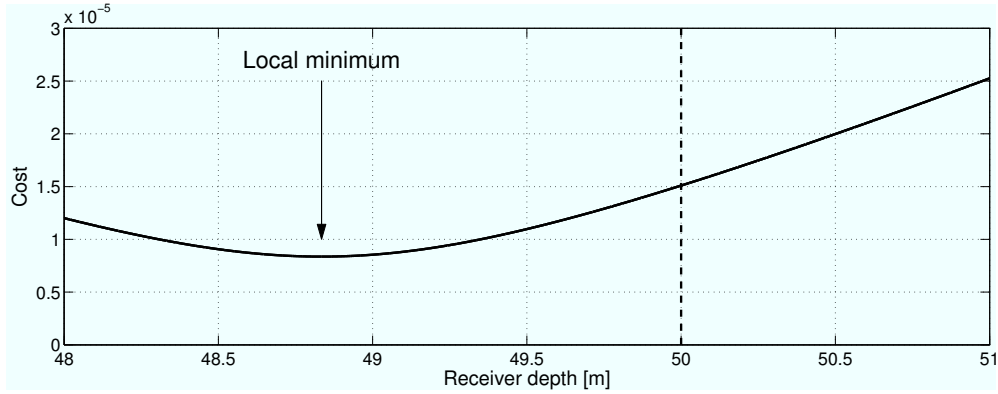


Figure 3.10: Detail of the cost function in Fig. 3.8, in the interval $[48, 51]$ m. In this interval, the function has the single minimum of 8×10^{-6} , at $z_E = 48.8$ m.

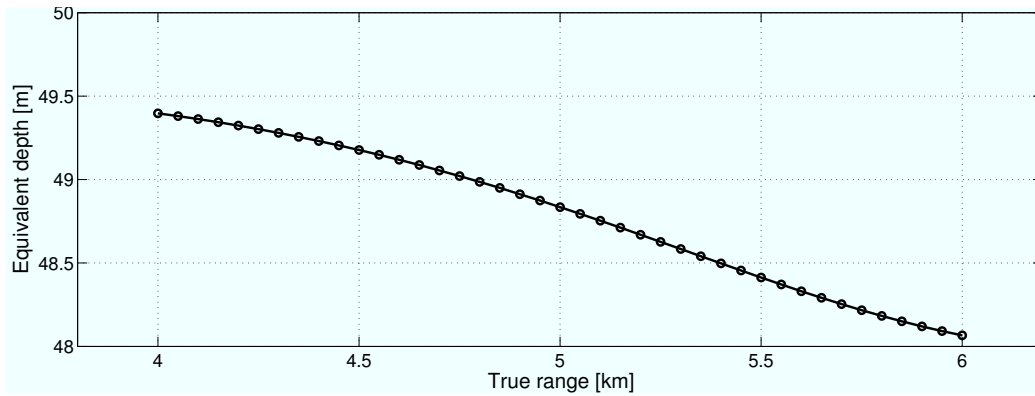


Figure 3.11: Local equivalent receiver depths defined as the values that locally minimize the cost in Eq. (3.16). The optimization search interval is defined as $[z - 10, z + 5]$, where z is the true receiver depth. The equivalent depths are shown as a function of true source-receiver range.

the receiver depth of 48.8 m is a local equivalent receiver depth which compensates for the source depth mismatch. When varying the true range between 4 and 6 km, and considering local search intervals defined as $[z - 10, z + 5]$, the obtained local equivalent receiver depths are those shown in Fig. 3.11. This result is to be compared with the one in Fig. 3.9. Similarly to what happened in the previous case, the local equivalent depths vary inversely with true range. However, all of them are contained in the small interval $[48.1, 49.4]$ m. In this example, the local equivalent model is seen as advantageous over the global equivalent model, in that it can be estimated at some acoustic observation points, and be used to model the field at other points. If the global equivalent model is used instead, it can be overfitted

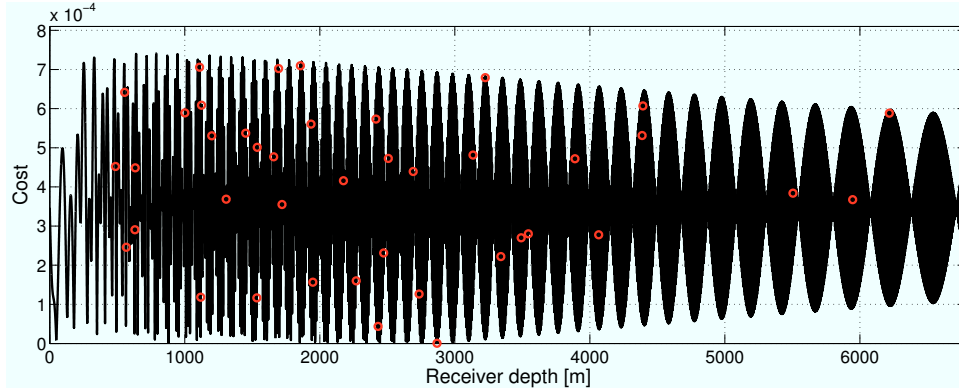


Figure 3.12: Cost in Eq. (3.16) evaluated with the acoustic field generated with the parameters in Eq. (3.17) and the acoustic field corresponding to the global equivalent depths in Fig. 3.9.

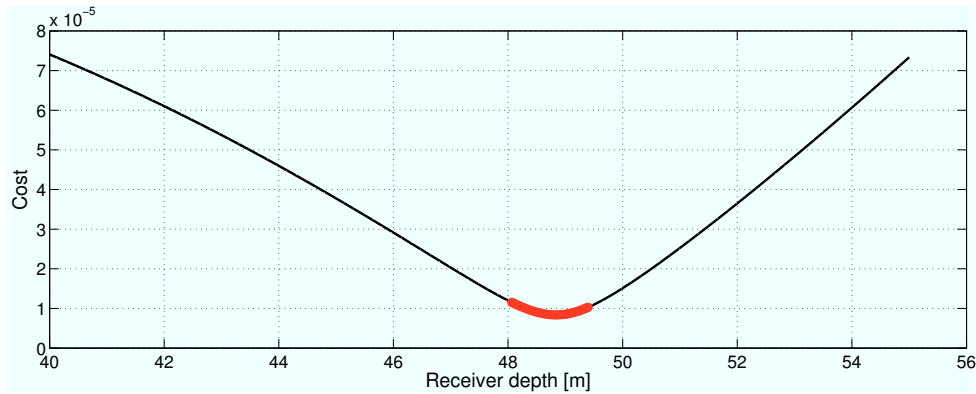


Figure 3.13: Cost in Eq. (3.16) evaluated with the acoustic field generated with the parameters in Eq. (3.17) and the acoustic field corresponding to the local equivalent depths in Fig. 3.11.

to the particular observation point, as seen in the following. An estimation exercise was performed, in which it is intended to model the acoustic field at the point described in the Eq. system (3.17), using every equivalent receiver depth from the ones in Fig. 3.9, one at a time. The quality of the acoustic estimate was measured by computing the cost in Eq. (3.16), with z_E equal to each of the global equivalent receiver depths. The result is shown on the red points in Fig. 3.12. This figure shows that large cost values do occur, evidencing that the equivalent receiver depths are overfitted to their respective spatial points. If the same exercise is done by considering local equivalent receiver depths, using the values shown in Fig. 3.11, then the modeling cost is as shown in Fig. 3.13. Clearly, the cost does not change significantly, since the values of local equivalent receiver depth are similar. Additionally,

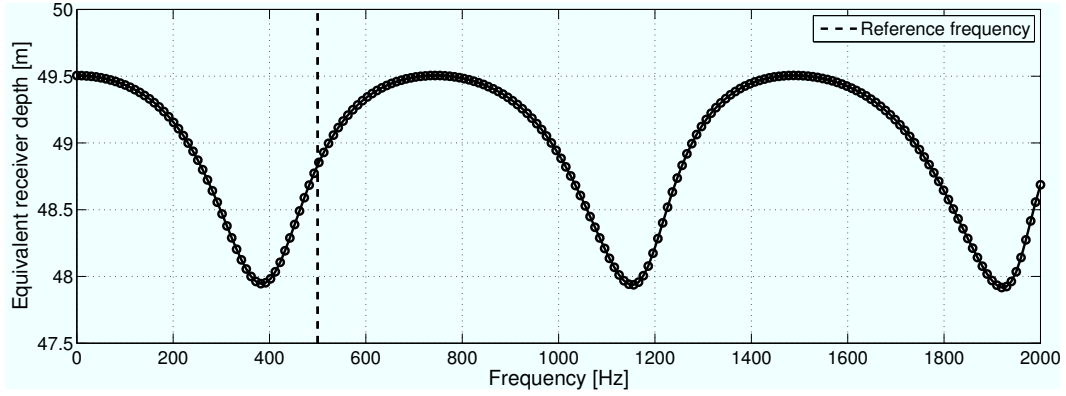


Figure 3.14: Equivalent receiver depth as a function of frequency, for the simulation parameters in Eq. (3.17).

and not less important, the cost values obtained with local equivalent receiver depths are in general significantly lower than the ones obtained with global equivalent receiver depths, as seen by comparing Figs. 3.13 and 3.12. This illustrates that local equivalent models may prevent overfitting, maintaining reduced residual acoustic errors.

An important issue is that the equivalent model is a function of frequency, which is illustrated in the following. For frequencies in $[0, 2000]$ Hz, the local equivalent receiver depth, for the parameter values in the Eq. system (3.17), is shown in Fig. 3.14. As seen in this figure, the equivalent receiver depth exhibits a (non-periodic) oscillating pattern. This is due to the dependence of the pressure phase on frequency, as seen in Eq. (3.14). The frequency dependence of the equivalent receiver depth presents essentially two regimes. In one of them, the frequency bands are modeled with an almost frequency-independent equivalent receiver depth (e.g. the 1400–1600-Hz band). In the other one, the dependence on frequency is stronger, demanding for acoustic observations to be made at finer-discretization frequency intervals, in order to better capture the frequency-dependence of the equivalent model (e.g. the 1800–1900-Hz band).

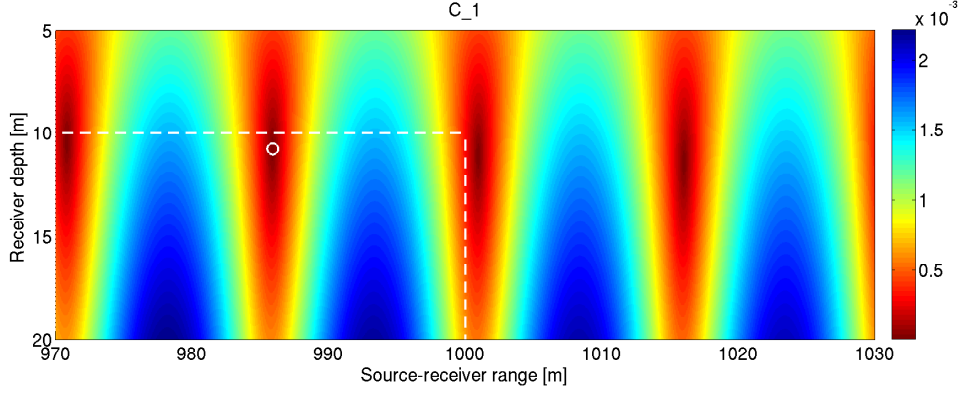


Figure 3.15: Cost function used to determine the equivalent (source-receiver range, receiver depth) pair to compensate for source depth mismatch (90 m, as compared to the true 100 m), in the fluid halfspace scenario. In the (source-receiver range, receiver depth) search space, the minimum is 7.0×10^{-6} , giving the equivalent values (986, 11) m for the equivalent source-receiver range and depth, respectively.

Source Depth Mismatch Compensation by Equivalent Receiver Depth and

Source-receiver Range

Let us consider the search for both equivalent receiver depth and source-receiver range that compensate for a mismatch in source depth. In this case, it is required to solve an equation with the same structure as Eq. (3.15) w.r.t. the pair (z_E, r_E) :

$$\frac{e^{i2\pi f \sqrt{r^2 + (z - z_s)^2} / c}}{\sqrt{r^2 + (z - z_s)^2}} - \frac{e^{i2\pi f \sqrt{r^2 + (z + z_s)^2} / c}}{\sqrt{r^2 + (z + z_s)^2}} = \frac{e^{i2\pi f \sqrt{r_E^2 + (z_E - z_{sM})^2} / c}}{\sqrt{r_E^2 + (z_E - z_{sM})^2}} - \frac{e^{i2\pi f \sqrt{r_E^2 + (z_E + z_{sM})^2} / c}}{\sqrt{r_E^2 + (z_E + z_{sM})^2}}. \quad (3.18)$$

The presence of two degrees of freedom is not enough to provide a solution to the equation. Proceeding as above, an approximate equivalent depth-range pair is then searched for, such that it minimizes the cost function in Eq. (3.16). Fig. 3.15 shows the cost, in the intervals [5, 20] m and [970, 1030] m for receiver depth and source-receiver range, respectively. The minimum cost in Fig. 3.15 is 116 times smaller than the one attained via the compensation given only by the receiver depth (see Fig. 3.8). This shows that, by giving freedom to more parameters, thus increasing the number of degrees of freedom intrinsic to the equivalent

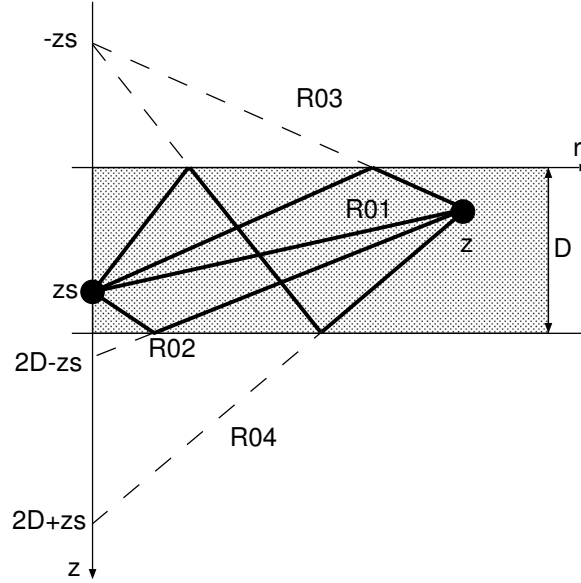


Figure 3.16: Point source in an ideal waveguide. The distances $R0n, n = 1, 2, \dots, 4$ are relative to the depth (z) axis.

model vector, it is possible to obtain more accurate acoustic estimates.

3.1.3 Ideal Waveguide

Let us consider an acoustic source in an ideal waveguide, as illustrated in Fig. 3.16. In this type of scenario, it is known that the acoustic field produced by the source is exactly given by:

$$\Psi_0(r, z) = -\frac{S_\omega}{4\pi} \sum_{m=0}^{\infty} \left[\frac{e^{ikR_{m1}}}{R_{m1}} - \frac{e^{ikR_{m2}}}{R_{m2}} - \frac{e^{ikR_{m3}}}{R_{m3}} + \frac{e^{ikR_{m4}}}{R_{m4}} \right], \quad (3.19)$$

with

$$\begin{aligned} R_{mn} &= \sqrt{r^2 + z_{mn}^2}, \\ z_{m1} &= 2Dm - z_s + z, \\ z_{m2} &= 2D(m+1) - z_s - z, \\ z_{m3} &= 2Dm + z_s + z, \\ z_{m4} &= 2D(m+1) + z_s - z, \end{aligned} \quad (3.20)$$

where the meaning of the fundamental variables can be understood from Fig. 3.16, and D is the vertical depth of the duct (waveguide thickness)[JKPS93]. In the present context, let us consider, as an approximation to $\Psi_0(r, z)$, a reference field built only with the first three

image source solutions, which is to be estimated:

$$\Psi(r, z) = -\frac{S_\omega}{4\pi} \left[\frac{e^{ikR_{01}}}{R_{01}} - \frac{e^{ikR_{02}}}{R_{02}} - \frac{e^{ikR_{03}}}{R_{03}} + \frac{e^{ikR_{04}}}{R_{04}} \right], \quad (3.21)$$

where $k = 2\pi f/c$ is the wavenumber. It is seen that the field depends on five variables: frequency f , receiver range r , receiver depth z , source depth z_s and duct depth D . In the following, an equivalent modeling exercise is presented, in which the requirement is to find the equivalent source-receiver range that compensates for a duct depth mismatch. In this case, the following equation is to be solved w.r.t. equivalent source-receiver range r_E :

$$\Psi(f, r, z, z_s, D) = \Psi_E(f, r_E, z, z_s, D_M), \quad (3.22)$$

where Ψ_E is the acoustic estimate and D_M is the duct depth in mismatch. On the impossibility of solving Eq. (3.22), a numerical solution was searched for as the argument that minimizes the following cost:

$$\mathcal{C}(r_e) = |\Psi(f, r, z, z_s, D) - \Psi_e(f, r_e, z, z_s, D_M)|, \quad (3.23)$$

where r_e and Ψ_e designate a candidate equivalent source-receiver range and the corresponding candidate acoustic field, respectively. Illustrative results consider the following simulation parameters:

$$\begin{aligned} f &= 100 \text{ Hz}, \\ r &= 1 \text{ km}, \\ z &= 100 \text{ m}, \\ z_s &= 100 \text{ m}, \\ c &= 1500 \text{ m/s}, \\ D &= 200 \text{ m}, \\ D_M &= 202 \text{ m}. \end{aligned} \quad (3.24)$$

For the above parameters, the cost function in Eq. (3.23) is represented in Fig. 3.17, giving the value 957 m for the equivalent source-receiver range. The value of the equivalent source-receiver range as a function of duct depth in mismatch was computed, and is shown

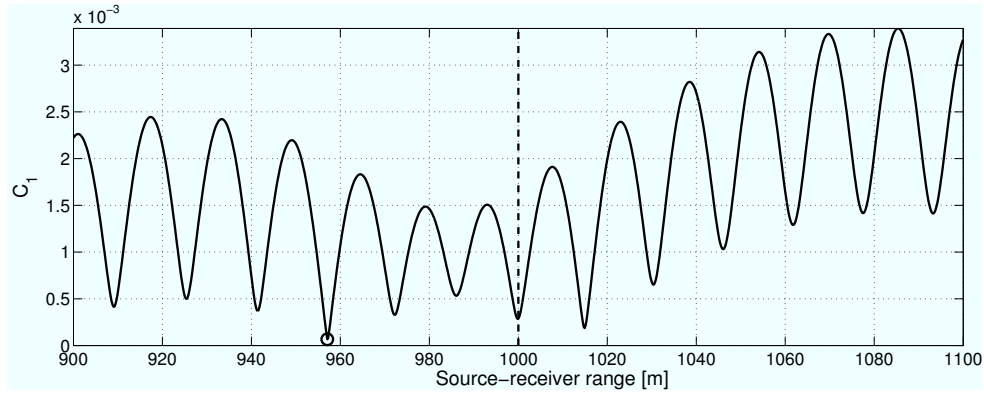


Figure 3.17: Cost function to determine the equivalent source-receiver range to compensate for duct depth mismatch (202 m, against the true 200 m), in the ideal waveguide scenario. The minimum cost is 6.0×10^{-10} .

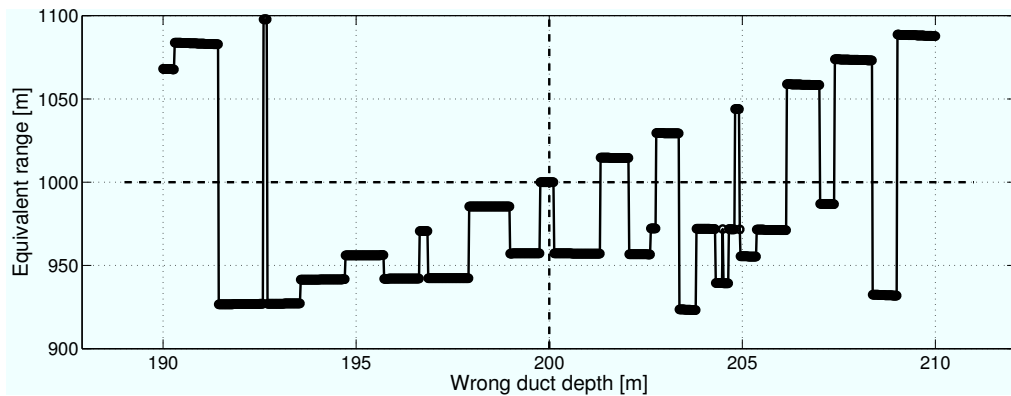


Figure 3.18: Equivalent source-receiver range as a function of duct depth in mismatch, to (approximately) model acoustic propagation in the ideal waveguide of Fig. 3.16.

in Fig. 3.18. This figure supports the classical result that an overestimated duct depth induces an overestimated source-receiver range [Tol92]. The difference between the true and the equivalent source-receiver range as a function of true source-receiver range and receiver depth is shown in Fig. 3.19. It is seen that the equivalent source-receiver range is a rather irregular function of the spatial point in which to estimate the acoustic field. This implies that a dense waveguide acoustic sampling might be necessary, if the acoustic modeler includes the source-receiver range in the equivalent model vector, in an acoustic estimation exercise.

A second acoustic estimation exercise was performed, in which (only) the source depth is adjusted to compensate for the duct depth mismatch. The result in terms of offset from true

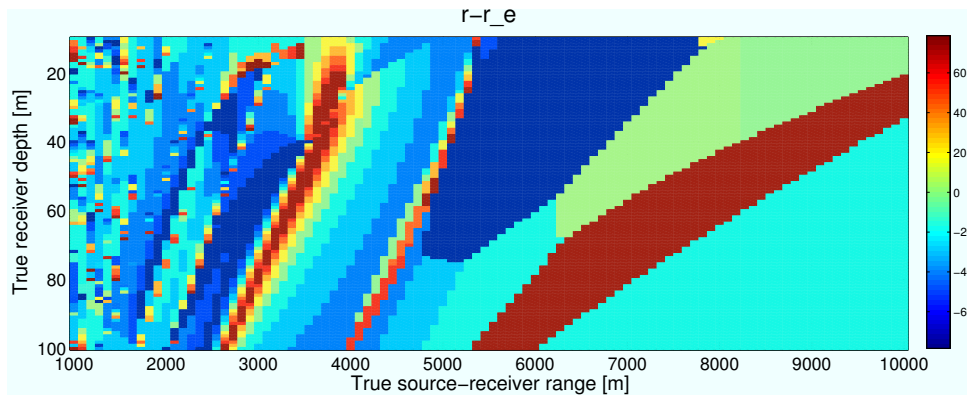


Figure 3.19: Difference between the true and the equivalent source-receiver range, as a function of true source-receiver range and receiver depth. The true duct depth and the one in mismatch are 200 and 202 m, respectively.

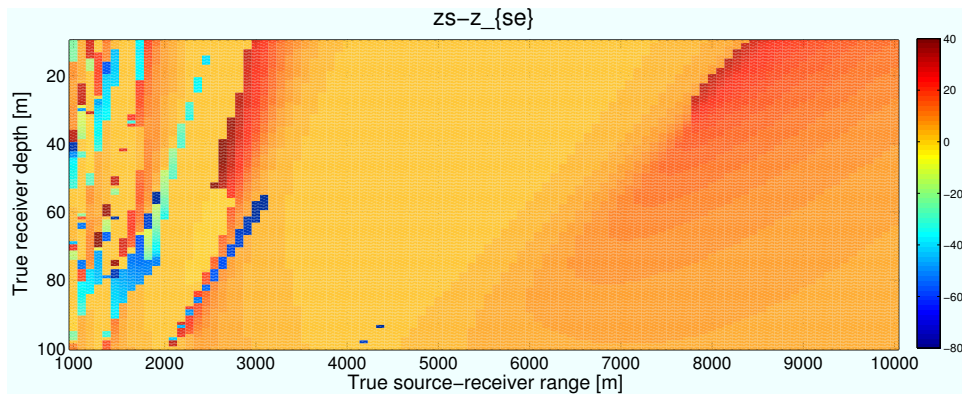


Figure 3.20: Difference between the true and the equivalent source depth, as a function of true source-receiver range and receiver depth. The true duct depth and the one in mismatch are 200 and 202 m, respectively.

value as a function of duct point, is shown in Fig. 3.20. This result shows the classical effect of the overestimated duct depth inducing the acoustic source to appear shallower [Tol92].

By comparing Figs. 3.20 and 3.19, it is seen that the generalization properties of the equivalent model depend strongly on the nature of the equivalent parameters. While the equivalent source-receiver range varies significantly with space (see Fig. 3.19), the same is not verified for the equivalent source depth (see Fig. 3.20). This applies for this particular case of duct depth mismatch and frequency.

3.1.4 Equivalent Models on Wave Reflection

Following is a description of interesting cases concerning the use of equivalent models on acoustic wave reflection. Here, the aim is to illustrate the interplay between the parameters that typically characterize the water column and the ocean bottom at the interface between these two media, in order to estimate the acoustic field using equivalent models. This analysis is derived from ray theory, which models acoustic propagation as a phenomenon in which the energy emanates from the acoustic source in all directions, following particular paths. These paths are structured mainly according to the refraction index, which is a function of sound speed, and the attenuation and density of the materials in which sound propagates. According to Refs. [JKPS93, ER12], in an ideal scenario in which a fluid halfspace overlays a viscoelastic halfspace (as in Fig. 3.21), it is possible to conclude that the acoustic pressure is a function of the same quantities as the reflection coefficient. The reflection coefficient for a fluid-viscoelastic interface is defined e.g. in Ref. [Pap94], and is a function of density, sound speed and attenuation in both media. The following sections elaborate on particular cases of reflection, illustrating the goal of computing the same reflection coefficient with an equivalent environmental parameterization. Two cases are considered, namely fluid-fluid and fluid-viscoelastic interfaces.

Reflection at a Fluid-fluid Interface

Let us concentrate on the case in which the two media are homogeneous fluids, with densities ρ_i and sound speeds c_i , $i = 1, 2$, i.e. a simplified version of the scenario in Fig. 3.21, where the bottom halfspace is described by zero shear speed and attenuation. In this type of scenario,

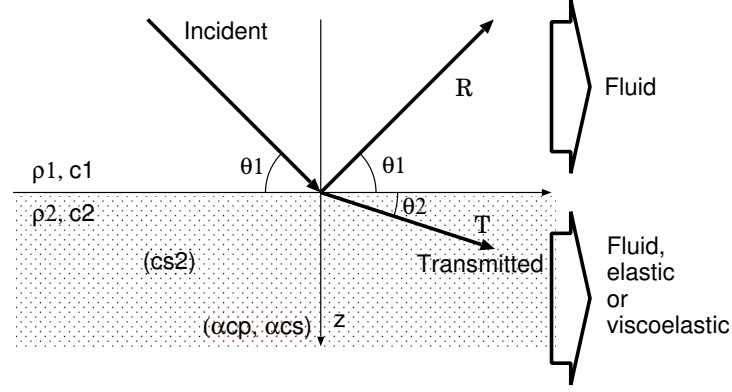


Figure 3.21: Reflection and transmission at a fluid-viscoelastic interface (adapted from Ref. [JKPS93]).

according to Ref. [Pap94], the reflection coefficient is exactly given by:

$$\mathcal{R} = \frac{\rho_2 c_2 / \sin \theta_2 - \rho_1 c_1 / \sin \theta_1}{\rho_2 c_2 / \sin \theta_2 + \rho_1 c_1 / \sin \theta_1}, \quad (3.25)$$

where

$$\theta_2 = \arccos \left(\frac{c_2}{c_1} \cos \theta_1 \right). \quad (3.26)$$

It is seen that the reflection coefficient depends on five variables: bottom density ρ_2 , bottom sound speed c_2 , water density ρ_1 , water sound speed c_1 and grazing angle θ_1 . In searching for equivalent environmental parameters in the present scenario, it was considered that any environmental parameter can be in mismatch. Taking into account that the starting point is to equate the reflection coefficients corresponding to the true environment and the one in mismatch, the equivalence is determined by solving the following equation:

$$\mathcal{R}(\rho_1, \rho_2, c_1, c_2, \theta_1) = \mathcal{R}'(\rho'_1, \rho'_2, c'_1, c'_2, \theta'_1), \quad (3.27)$$

where \mathcal{R}' designates the estimated reflection coefficient, and all the other quantities notated with a prime ' can be or not be in mismatch. Let us consider that only one among the five independent environmental parameters is optimized for equivalent modeling. In this case, the solution to the equivalence problem is the solution to Eq. (3.27) with respect to the

particular parameter to optimize for. The solution for each parameter (the subscript “E” designates an equivalent quantity), except the angle, is given as:

$$\rho_{1E} = \rho_1 \times \frac{c_1 c'_2 \rho'_2 \sin \theta'_1 \sqrt{1 - (c_2 \cos \theta_1 / c_1)^2}}{c'_1 c_2 \rho_2 \sin \theta_1 \sqrt{1 - (c'_2 \cos \theta'_1 / c'_1)^2}}, \quad (3.28)$$

$$\rho_{2E} = \rho_2 \times \frac{c_2 c'_1 \rho'_1 \sin \theta_1 \sqrt{1 - (c'_2 \cos \theta'_1 / c'_1)^2}}{c'_2 c_1 \rho_1 \sin \theta'_1 \sqrt{1 - (c_2 \cos \theta_1 / c_1)^2}}, \quad (3.29)$$

$$c_{1E} = c'_2 \frac{\sqrt{A - B + C}}{c_2 \rho_2 \rho'_1 \sin \theta_1}, \quad (3.30)$$

$$c_{2E} = c'_1 \frac{c_2 \rho_2 \rho'_1 \sin \theta_1}{\sqrt{A - B + C}}, \quad (3.31)$$

where

$$A = (c_1 \rho_1 \rho'_2 \sin \theta'_1)^2, \quad (3.32)$$

$$B = (c_2 \rho_1 \rho'_2 \cos \theta_1 \sin \theta'_1)^2, \quad (3.33)$$

$$C = (c_2 \rho_2 \rho'_1 \cos \theta'_1 \sin \theta_1)^2. \quad (3.34)$$

In particular, notice that the equivalent densities ρ_{1E} and ρ_{2E} are scaled versions of the true densities ρ_1 and ρ_2 , respectively. Among the various possibilities of mismatch and compensation, some interesting cases are reported in the following.

Density-density Compensation In the case that every parameter is correct except the density in one medium, then it is possible to obtain the true reflection coefficient with the density value in mismatch and an equivalent value for the density in the other medium (particular form of Eq. (3.28) or (3.29)). For example, if the density ρ_2 is in mismatch, with the value ρ_{2M} , then the equivalent density

$$\rho_{1E} = \rho_1 \times \rho_{2M} / \rho_2 \quad (3.35)$$

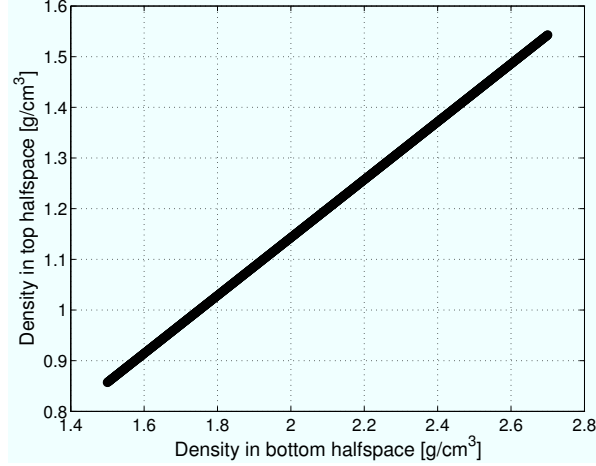


Figure 3.22: Family of top-bottom halfspace density pairs which lead to the same reflection coefficient, in the fluid-fluid reflection case.

assures that the estimated reflection coefficient \mathcal{R}' has zero error. The simplicity of this compensation can be understood by the fact that the reflection coefficient in Eq. (3.25) can be written as a function of the density ratio $\rho_r = \rho_2/\rho_1$ (among the other parameters):

$$\mathcal{R} = \frac{\rho_r c_2 / \sin \theta_2 - c_1 / \sin \theta_1}{\rho_r c_2 / \sin \theta_2 + c_1 / \sin \theta_1}. \quad (3.36)$$

An illustration is done in Fig. 3.22, for the following parameters:

$$\begin{aligned} \rho_1 &= 1 \text{ g/cm}^3, \\ \rho_2 &= 1.75 \text{ g/cm}^3. \end{aligned} \quad (3.37)$$

The equivalent density does not depend on grazing angle. Thus, if the top halfspace is replaced by a homogeneous fluid waveguide, then the relationship in Eq. (3.35) will be applicable to any reflection angle, independently of the interaction of the acoustic energy with the top boundary, and of ray refraction, consequently allowing to obtain a zero-error acoustic pressure with the equivalent density (see, for example, Refs. [JKPS93, ER12], for the relation between reflection coefficient and acoustic pressure). This equivalence relation holds independently of acoustic source and receiver geometry, which cannot be in mismatch.

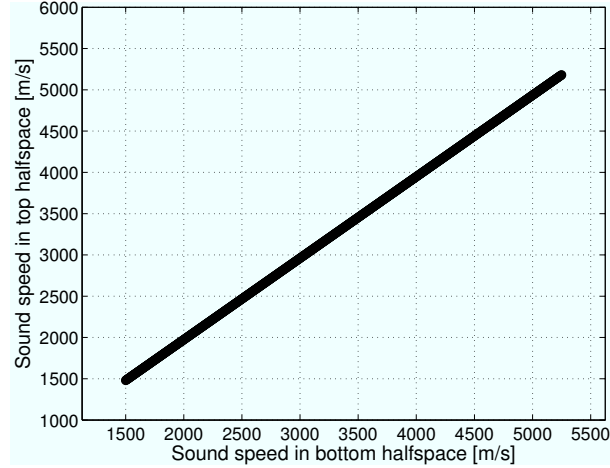


Figure 3.23: Family of top-bottom halfspace sound speed pairs which lead to the same reflection coefficient, in the fluid-fluid reflection case.

Sound Speed-Sound Speed Compensation As compared to density, a similar relation exists for sound speed. In other words, it is possible to obtain the true reflection coefficient by using a value of sound speed in mismatch for one medium and a compensating value of equivalent sound speed for the other medium. These values must satisfy the relation:

$$c'_1/c_1 = c'_2/c_2, \quad (3.38)$$

where the prime ' denotes either a situation in which c_1 is in mismatch, compensated by an equivalent c'_2 , or a situation in which c_2 is in mismatch, compensated by an equivalent c'_1 .

This relation is understood by the fact that the reflection coefficient can be written in terms of sound speed ratio $c_r = c_2/c_1$ (among others), as follows:

$$\mathcal{R} = \frac{\rho_2 c_r / \sqrt{1 - c_r^2 \cos^2 \theta_1} - \rho_1 / \sin \theta_1}{\rho_2 c_r / \sqrt{1 - c_r^2 \cos^2 \theta_1} + \rho_1 / \sin \theta_1}. \quad (3.39)$$

An illustration is done in Fig. 3.23, for the following parameters:

$$\begin{aligned} c_1 &= 1500 \text{ m/s}, \\ c_2 &= 1520 \text{ m/s}. \end{aligned} \quad (3.40)$$

It is seen that an exaggerated error in the bottom fluid sound speed can be completely

compensated by an exaggerated error in the top fluid sound speed. As in the previous case, any layer or both layers can be replaced by finite layers, hence it is possible to obtain a modeled acoustic pressure with zero error.

Reflection at a Fluid-elastic or Fluid-viscoelastic Interface

For this type of scenario, an expression for the reflection coefficient can be found in Ref. [Pap94]. Similarly to what is verified for the fluid-fluid interface, the reflection coefficient is invariant to density ratio. However, an invariance to sound speed ratio does not exist, possibly because upon reflection of a fluid-incoming compressional wave, the refracted wave is split into a compressional and a shear wave propagating in the bottom halfspace. In a fluid-elastic or fluid-viscoelastic interface, several cases of equivalence can be defined, though the equivalent model is a function of grazing angle, except in the case of a mismatch exclusively in density. Thus, when aiming to model the full pressure field with an equivalent model, a different equivalent model has to be used for each grazing angle. This implies that the equivalent model can be fully characterized only after a ray-by-ray computation is issued. This demands the knowledge of the grazing angle of every reflection instance of every acoustic ray that connects the source to the receiver (eigenray), which is impractical, when not impossible.

3.2 Summary

The present chapter illustrates by examples the main properties and categories of equivalent models, using simple and idealized acoustic propagation media. Four notes are worth mentioning, as follows. First, environmental mismatch does not always preclude obtaining an accurate acoustic estimate. For example, there are cases in which the transmission loss

is insensitive to some parameters, hence the latter are allowed to be unknown. This lack of knowledge is not tolerated, if the quantity to be modeled is the acoustic pressure in magnitude and phase, for the same scenario. Nevertheless, should the parameters relevant to define the transmission loss have incorrect values, the latter cannot be compensated by any value of the parameters to which the loss is insensitive. The same does not happen for complex acoustic pressure. The above statements apply also to the space-frequency domain, in which the particular point will determine the consequence of environmental mismatch, and the possibility of compensation for this mismatch. Second, the complexity of the equivalent model determines the accuracy of the acoustic estimate. The final acoustic error decreases with an increasing number of equivalent environmental parameters. Third, the value of the equivalent model depends on space and frequency, and also on the cost function employed to compute the model. This fact comes from the definition of equivalent model. Finally, in terms of typology, and taking into account the characteristics of the cost function that defines the equivalent model, the latter can be classified as:

- *global* —if it globally minimizes the cost function— or *local* —if it corresponds to a local minimum;
- *exact* —if it makes the cost function to vanish— or *approximate* —otherwise;
- *single* —if it is the unique minimizer in the search interval— or *multiple* —otherwise.

Chapter 4

Equivalent models in realistic media

“A couple of months in the laboratory can save a couple of hours in the library.”

Frank H. Westheimer

THE problem to be solved in the present work is to estimate the acoustic field in an ocean transect. The acoustic field to be estimated (“true field”) was synthesized from the real oceanographic data collected during the Maritime Rapid Environmental Assessment 2003 (MREA’03) sea trial, for a period of approximately one month. The estimation of the acoustic field at future times (acoustic forecast) makes use of the oceanographic forecasts computed with the Navy Coastal Ocean Model (NCOM). This chapter starts with a description of the real environmental data (Sec. 4.1), detailing the oceanographic measurements and predictions relevant for the present work. Taking into account the importance of using equivalent models, Sec. 4.2 describes important inter-parameter compensation possibilities, relevant for defining the structure of the equivalent model whose application to a realistic estimation exercise is shown in the next chapter.

4.1 Real and forecast environmental data

This section summarily describes the MREA'03 sea trial, and presents relevant oceanographic aspects of the experimental area. The MREA'03 acoustic-oceanographic sea trial took place in the vicinity of Elba Island, in the Ligurian Sea (Italy), during the period May 26–June 27, 2003. Extensive ground truth measurements were performed, including those made with conductivity, temperature and depth (CTD) profilers, expendable bathythermograph (XBT) profilers, vessel-mounted acoustic Doppler current profilers (ADCPs), one shallow water environmental profiler in trawl-safe real-time configuration (SEPTR) buoy[TdSGG00], two bottom-mounted ADCPs, two thermistor chains, one meteo buoy and one wave buoy. Most of this equipment was operated aboard or deployed from the R/Vs ALLIANCE and LEONARDO. On June 21 and 23, acoustic transmissions and inversions were performed (not considered in the present work), making use of a free-drifting Acoustic Oceanographic Buoy (AOB)[SZM06], to complement rapid environmental assessment (REA) measurements and to test acoustic communications, using signals emitted by a ship-towed sound source[JSSC04]. The area of the MREA'03 sea trial is shown in Fig. 4.1, along with the oceanographic modeling domains and the acoustic transmission domain. The Ligurian Sea is an arm of the Mediterranean Sea which, in generic oceanographic terms, is a high-salinity marginal basin with limited tides. Below the sediment layer, there is a bottom substrate which can be modeled, with a reasonable approximation, as an acoustic halfspace. At finer levels of detail, Holland and Osler[HO00] have noted the existence of some randomly placed thin, high-speed layers within sediment core samples.

Regarding the oceanographic data collected during the MREA'03 experiment, several

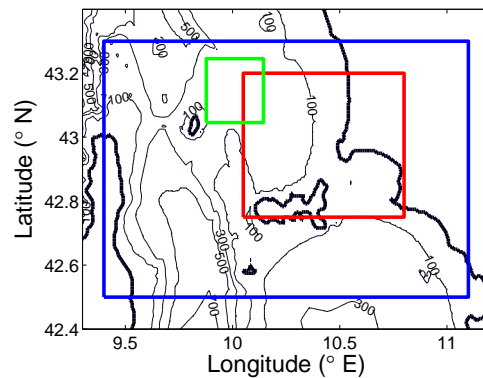


Figure 4.1: Maritime Rapid Environmental Assessment 2003 area: Elba channel (blue) and Northern Elba (red) working boxes for the ocean prediction system MODAS-NCOM, and acoustic transmission box (green).

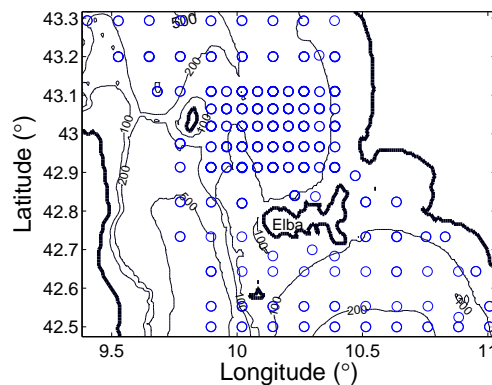


Figure 4.2: View of a (42.5–43.3 °N, 9.40–11.0 °E) area, showing the locations of the CTD casts (circles) performed during the MREA'03 sea trial.

CTD casts were performed between May 28 and June 25, as represented in Fig. 4.2. The time series of the sound speed profiles (SSPs) computed from the CTD measurements, as well as the average sound speed profile (SSP), are shown in Fig. 4.3, for the top 200 m. The oceanographic forecasts taken into consideration in this work were computed at the Naval Research Laboratory (NRL). These ocean modeling results are obtained with: 1) a regional relocatable run of the NCOM model, for the Elba channel region (blue box in Fig. 4.1), and 2) a nested high-resolution relocatable version of the Princeton Ocean Model, implemented at the Naval Research Laboratory (NRLPOM), for the Northern Elba domain (red box in Fig. 4.1)[Mar00, PFB01, FCPR⁺09]. Prior to running these models, a larger-domain

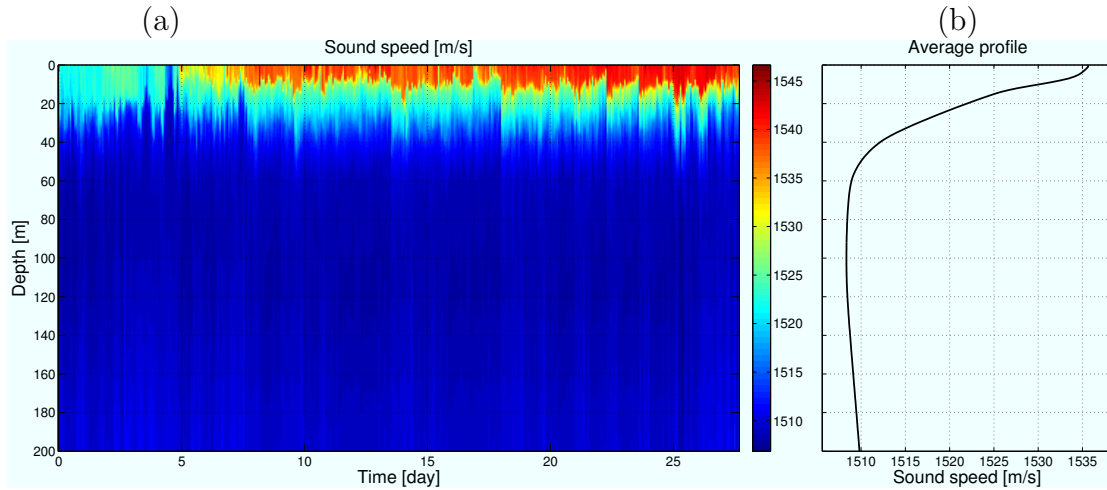


Figure 4.3: (a) Sound speed profiles along time, and (b) average sound speed profile over all the casts from the MREA'03 sea trial.

(including the Tyrrhenian Sea) model was run. This model was initialized by the global NCOM. All the models were forced by the Coupled Ocean/Atmosphere Mesoscale Prediction System (COAMPS) winds (no heat fluxes were included)[Hod97, HHD⁺13]. Outputs at three-hour intervals were used for specification of the open boundary conditions for the regional relocatable NCOM for the Elba channel domain, at approximately 1.5-km resolution and 35 vertical sigma-levels. The larger-domain model was initialized with the previous day's nowcast, and nudged to the current day's Modular Ocean Data Assimilation System (MODAS) field during the hindcast[PFB01, FBC⁺02, FTB⁺02, PFB02]. No assimilation was done during the forecast. An NCOM run for the Elba channel domain was performed, providing initial conditions for the high-resolution (0.5 km and 25 sigma-levels) NRLPOM for the Northern Elba domain, which included tide flow. Both regional relocatable NCOM and high-resolution NRLPOM models produced forecasts every three hours[PFB01].

4.2 Equivalent modeling

In any oceanic region of choice, the acoustic field is defined by a large set of environmental properties. Furthermore, these properties vary with space and time. Due to the limitations in observing these quantities with a fine space-time discretization, it is essential to know the degree of dependence of the acoustic field on each of them. In operational setups, this allows to schedule the sampling task to observe at minimum the parameters for which a small error can induce a large acoustic error, or parameters for which, even after compensation performed by other parameters, the residual mismatch can lead to unacceptable acoustic errors. After summarizing the concept of empirical orthogonal function representation, the next sections will elaborate on the importance of the different parameters for the acoustic field, and illustrate the parameter-to-parameter fundamental compensation characteristics for the main realistic scenario considered in the present work.

Several oceanic properties vary in space, in range and/or in depth, with various scales, from the meter to the hundred-kilometer scale. One example of such a property is the water column depth-dependent SSP which, for acoustic propagation modeling purposes, has to be described with a fine discretization. One way of simplifying the sound speed parameterization, borrowed from oceanography, is the use of empirical orthogonal functions. Empirical orthogonal functions —termed in [Lor56], and also called principal vectors or loadings— are very common in acoustic inversion research, to regularize the estimation of sound speed at a large number of depths, and to minimize the computation time. According to the empirical orthogonal function (EOF) representation, every (random-modeled) SSP $c(z, t)$, where z and t represent depth and time, respectively, is modeled as a sum of a

mean profile $\bar{c}(z)$ with weighted versions of basis functions $\varphi_k(z)$ —the empirical orthogonal functions (EOFs):

$$c(z, t) \approx \bar{c}(z) + \sum_{k=1}^K \alpha_k(t) \varphi_k(z). \quad (4.1)$$

One interpretation of Eq. (4.1) is that the space-time dependence of the sound speed is split into the random time-dependent coefficients $\alpha_k(t)$ (sometimes labeled principal components or scores) and the deterministic space-dependent functions $\varphi_k(z)$. Considering the depth z as a discrete variable with M possible values, the SSP $c(z, t)$ can be represented by a vector with M components containing the sound speed at every depth. The EOFs are the $K \leq M$ eigenvectors of the covariance matrix of a random vector variable assumed to generate every SSP. The EOF estimates are defined as the eigenvectors of an estimate of the covariance matrix.

4.2.1 Environmental parameter hierarchy

When aiming to use equivalent environmental models to model the acoustic field in a particular oceanic area, one of the first steps is to understand the relative importance of each environmental parameter. This gives an insight of which parameters may need to be ‘fine tuned’ for acoustic modeling: the more sensitive the acoustic field is to a given parameter, the more important is to accurately know or to tune this parameter. In the present work, the relative significance of every environmental parameter is assessed by cost analysis, as follows.

First, a canonical scenario was defined, as shown in Fig. 4.4, consisting of an ocean medium with geoacoustic properties taken from Ref. [Gin94] (describing a past experiment in North Elba Island), and a fixed water column SSP coincident with the average SSP shown in Fig. 4.3 (b). This scenario is associated with a canonical acoustic field $u_c(r, z, f, \boldsymbol{\theta}_T)$, where $\boldsymbol{\theta}_T$

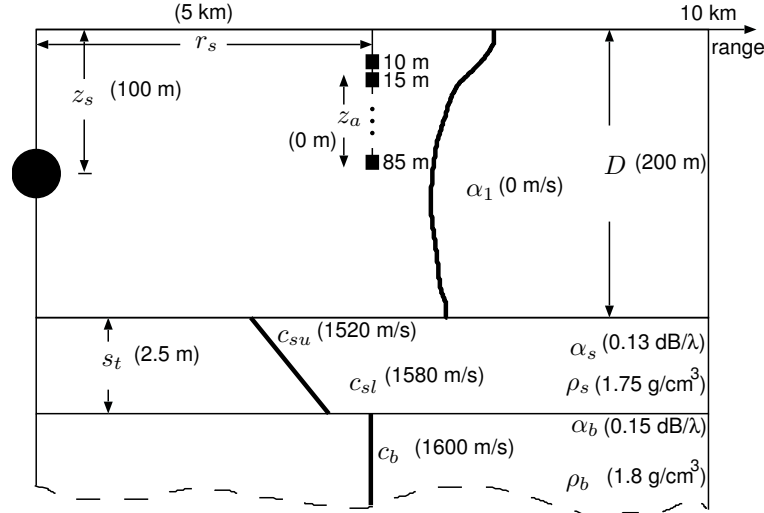


Figure 4.4: Parameters that describe the realistic underwater scenario for which the concept of equivalent model is characterized in the present chapter. The meaning of the parameters is explained in Tab. 4.1.

is the true environment, for $r = 0.5$ to 10 km, with 0.5-km step, $z = 10$ to 85 m, with 5-m step, and $f = 100$ to 1000 Hz, with 100-Hz step. Afterwards, a variable scenario was defined, in which one parameter at a time is varied between chosen bounds. For this scenario, the acoustic field corresponding to each value of the varying parameter was computed and compared to the canonical field through an acoustic cost. The latter was defined as the overall relative error, taken as an average over range, depth and frequency:

$$\mathcal{C}_0(\theta_k) = \frac{1}{N_r N_z N_f} \sum_r \sum_z \sum_f \frac{|u_s(r, z, f, \theta_0) - u_s(r, z, f, \theta_k)|}{|u_s(r, z, f, \theta_0)| + |u_s(r, z, f, \theta_k)|}. \quad (4.2)$$

The maximum of $\mathcal{C}_0(\theta_k)$ gives the sensitivity of the acoustic field to parameter θ_k : higher values for the maximum value indicate that the acoustic field deviates significantly from the canonical value, hence is more sensitive to θ_k . The parameters varied according to the following rules:

- Source depth (z_s): 90–110 m (100 m (canonical value) $\pm 10\%$);
- Hydrophone array depth shift (z_a): -1–1 m (shallowest hydrophone depth $\pm 10\%$);

Table 4.1: Environmental parameters.

Group	Layer	Sub-layer	Name	Notation
Instrumentation			Source depth	z_s
			Source-receiver range	r_s
			Receiver array depth shift	z_a
Oceanographic	Water column		Water depth	D
			Sound speed profile first EOF coefficient	α_1
	Bottom	Sediment	Thickness	s_t
			Density	ρ_s
			Upper compressional speed	s_u
	Bottom	Basement	Lower compressional speed	s_l
			Compressional attenuation	s_a
			Density	ρ_b
			Compressional speed	c_b
	Bottom	Basement	Compressional attenuation	b_a

- Source-receiver range (r_s): 4.5–5.5 km (5 km (canonical value) \pm 10%);
- Water depth (D): 180–220 m (200 m (canonical value) \pm 10%);
- Sediment thickness (s_t): 0–5 m (2.5 m (canonical value) \pm 100%);
- Other sediment and basement properties: bounds chosen according to typical minima and maxima as indicated in Ref. [JKPS93], namely:
 - Compressional speeds (c_{su} , c_{sl} and c_b): 1500–5250 m/s;
 - Densities (ρ_s and ρ_b): 1.5–2.7 g/cm³;
 - Compressional wave attenuation (α_s and α_b): 0.1–1.0 dB/wavelength.

For the geoacoustic parameters, the criterion to define the bounds is to evaluate the consequence of erroneously considering an ocean bottom parameter to be from a different material. For the source-receiver range, only the acoustic field at 5 km was considered for the computation of the cost in Eq. (4.2). The cost for each parameter variation is shown in Fig. 4.5. By sorting the values of the maxima mentioned in Fig. 4.5, a hierarchy of importance (for

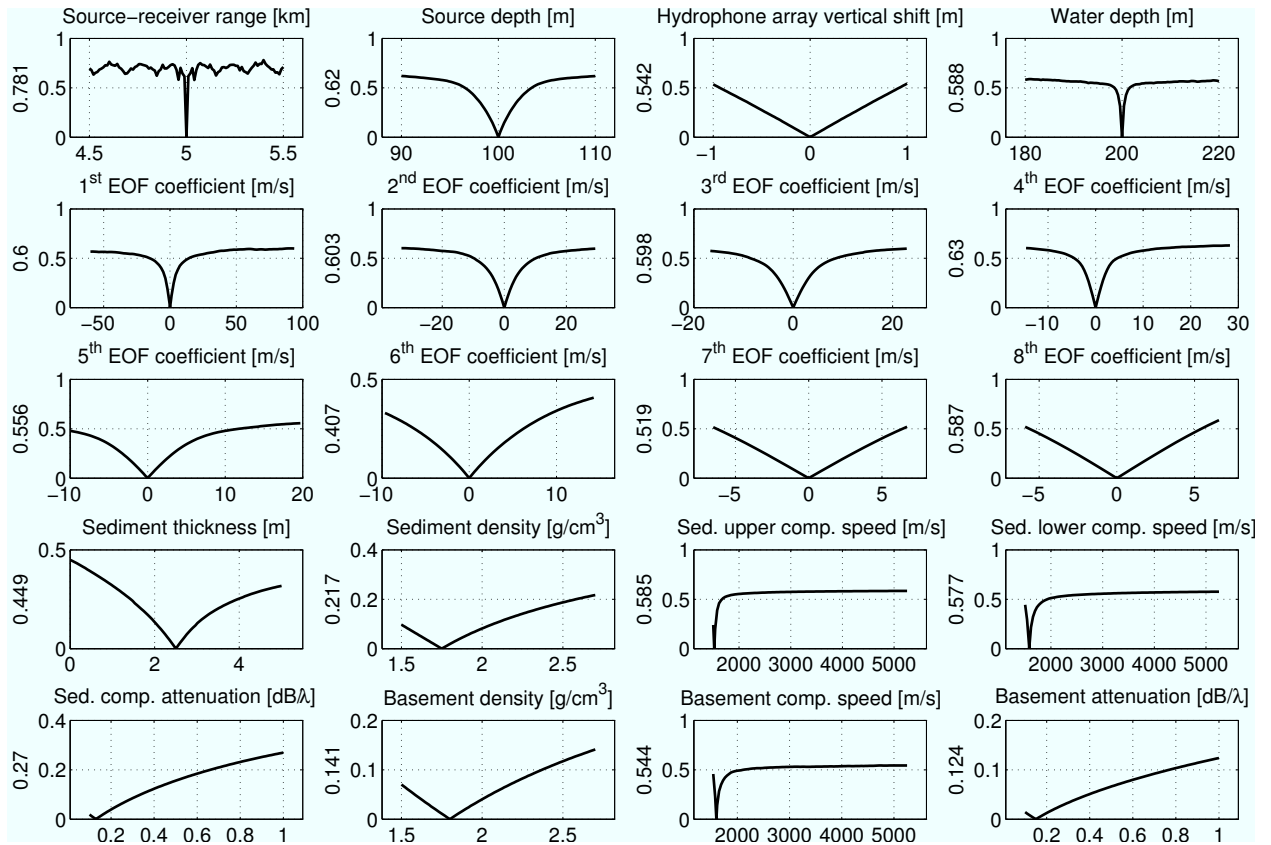


Figure 4.5: Environmental sensitivity analysis for the realistic simulations of the present work. The consequence of introducing an offset in each parameter at a time (see Tab. 4.1) on the acoustic field, is represented in terms of an acoustic cost (eq. (4.2)).

the acoustic field) is obtained, shown in Tab. 4.2. This hierarchy agrees with several previous works dealing with relative sensitivity of the acoustic field to the environment, grouping geometrical properties and sound speed together into the highest importance to define the acoustic field[CK91, MB99].

Table 4.2: Hierarchy of the parameters that define the acoustic field. The hierarchy was computed according to the maximum value of each of the costs in Fig. 4.5.

Importance	Parameter	Sensitivity
Most important	Source-receiver range	0.781
	4 th EOF coefficient	.63
	Source depth	.62
	2 nd EOF coefficient	.603
	1 st EOF coefficient	.6
	3 rd EOF coefficient	.598
	Water depth	.588
	8 th EOF coefficient	.587
	Sediment upper compressional speed	.585
	Sediment lower compressional speed	.577
	5 th EOF coefficient	.556
	Basement compressional speed	.544
	Hydrophone array depth shift	.542
	7 th EOF coefficient	.519
	Sediment thickness	.449
	6 th EOF coefficient	.407
	Sediment compressional attenuation	.27
	Sediment density	.217
	Basement density	.141
	Least important	Basement attenuation

4.2.2 Environmental mismatch compensation

According to the claim of the present work, in order to obtain an accurate acoustic prediction, in a situation of environmental mismatch, it is essential that some environmental parameters compensate for that mismatch. This section presents a study quantifying the compensation in every parameter pair, when the goal is to model the acoustic field at the hydrophone array at 5-km range from the acoustic source, at frequencies of 100–1000 Hz, with 100-Hz

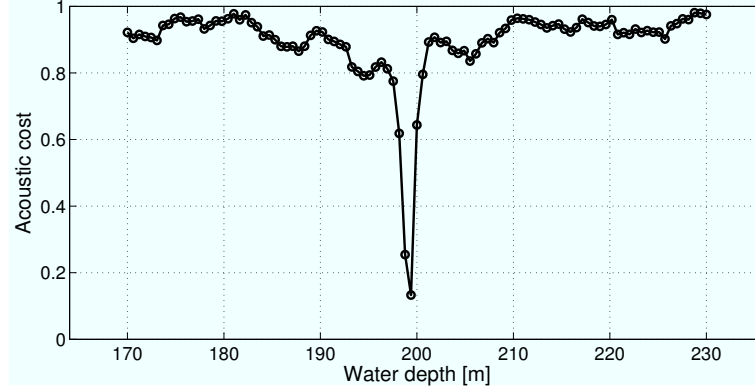


Figure 4.6: Environmental mismatch compensation: the source-receiver range is taken as 50 m inferior to the true value of 5 km. This environmental mismatch is compensated by an offset in the water depth, which subtracts 60 cm to the true 200 m.

step, using values for the fixed parameters as shown in Fig. 4.4. Each parameter at a time, playing the role of a parameter in mismatch, was allowed to vary essentially within the same bounds as shown in Fig. 4.5. For each value of a particular parameter in mismatch, the value of every other at a time was optimized by resorting to an acoustic cost function, such that the cost is minimized. The cost function is a complementary form of the depth-coherent, frequency-incoherent Bartlett processor, and defined as:

$$\mathcal{C}_1(\theta_k) = 1 - \frac{1}{N_f} \sum_f \frac{\mathbf{w}^H(f, \theta_k) \mathbf{C}_{RR}(f, \boldsymbol{\theta}_0) \mathbf{w}(f, \theta_k)}{\|\mathbf{w}(f, \theta_k)\|^2 \text{tr} \mathbf{C}_{RR}(f, \boldsymbol{\theta}_0)}, \quad (4.3)$$

where $\mathbf{C}_{RR}(f, \boldsymbol{\theta}_0)$ is an estimate of the receiver data correlation matrix at frequency f , and \mathbf{w} is a vector of acoustic pressure candidates and a function of the parameter value θ_k . The processor, whose values are normalized between 0 and 1, is to be minimized with respect to θ_k . One example of optimization/compensation is shown in Fig. 4.6, in which the source-receiver range was negatively offset by 50 m, and the water depth was optimized to compensate for this mismatch. In order to obtain a high acoustic similarity between the true and modeled acoustic fields, it was necessary to subtract 60 cm to the true water depth of 200 m, as indicated by the value that minimizes the cost. The minimum cost is

not zero, indicating that the canonical acoustic field could not be reproduced exactly. In order to quantify the extent of inter-parameter compensation, several values of mismatch were tested, and for each one, a functional cost as the one of Fig. 4.6 was computed, in order to find the equivalent water depth. A contour plot of cost, superimposed by values of optimum water depth, is shown in Fig. 4.7. It can be recognized the well-known fact that source-receiver range is highly correlated with water depth, implying that errors in excess on source-receiver range can be compensated by errors in excess on water depth [DMH⁺99]. Taking into account the possibility of not modeling the acoustic field with zero error, even after compensation for mismatch, it is necessary to decide on a threshold which is acceptable as the maximum cost allowing for a sufficiently accurate acoustic modeling. For the current study, this threshold was set to 0.1. For the parameters at hand, as represented in Fig. 4.7, this threshold is respected only for source-receiver range values between 4.94 and 5.07 km. The maximum difference between each of these values and the true value of 5 km was considered the maximum allowed mismatch for accurate acoustic modeling. For this case, it represents approximately 1.3% of the true 5 km. This procedure was repeated for every possible parameter pair, taken from Tab. 4.1. Selected cases of compensation from all the possible ones are shown in Figs. 4.7–4.19. Every value in mismatch is compensated by an equivalent value of the compensating parameter, as represented by the circles in these figures. In all the figures, the mismatch bounds and search bounds for which the acoustic error is below the threshold of 0.1, correspond to the bounds of the yellow lines. Figure 4.8 shows the result of compensation for source depth mismatch performed by optimization for sediment compressional attenuation. Only a small mismatch ($\leq 0.82\%$) can be compensated. This behavior is verified for other compensating parameters (see Tab. 4.3, which lists all the

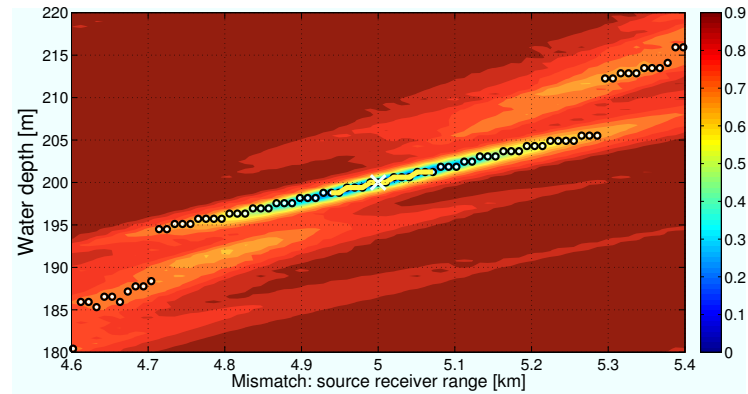


Figure 4.7: Contour plot of the acoustic cost, and optimal water depth that compensates for source-receiver range mismatch.

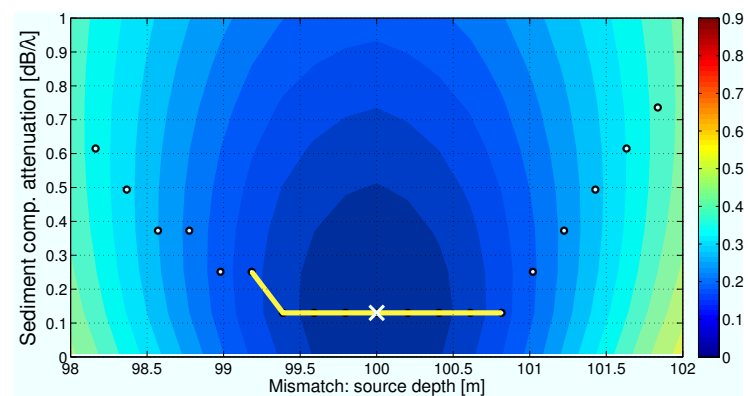


Figure 4.8: Contour plot of the acoustic cost (background), and optimal sediment compressional attenuation that compensates for source depth mismatch (circles). The optimal values minimize the cost computed for each value in mismatch. The case of no mismatch is indicated by the white cross. The points for which the acoustic error is below the threshold of 0.1 are connected by the yellow line.

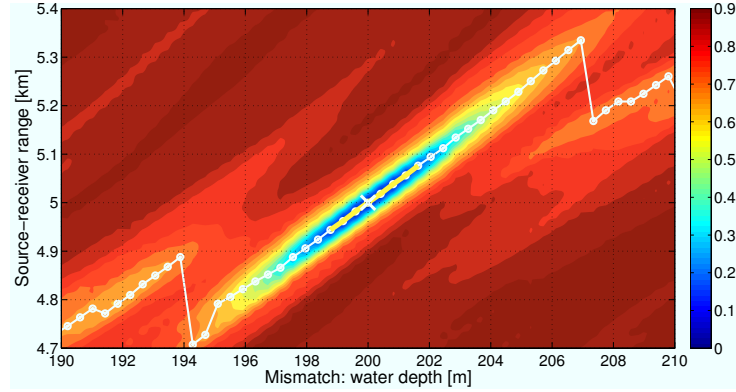


Figure 4.9: Contour plot of the acoustic cost (background), and optimal source-receiver range that compensates for water depth mismatch (circles). The optimal values minimize the cost computed for each value in mismatch. The case of no mismatch is indicated by the white cross. The points for which the acoustic error is below the threshold of 0.1 are connected by the yellow line.

pairwise compensation possibilities), revealing that the source depth constitutes essentially an ‘independent’ contribution to acoustic propagation. Figure 4.9 shows the result of compensation for water depth mismatch performed by optimization for source-receiver range. In a situation of coincident discretization and bounds for water depth and source-receiver range, the contour plot in this figure would be exactly the transpose of the one in Fig. 4.7. The discontinuities in the pattern defined by all the equivalent source-receiver range values are due to abrupt variations on the number of propagating modes in the water channel, induced by water depth changes. Figure 4.10 shows the result of compensation for water column SSP mismatch —generated by a mismatch in the first EOF coefficient— performed by optimization for source-receiver range. As for the source depth (see Fig. 4.8), only a small mismatch is allowed in the first EOF coefficient, to follow the criterion of having an acoustic error ≤ 0.1 , evidencing that this parameter also constitutes an independent contribution to acoustic propagation. Figure 4.11 shows the result of compensation for sediment thickness mismatch performed by optimization for source-receiver range. In this case, two factors contribute to allow a mismatch as high as 100% (see column “ s_t ” of Tab. 4.3) in sediment

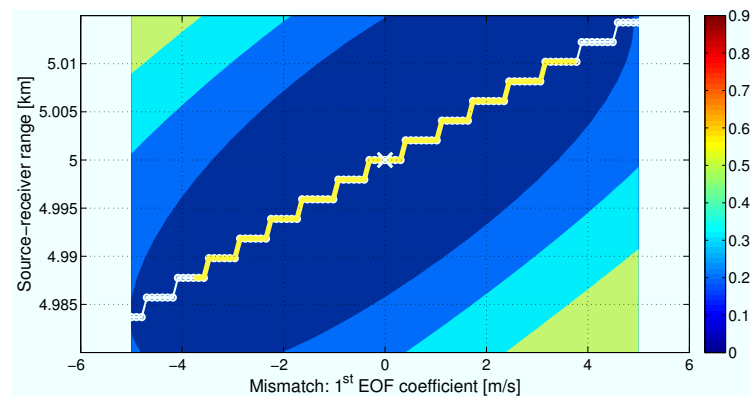


Figure 4.10: Contour plot of the acoustic cost (background), and optimal water depth that compensates for water column SSP mismatch (circles). The optimal values minimize the cost computed for each value in mismatch. The case of no mismatch is indicated by the white cross. The points for which the acoustic error is below the threshold of 0.1 are connected by the yellow line.

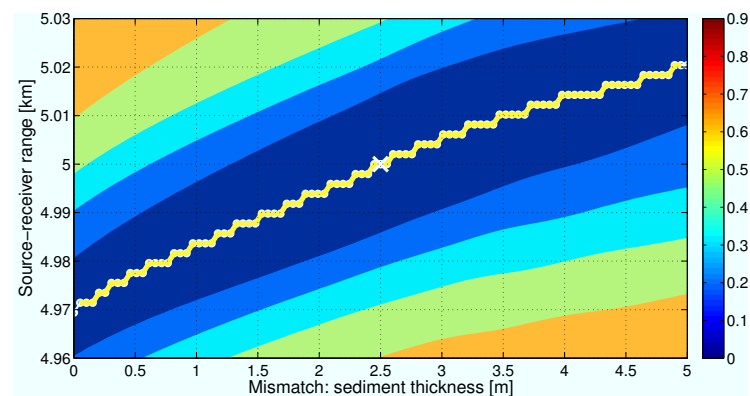


Figure 4.11: Contour plot of the acoustic cost (background), and optimal source-receiver range that compensates for sediment thickness mismatch (circles). The optimal values minimize the cost computed for each value in mismatch. The case of no mismatch is indicated by the white cross. The points for which the acoustic error is below the threshold of 0.1 are connected by the yellow line.

thickness: 1) the latter is not more than moderately relevant for acoustic propagation (see Fig. 4.5 or Tab. 4.2, indicating a sensitivity of 0.45); 2) the sediment thickness is highly “correlated” with source-receiver range, also a property of geometric nature. Figure 4.12 shows the result of compensation for sediment density mismatch performed by optimization for water depth. High values of mismatch are allowed for sediment density (as high as 54%), due to the fact that: 1) it is one of the least relevant parameters to define the acoustic field (see Tab. 4.2); 2) it is correlated with water depth. Other parameters are correlated with sediment density, as seen on the high values in column “ ρ_s ” of Tab. 4.3. Figure 4.13 shows

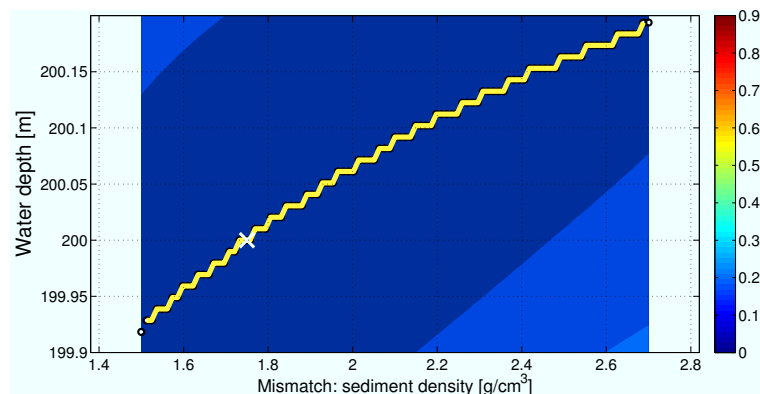


Figure 4.12: Contour plot of the acoustic cost (background), and optimal water depth that compensates for sediment density mismatch (circles). The optimal values minimize the cost computed for each value in mismatch. The case of no mismatch is indicated by the white cross. The points for which the acoustic error is below the threshold of 0.1 are connected by the yellow line.

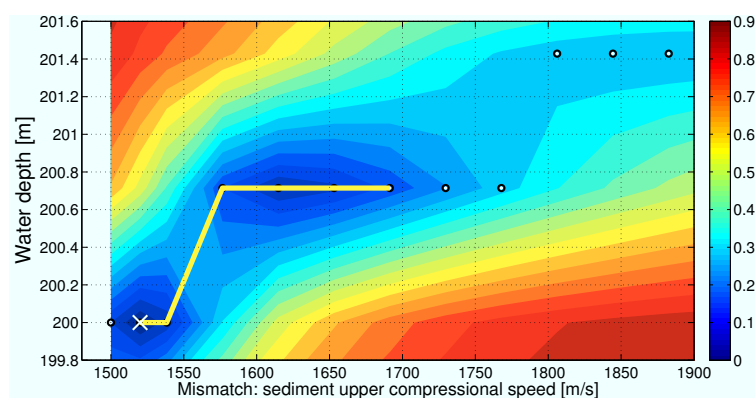


Figure 4.13: Contour plot of the acoustic cost (background), and optimal water depth that compensates for sediment upper compressional speed mismatch (circles). The optimal values minimize the cost computed for each value in mismatch. The case of no mismatch is indicated by the white cross. The points for which the acoustic error is below the threshold of 0.1 are connected by the yellow line.

the result of compensation for sediment upper compressional speed mismatch performed by optimization for water depth. A reasonable mismatch is allowed, with a percentage of 9.5%. Interestingly, an approximate value of mismatch (7.1%) is allowed when the compensating parameter is the source-receiver range (see Tab. 4.3). This is not surprising, taking into account the high correlation between water depth and source-receiver range (see Figs. 4.7 and 4.9). Figure 4.14 shows the result of compensation for sediment lower compressional speed mismatch performed by optimization for sediment thickness. Though the sediment lower compressional speed is a significant parameter for acoustic propagation (see Tab. 4.2),

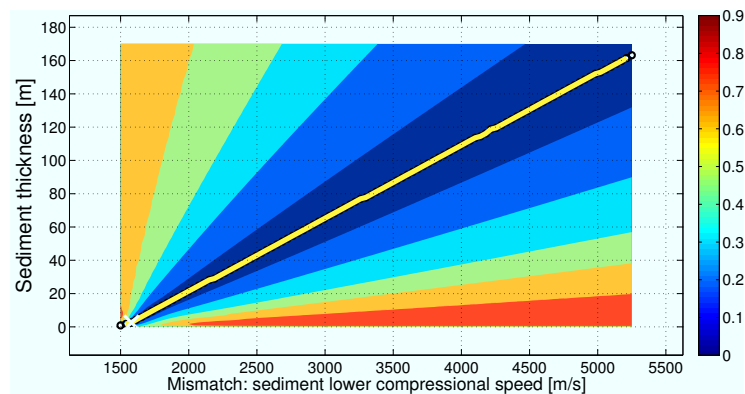


Figure 4.14: Contour plot of the acoustic cost (background), and optimal sediment thickness that compensates for sediment lower compressional speed mismatch (circles). The optimal values minimize the cost computed for each value in mismatch. The case of no mismatch is indicated by the white cross. The points for which the acoustic error is below the threshold of 0.1 are connected by the yellow line.

it is allowed to have a high mismatch, due to a high correlation with sediment thickness.

All the values in mismatch were compensated according to the 0.1-threshold criterion. In-

terestingly, the compensating values of sediment thickness can deviate significantly from the

true value of 2.5 m. It is important to point out that, as mentioned in the first chapters of

the present work, the environmental outcomes appropriate for acoustic modeling or the ones

appropriate for environmental estimation have to be interpreted according to their context.

While in environmental estimation of sediment thickness, a search will be done within ac-

ceptable values for the thickness, in ocean acoustic modeling constrained by environmental

mismatch, it is necessary to not discard the possibility of using exaggeratedly high values for

the thickness, to minimize the effect of mismatch. The drawback of using too high values for

thickness might be a situation of overfitting. Figure 4.15 shows the result of compensation

for sediment compressional attenuation mismatch performed by optimization for sediment

density. According to Tab. 4.2, the sediment compressional attenuation is not a significant

parameter for acoustic propagation, which explains that all the values of mismatch were

compensated. Figure 4.16 shows the result of compensation for basement density mismatch

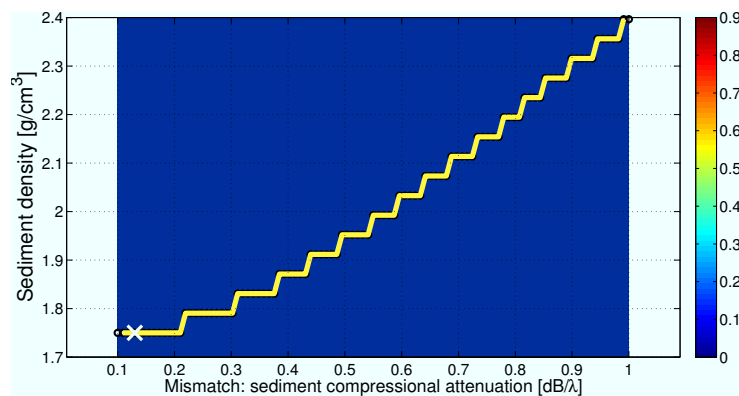


Figure 4.15: Contour plot of the acoustic cost (background), and optimal sediment density that compensates for sediment compressional attenuation mismatch (circles). The optimal values minimize the cost computed for each value in mismatch. The case of no mismatch is indicated by the white cross. The points for which the acoustic error is below the threshold of 0.1 are connected by the yellow line.

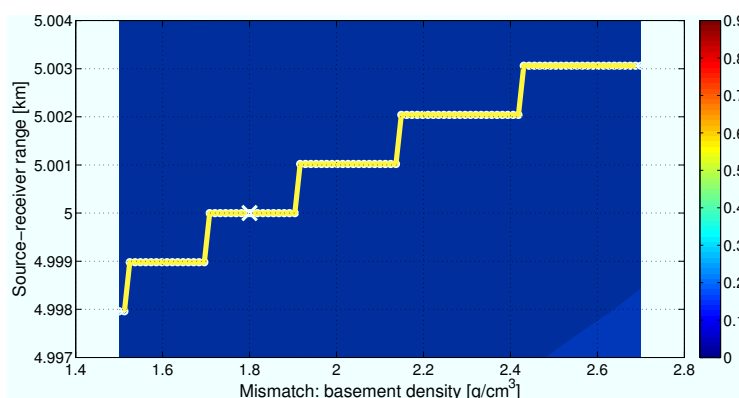


Figure 4.16: Contour plot of the acoustic cost (background), and optimal source depth that compensates for basement density mismatch (circles). The optimal values minimize the cost computed for each value in mismatch. The case of no mismatch is indicated by the white cross. The points for which the acoustic error is below the threshold of 0.1 are connected by the yellow line.

performed by optimization for source-receiver range. According to Tab. 4.2, the basement density is not significant for acoustic propagation, which explains that every value of mismatch was compensated by source-receiver range. As seen in Tab. 4.3, every parameter can compensate for a mismatch in basement density. Figure 4.17 shows the result of compensation for basement compressional speed mismatch performed by optimization for basement compressional attenuation. Similarly to the result shown in Fig. 4.14, it is noticeable the interference of two important phenomena: first, the basement compressional speed is significant for acoustic propagation (recall that the sound speed of the acoustic propagation

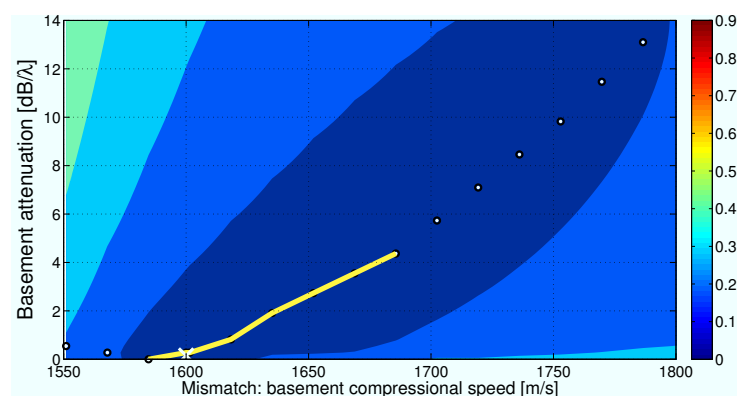


Figure 4.17: Contour plot of the acoustic cost (background), and optimal basement compressional attenuation that compensates for basement compressional speed mismatch (circles). The optimal values minimize the cost computed for each value in mismatch. The case of no mismatch is indicated by the white cross. The points for which the acoustic error is below the threshold of 0.1 are connected by the yellow line.

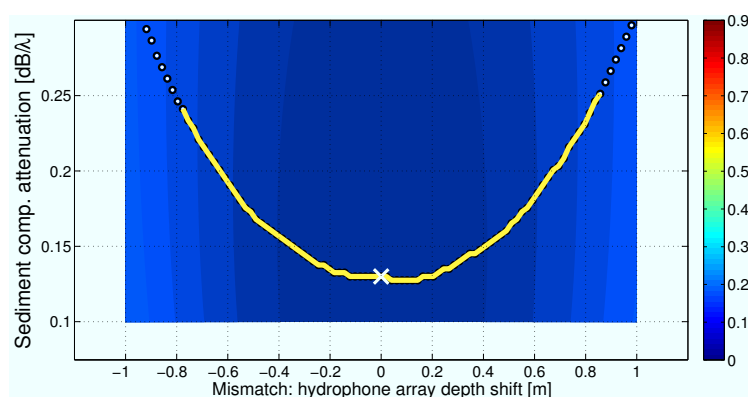


Figure 4.18: Contour plot of the acoustic cost (background), and optimal sediment compressional attenuation that compensates for receiver array depth shift mismatch (circles). The optimal values minimize the cost computed for each value in mismatch. The case of no mismatch is indicated by the white cross. The points for which the acoustic error is below the threshold of 0.1 are connected by the yellow line.

channel is one of the most important parameters defining propagation paths, and see Tab. 4.2), which does not allow high values of mismatch per se; second, the basement compressional speed is highly correlated with basement compressional attenuation, as deduced from a moderate maximum allowable mismatch of 4.9% (see Tab. 4.3) and the regular relationship between the mismatch and the compensating values (see Fig. 4.17). Figure 4.18 shows the result of compensation for receiver array depth shift performed by optimization for sediment compressional attenuation. The low value for the maximum acceptable mismatch,

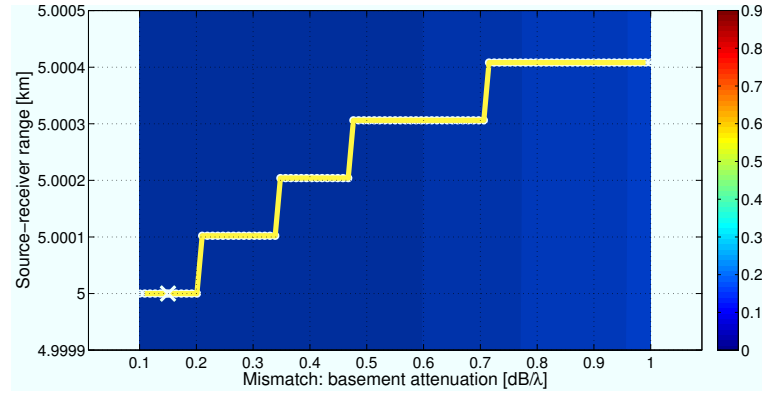


Figure 4.19: Contour plot of the acoustic cost (background), and optimal source-receiver range that compensates for basement compressional attenuation mismatch (circles). The optimal values minimize the cost computed for each value in mismatch. The case of no mismatch is indicated by the white cross. The points for which the acoustic error is below the threshold of 0.1 are connected by the yellow line.

0.85 m (almost independent of the compensating parameter —see Tab. 4.3), indicates that the receiver array depth shift also carries essentially independent information concerning the acoustic field, similarly to source depth (see Fig. 4.8) and water column SSP (see Fig. 4.10). Figure 4.19 shows the result of compensation for basement compressional attenuation mismatch performed by optimization for source-receiver range. The basement compressional attenuation is the least significant parameter for acoustic propagation (see Tab. 4.2), which explains that the full interval of mismatch could be compensated by source-receiver range (as well as by any other parameter, as seen in Tab. 4.3). Table 4.3 lists all the possibilities of compensation. Three essential classes of behavior can be deduced from Tab. 4.3. The first one concerns parameters which have low significance for the acoustic field, namely sediment thickness, sediment density, sediment attenuation, basement density and basement attenuation (columns “ s_t ”, “ s_d ”, “ s_a ”, “ b_d ” and “ b_a ”, respectively, in Tab. 4.3) —recall Tab. 4.2. For such parameters, a high mismatch is allowed, independently of the compensating parameter, since the mismatch does not significantly compromise acoustic accuracy. The second class of behavior concerns correlated parameters. This is the case of the following parameters in

Table 4.3: Pairwise environmental mismatch compensation. Each column represents one parameter in mismatch, and each row, one parameter which was given freedom to compensate the mismatch. The values filling the table are the maximum allowed mismatch such that the acoustic cost is ≤ 0.1 , after the mismatch compensation (expressed in percentage, except for α_1 and z_a (with a null true value), for which the absolute values are used). The values in bold are the maximum for each column. The notation is explained in Tab. 4.1.

	r_s	α_1	z_s	D	s_t	ρ_s	s_u	s_l	s_a	b_d	c_b	z_a	b_a
r_s	-	3.8	0.81	0.69	100	54	7.1	7.1	520	50	1.5	0.83	570
α_1	0.32	-	0.84	0.14	52	48	2	2.6	520	50	1.7	0.85	570
z_s	0.22	2.6	-	0.081	42	47	1.6	2.3	520	50	1.5	0.83	570
D	1.3	3.1	0.81	-	100	54	9.5	2.4	520	50	1.5	0.83	570
s_t	0.51	2.9	0.81	0.41	-	54	2.1	230	620	50	1.8	0.83	570
ρ_s	0.31	2.7	0.81	0.14	79	-	1.7	3.4	670	50	1.9	0.83	570
s_u	0.64	3.3	0.81	0.48	100	54	-	7.2	540	50	1.8	0.83	570
s_l	0.25	2.9	0.81	0.28	100	54	1.6	-	570	50	1.7	0.83	570
s_a	0.23	2.7	0.82	0.093	45	54	1.6	2.3	-	50	4.1	0.85	570
ρ_b	0.27	2.8	0.81	0.12	55	51	1.6	2.3	530	-	1.9	0.83	570
c_b	0.24	2.7	0.81	0.098	46	54	1.7	2.6	520	50	-	0.83	570
z_a	0.22	2.6	0.81	0.081	42	47	1.6	2.3	520	50	1.5	-	570
b_a	0.22	2.6	0.76	0.084	42	47	1.6	2.3	550	50	4.9	0.83	-

mismatch: source-receiver range, water column depth, sediment upper compressional speed, sediment lower compressional speed and basement compressional speed (columns “ r_s ”, “ D ”, “ s_u ”, “ s_l ” and “ c_b ”, respectively, in Tab. 4.3). Each of these parameters is highly correlated with another parameter, a ‘peer’ parameter. When the ‘peer’ parameter is used to compensate for the mismatch, the value in mismatch can deviate more from the true value, than if only any parameter other than the ‘peer’ is used to compensate for the mismatch. In physical terms, it is possible to infer that each of the parameters in the second class plays a role similar to its ‘peer’ parameter in defining the acoustic field. The third class of behavior is defined by low-correlated parameters. This is the case of: first EOF coefficient, source depth and receiver array depth shift (columns “ α_1 ”, “ z_s ” and “ z_a ”, respectively, in Tab. 4.3). These parameters define acoustic propagation features which are difficult to reproduce by other parameters. This makes it difficult to “counterbalance” any mismatch that might

exist in these parameters. As a consequence, the corresponding columns in Tab. 4.3 contain relatively small, constant values. A summary of the compensation characteristics mentioned above, when facing the goal of accurately modeling the acoustic field, is:

- Parameters which are not significant for acoustic propagation can deviate significantly from their true values, and their mismatch can be compensated by any from a large diversity of parameters;
- Parameters which are significant for acoustic propagation cannot deviate significantly from their true values, unless their mismatch is compensated by a highly correlated parameter.

4.3 Summary

This chapter started by describing the oceanographic data set at hand and defining the scenario for application of the proposed acoustic estimation method. The full environmental parameter vector was analyzed, allowing to quantify the importance of each parameter on the estimation of the acoustic field. Then, by departing from a canonical scenario which will be the working scenario in the next chapter, several examples of equivalent environmental modeling were worked out. It was observed that there are numerous possible situations of environmental mismatch in which the latter can be almost completely removed, in terms of acoustic output. This is due to the presence of a sufficiently high number of degrees of freedom in the considered realistic oceanic scenario. According to the compensation for mismatch, the parameters were grouped into three categories: low-significant, correlated and low-correlated. The first category concerns the least important parameters for acoustic propagation, whose mismatch does not compromise the acoustic estimate quality. It is

not essential to compensate for a mismatch in such a parameter, when the acoustic error imposed by the mismatch lies within acceptable bounds for the particular application. The second category is made up of parameters whose mismatch can be compensated by correlated parameters. The third category is made from parameters whose influence on the acoustic field cannot be easily reproduced by any other parameter, hence whose mismatch cannot be easily compensated. For parameters of this type that are relevant for acoustic propagation, they should either: 1) be known with high accuracy, or 2) be included in the equivalent environmental vector. In the latter case, they will be free parameters whose true value can eventually be determined by acoustic inversion.

Chapter 5

Application of Equivalent Models in Acoustic Nowcast and Forecast

“The most reliable way to forecast the future is to try to understand the present.”

John Naisbitt

THE present chapter describes the application of the approach adopted in the present work to the problems of acoustic nowcast (Sec. 5.1) and forecast (Sec. 5.2), in a realistic setup. For each exercise (nowcast or forecast), a different data set is worked out. The presented numerical tests consider synthetic acoustic data, with the objective of representing long (\approx one month) time series, to illustrate the approach with statistical significance. The following sections put in evidence the equivalent model as a relevant component in the determination of the acoustic nowcast/forecast. The oceanographic measured/predicted data is taken from the Maritime Rapid Environmental Assessment 2003 (MREA'03) sea trial, described in Sec. 4.1.

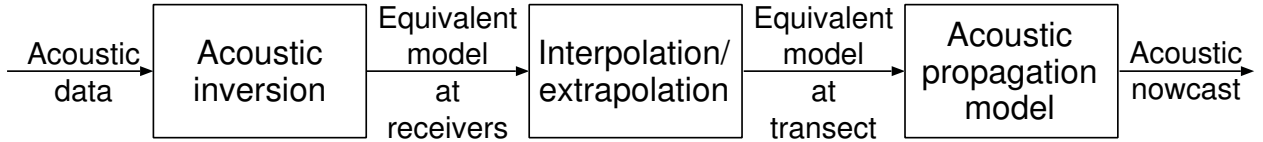


Figure 5.1: Acoustic nowcast estimator.

5.1 Acoustic Nowcast

This section describes the approach adopted in the present work to solve the problem of acoustic nowcast. By “nowcast” it is meant the estimation of the acoustic field at the most recent time sample of acoustic-oceanographic observation. The nowcast estimator consists of three steps, outlined in Fig. 5.1. The first one is the inversion of acoustic data, producing frequency-independent equivalent model estimates for the time sample of nowcast. The second one is the interpolation/extrapolation of the estimates to all the required space points in which to estimate the acoustic field. The third one consists in running the acoustic propagation model with the interpolation/extrapolation outcomes. The output of this run is the acoustic nowcast for the ocean transect. The following sections describe the approach and numerical results of the above nowcast estimator.

5.1.1 Acoustic Nowcast Test Case

The approach for acoustic nowcast developed in the present work is illustrated with synthetic data produced on a real scenario. The practical objective is to estimate the acoustic field in an ocean transect whose water column properties are set to coincide with the water column measurements cast during the MREA’03 sea trial (described in Ch. 4), and whose ocean bottom properties are taken from Ref. [JKPS93], as shown in Fig. 5.2. These are labeled as “true” environmental properties. Simultaneously, baseline environmental properties are considered, defining the environmental model that a hypothetical user has at hand, which

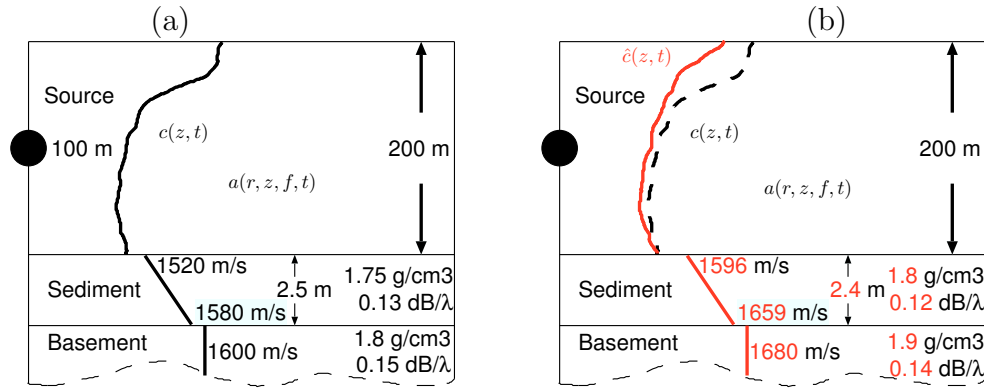


Figure 5.2: Idealized ocean transect in which the acoustic field nowcast is to be computed: (a) true and (b) baseline environmental properties. The environmental components in mismatch are represented by the red values/lines in (b). At every time sample, the presumably known sound speed profile has smaller or equal values than the true sound speed profile, and deviates linearly from the surface to the bottom, starting at 2 m/s and finishing at 0.

is the “best” (logical) —according to the user’s knowledge— environmental representation of the ocean transect under consideration. Several properties are different between the true and modeled scenarios, as seen in Fig. 5.2. Every instantaneous water column sound speed profile (SSP) is assumed to be less downward-refracting than its corresponding true SSP. The ocean bottom is assumed to be more reflective than the true one; this is quantified by larger density and sound speed values, and a smaller attenuation; the error in the geoacoustic properties has a magnitude of 5%. The present method assimilates acoustic measurements obtained in the transect. For this purpose, two acoustic receiver arrays are placed at 5- and 10-km range from the source —see Fig. 5.3. The acoustic nowcast exercise was repeated according to an idealized timeline, composed of 465 uniformly spaced time samples between May 28 (time $t_0 = 0$) and June 25 (time $t_E = \text{day } 28$) (bounds coincident with actual conductivity, temperature and depth (CTD) cast time bounds during the MREA’03 sea trial) —see Fig. 5.4, and recall Fig. 2.2. The time sample t_F represented in Fig. 2.2 will be important for the acoustic forecast exercise, in Sec. 5.2. The time step between two acoustic nowcast exercises is 1.4 h. For every time sample, one CTD-derived SSP, together with

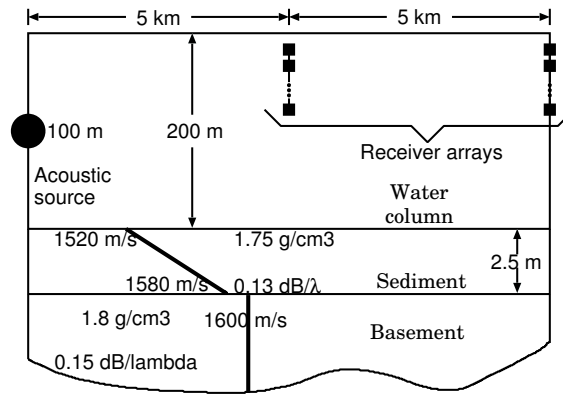


Figure 5.3: Ocean transect in which to estimate the acoustic field, monitored with two acoustic receiver arrays. The acoustic data observed at these array locations is inter/extrapolated in space and time, which is the main idea behind the approach to acoustic nowcast presented in the present work. The true geoaoustic properties are also shown (refer to Fig. 5.2 (a)).

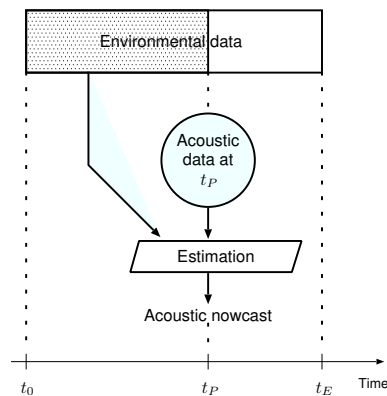


Figure 5.4: Idealized timeline for acoustic nowcast, bounded by times $t_0 = 0$ (initial time sample) and $t_E = 28$ days (final time sample) —recall Fig. 2.2. At time t_P , the past acquired (erroneous) CTD data, together with baseline geoaoustic and geometric properties, and acoustic measurements at t_P , enter an estimation block. This block has the acoustic nowcast as output. Several nowcast exercises are executed, hence the “present time” t_P runs from t_0 to t_E .

the geoaoustic properties in Fig. 5.2, was used to generate the “true” acoustic field, with the SACLANTCEN Normal-Mode Acoustic Propagation Model (SNAP) [JF79], at ranges between 0.5 and 10 km with 0.5-km step, depths between 10 and 85 m with 5-m step, and frequencies between 100 and 1000 Hz with 100-Hz step, which contains the noiseless data observed at the two receiver arrays in Fig. 5.3. By referring to the scheme in Fig. 5.1, in order to solve the problem of nowcast, the acoustic data snapshots observed at each receiver array were processed separately by acoustic inversion, providing an equivalent environmental

parameterization for the array position. The two equivalent model outcomes corresponding to the two receiver arrays were interpolated/extrapolated to the required spatial points. This result was then used in an acoustic forward modeling exercise whose output constitutes the acoustic nowcast.

A fundamental question when using an equivalent model is to decide which parameters to invert for. Since every parameter acts as an additional degree of freedom in modeling the acoustic field, ideally all the environmental parameters should be included in the equivalent model. This would lead to a highly accurate modeled acoustic field at the receiver array locations. Nevertheless, a high number of parameters may cause overfitting (as seen in Ch. 3), which demands for establishing a trade-off between acoustic accuracy and equivalent model generalization. Some preliminary tests not shown here (nevertheless with results similar to those shown in Fig. 3.19, for the ideal waveguide) demonstrated that source-receiver range, source depth or water depth, if used as components of the equivalent model, vary significantly with range. When using these parameters in the equivalent model, the interpolation of their values to ranges other than the receiver array positions (5 and 10 km) very rarely produces useful outcomes for acoustic estimation in the full ocean transect. This reason motivated to not use these parameters as components of the equivalent model, though they are able to compensate for errors in several other parameters (source-receiver range and water depth can compensate for errors in approximately half of the total number of parameters —see Tab. 4.3). Moreover, in the present test case, there is no mismatch in these environmental properties. In a real setup for which a mismatch might exist, it is important to include some of these parameters in the equivalent model vector, since they are among the most important parameters for defining the acoustic field. A mismatch in one of

these parameters (for example, in source depth, which is an ‘independent’ parameter —see column “ z_s ” in Tab. 4.3) that is not minimized by acoustic inversion for the parameter itself can lead to high acoustic errors. As seen in Tab. 4.3, the sound speed in water, in sediment and in basement, is relevant for the definition of the acoustic field, and can compensate for mismatch in some of the geoacoustic parameters, such as sediment compressional attenuation (see Tab. 4.3). In practice, sound speed does not exhibit significant range-dependence, when included in the equivalent model vector. Thus, the equivalent model was built from the sound speed in water, in sediment —at the water-sediment interface and the sediment-basement interface, assuming a linear variation of sound speed with depth—, and in basement —with a depth-independent sound speed. Regarding the water column, the correlation matrix of the sound speed data was estimated only from the sound speed profiles (SSPs) (in mismatch, as shown in Fig. 5.2 (b)) corresponding to times t_0, \dots, t_P —see Fig. 5.4. Thus, it is assumed that, at the initial time t_0 , only one SSP cast is available to build the database of SSPs. At each new time sample, an SSP cast is added to the database, which is used to update the average profile and the empirical orthogonal functions (EOFs). The resulting time-dependent empirical orthogonal function (EOF) representation can be written as:

$$c(z, t) \approx \bar{c}(z, t) + \sum_{k=1}^K \alpha_k(t) \hat{\varphi}_k(z, t). \quad (5.1)$$

This constitutes a time-variant form of Eq. (4.1), and $K = 8$ EOFs were considered sufficient to model the acoustic field with low error. The value of K was selected by trial-and-error, in which several acoustic snapshots were inverted, and a candidate K was progressively increased such as to attain a Bartlett misfit less than 0.1 at the end of the inversion. The chosen value of K is the minimum value that satisfies this criterion. In a generic application, this exercise can be done by adjusting the value of K to the required acoustic accuracy. The

Table 5.1: Parameters to invert for.
1 st –8 th EOF coefficient
Basement compressional speed
Sediment upper compressional speed
Sediment lower compressional speed

time series of the first EOF at selected depths is shown in Fig. 5.5. It is seen that only after

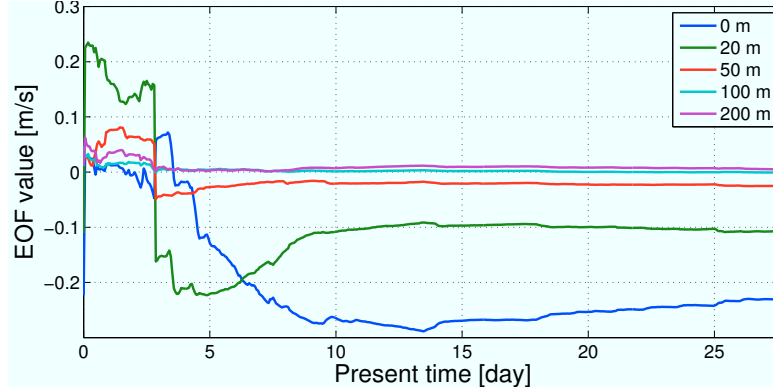


Figure 5.5: Time series of the first EOF at selected depths, for the complete timeline of the nowcast exercise.

day 10 the EOF values stabilize. The complete equivalent model vector is summarized in Tab. 5.1.

5.1.2 Solution to Acoustic Nowcast

Let us recall the definition of equivalent model (same as Eq. (2.4)):

$$\begin{aligned}
 \Theta_E(r, z, f, \Theta_T, \mathcal{C}, \mathcal{P}, \hat{\mathcal{P}}) &= \arg \min_{\Theta} \mathcal{C}(u, \hat{u}) \\
 &= \arg \min_{\Theta} \mathcal{C}(\mathcal{P}(r, z, f, \Theta_T), \hat{\mathcal{P}}(r, z, f, \Theta)). \quad (5.2)
 \end{aligned}$$

In exact terms, for fixed $\Theta_T, \mathcal{C}, \mathcal{P}$ and $\hat{\mathcal{P}}$, the equivalent model is a function of space and frequency. In this case, it can be noted as: $\Theta_E(r, z, f)$. The first implication of this dependence is that the equivalent model can be completely characterized only in a situation on which acoustic receivers observe the acoustic field at every space-frequency point in

which to estimate the acoustic field. The impossibility of executing such a huge acoustic observation exercise (which would even turn an estimation exercise into an observational one) demands for approximations regarding the structure of the equivalent model. The present work resorted to the approximation expressed in Rem. 5.1.

Remark 5.1: Consider a discrete set \mathcal{E} of space-frequency points (r, z, f) at which it is required to estimate the acoustic field. For every point (r, z, f) in \mathcal{E} there exists an equivalent model $\Theta_E(r, z, f)$. Consider now a subset of \mathcal{E} consisting of a fixed range r_0 and several depth and frequency points, (r_0, z, f) . If acoustic observations are done at these points, then an equivalent model constant in depth and frequency, $\theta_E(r_0)$, can be defined. Any estimator of $\theta_E(r_0)$ is a depth-frequency-independent estimator of $\Theta_E(r_0, z, f)$.

Remark 5.1 expresses that the range-depth-frequency-dependent equivalent model can be approximated by a range-dependent, depth-frequency-independent version. This is the approximation applied in the present work. This subjective choice is well adapted to conventional acoustic inversion approaches in the context of acoustic environmental assessment. For this purpose, the acoustic field observed at all the receivers of a vertical array, at a chosen set of frequencies, is mapped into a single environmental description, which minimizes an acoustic data-model error. Here, the same procedure is applied, but now interpreted as an acoustic propagation model calibrator, which provides a single equivalent model associated with a particular observation range. In an operational application, other approximations might be preferred. For example, when using a horizontal receiver array, depth-dependent, range-independent equivalent models may naturally be defined.

It is important to notice that, taking into account the inevitable subjective nature of the cost function that defines the equivalent model, the equivalent models $\Theta_E(r, z, f)$ and $\theta_E(r)$ may each one be defined by a different cost function. This is an important matter, regarding the needs of the end-user of the acoustic estimate, and the limitations of acoustic observation systems. On the one hand, the end-user might be interested in minimizing e.g. the difference

between the complex acoustic pressure and its estimate. The environmental model that satisfies this objective is the equivalent model that serves the user's purpose, $\Theta_E(r, z, f)$. On the other hand, such a cost function cannot be considered for acoustic inversion, due to noise from acoustic and electronic nature (to mention only a few), demanding for (noise-robust) correlation-based cost functions. The minimization of a cost function of this type gives rise to an equivalent model $\theta_E(r)$ which, in principle, will not minimize the acoustic error that interests the user. This issue is independent from the fact that $\theta_E(r)$ is a depth-frequency-independent vector. In the present work, $\theta_E(r)$ is defined as the value that minimizes the cost function specified as a complementary form of the depth-coherent, frequency-incoherent Bartlett processor (transcription of Eq. (4.3)):

$$\mathcal{C}_1(\boldsymbol{\theta}) = 1 - \frac{1}{N_f} \sum_{f=1}^{N_f} \frac{\mathbf{w}^H(f, \boldsymbol{\theta}) \mathbf{C}_{RR}(f, \boldsymbol{\theta}_0) \mathbf{w}(f, \boldsymbol{\theta})}{\|\mathbf{w}(f, \boldsymbol{\theta})\|^2 \text{tr} \mathbf{C}_{RR}(f, \boldsymbol{\theta}_0)}, \quad (5.3)$$

where $\mathbf{C}_{RR}(f, \boldsymbol{\theta}_0)$ is an estimate of the receiver data correlation matrix at frequency f , $N_f = 10$ is the number of acoustic frequencies (100 to 1000 Hz, with 100-Hz step), and \mathbf{w} is a vector of acoustic pressure candidates and a function of the candidate equivalent model value $\boldsymbol{\theta}$.

5.1.3 Numerical Results

This section presents the results of acoustic nowcast for the test case described in Sec. 5.1.1. At every time sample, the acoustic data from the receiver arrays was inverted, and the inversion outcomes were used for forward modeling the synchronous acoustic field in the ocean transect at every space-frequency point (r, z, f) . The next two sections describe the acoustic inversion results and the nowcast estimates.

Table 5.2: Parameter search bounds and discretization for acoustic inversion, to solve the problem of acoustic nowcast.

Parameter	Lower bound	Upper bound	Discretization [m/s]
Basement compressional speed [m/s]	1530	1690	5.2
Sediment upper compressional speed [m/s]	1360	1610	8.1
Sediment lower compressional speed [m/s]	1510	1800	9.4
1 st EOF coefficient [m/s]	-26	24	1.6
2 nd EOF coefficient [m/s]	-19	31	1.6
3 rd EOF coefficient [m/s]	-4.7	45	1.6
4 th EOF coefficient [m/s]	3.2	53	1.6
5 th EOF coefficient [m/s]	-5.3	45	1.6
6 th EOF coefficient [m/s]	-28	22	1.6
7 th EOF coefficient [m/s]	-25	25	1.6
8 th EOF coefficient [m/s]	-24	26	1.6

Acoustic Inversion

For the acoustic inversion, the software package SAGA was employed [Ger07], in which SNAP was used as the forward model. This package implements a genetic algorithm-based global search to minimize the cost function in Eq. (5.3) with respect to ocean-environmental parameters, defined here as the components of the equivalent model vector. For the inversion, the search bounds and discretization for the parameters are described in Tab. 5.2. The search bounds and discretization were chosen by trial-and-error, in such a way to have a sufficiently fine discretization, without compromising the computational load, and have a low acoustic error at the end of the inversion. It is observed in Tab. 5.2 that some values are rather unrealistic, such as the minimum bound of 1360 m/s for the sediment upper compressional speed. However, taking into account that the objective of the present work is to accurately model the acoustic field (and not to estimate environmental parameters), in a context of environmental mismatch, unrealistic bounds are expected and necessary for some parameters. The search was performed with 12 independent populations, each with 2000 forward modeling runs, and 100 individuals per population. The acoustic inversion results

corresponding to the equivalent model parameters listed in Tab. 5.1, for all the time samples, are shown in Fig. 5.6. The results differ from array to array, which demonstrates the space-

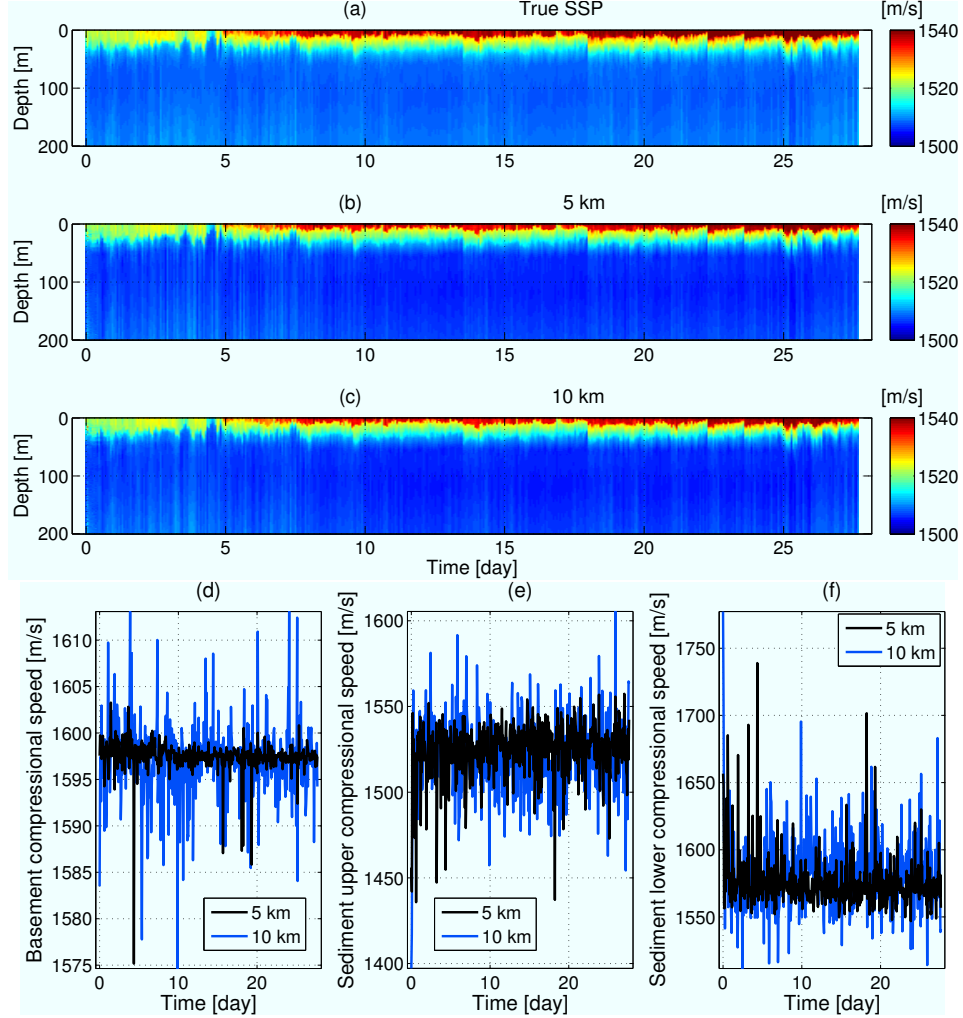


Figure 5.6: Acoustic inversion results for the parameters in Tab. 5.2. The true sound speed profile time history is shown in (a), followed by its corresponding inversion results (computed from the empirical orthogonal function coefficients), at the 5- (b) and the 10-km acoustic receiver array (c). The bottom three graphs show the inversion results for basement compressional speed (d) and sediment compressional speed (upper (e) and lower (f)). Here, the black and the blue lines correspond to the 5- and the 10-km receiver array, respectively.

dependence of the equivalent model. Figure 5.7 shows the sum of the difference between the true and the equivalent SSP, computed as $\sum_{m=1}^M [c(z_m) - \hat{c}(z_m)]$, $m = 1, 2, \dots, M$, where M , z_m , c and \hat{c} designate the number of profile depths, the m^{th} depth, the true sound speed and the estimated sound speed, respectively. It is seen that the difference between the true

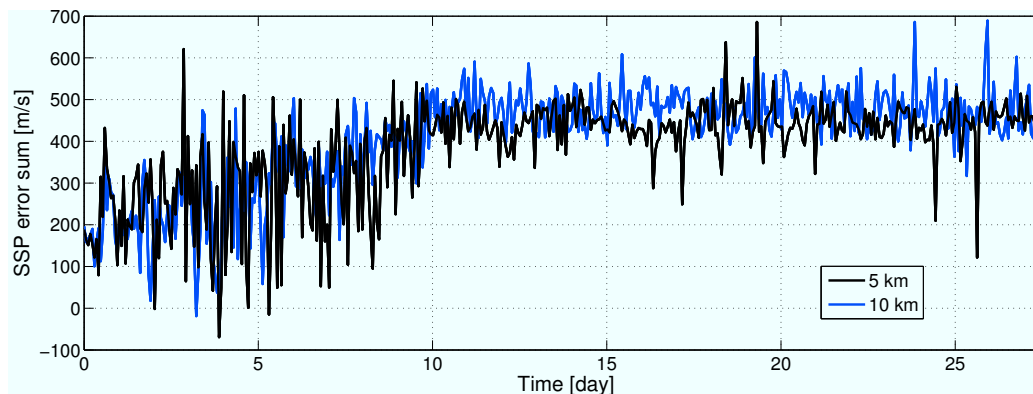


Figure 5.7: Sum of the difference between the true and the equivalent sound speed profile. The black and the blue lines correspond to the 5- and the 10-km receiver array, respectively.

and the estimated SSPs has an increasing trend before day 10, presenting a smaller variability afterwards. This behavior correlates with the evolution of the EOFs' structure, as seen in Fig. 5.5. The EOFs and the average SSP, which are computed from the SSPs in mismatch (see Fig. 5.2), define a structure for the equivalent SSPs which is less downward-refracting than for the true SSPs. This structure becomes more prominent over time, stabilizing according to the EOF smaller time variability. Regarding the geoacoustic component of the equivalent model, four observations can be made. As a first observation, the equivalent geoacoustic values are in general smaller than their true counterparts, for both arrays. This can be due to two reasons: 1) the baseline model assumes that the ocean bottom is more reflective than in reality, which is expressed in every property, as seen in Fig. 5.2; a lower value than the true one for the equivalent geoacoustic sound speeds, combined with the other presumably more reflective bottom parameters, will 'restore' the bottom absorption; 2) lower values for the equivalent geoacoustic parameters compensate for the equivalent SSP structure (less downward-refracting than in the true SSP), acting in the sense of trapping the acoustic energy that reaches the bottom. In particular, after day 10, the equivalent basement compressional speed stabilizes to lower values (see Fig. 5.6 (d)). As a second observation,

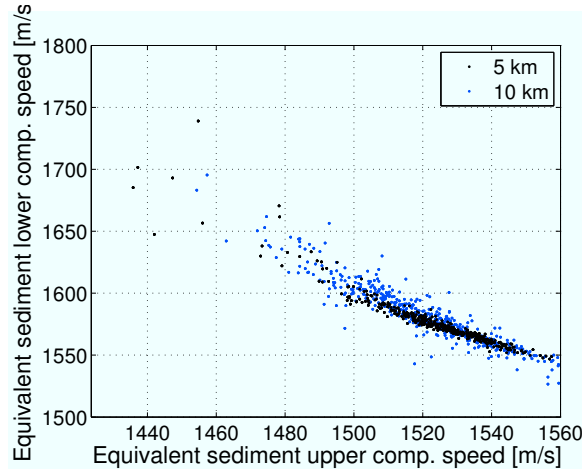


Figure 5.8: Equivalent sediment speeds shown against each other, for the acoustic nowcast exercise.

the equivalent geoacoustic values have more variance for the array at 10 km. This result is in principle explained by the cumulative acoustic error imposed by the environmental mismatch, whose effect is enhanced and less stable as the acoustic energy travels along the waveguide. As a third observation, it is seen in Fig. 5.6 (e) that the equivalent sediment upper compressional speed has a slightly increasing trend, as opposed to the equivalent sediment lower compressional speed —Fig. 5.6 (f). This can be explained as a mechanism to compensate for the structure of the equivalent SSP. The equivalent sound speed values in the sediment define a progressively smaller gradient over time, which reflects less energy back to the water column (the true gradient is 24 s^{-1} , represented in Fig. 5.2 (a)). As a fourth observation, the equivalent sediment sound speeds are strongly ‘correlated’. This is made explicit in Fig. 5.8, which shows a strong relationship between the sound speeds, and is an example of a ‘partial’ equivalent model. By taking for example a point close to the true values of sediment sound speed as a reference, a much lower sediment upper compressional speed (acting as an acoustic energy attractor) can be compensated by a much higher sediment lower compressional speed, and conversely, still producing a similar acoustic field.

The acoustic misfit at the end of the inversion exercise as defined in Eq. (5.3), is shown in Fig. 5.9. It is seen that before day 1, the acoustic misfit is relatively high, stabilizing

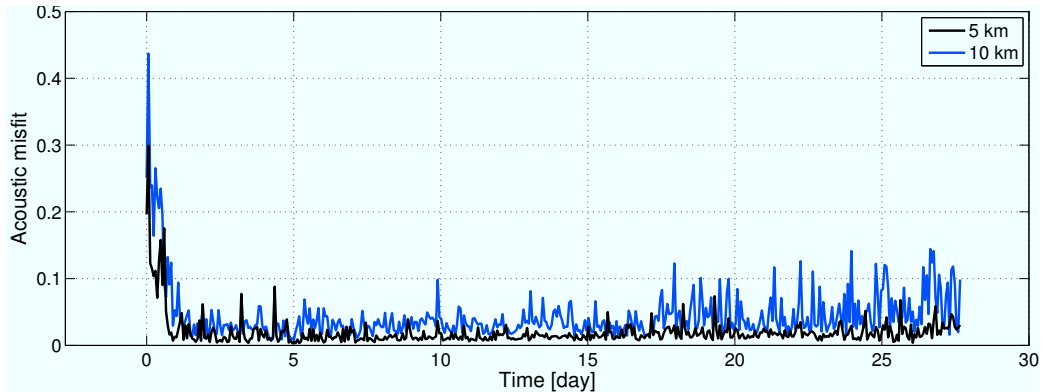


Figure 5.9: Acoustic cost in Eq. (4.3) at the end of the inversion, for the arrays at 5 (black) and 10 km (blue).

to lower values (< 0.15) after day 3, in both receiver arrays. The initial values correspond to a period of little water column information (it is only after 11 h of data acquisition that eight SSP casts are available, the minimum necessary to estimate the shape of the eight EOFs used in the SSP parameterization). The average acoustic misfit corresponding to the receiver array at 10 km is larger than its homolog for 5 km, mainly after day 17. This is probably due to the fact that the range-accumulated effect of mismatch at 10 km is more difficult to be canceled than the one at 5 km, specially in the situation in which there is a significant interaction of the acoustic energy with the ocean bottom, due to the more pronounced downward-refracting true SSPs after day 17, as seen in Fig. 5.6 (a).

Acoustic Field Nowcast

Taking into account the range-dependent approximation for the equivalent model established in Rem. 5.1, the first question, after having at hand equivalent outcomes representing the 5- and 10-km range, is how to interpolate/extrapolate these values in space, in order to obtain an equivalent model outcome representative of every ocean transect range. In order to answer

this question, five environmental parameterizations of the full transect were considered:

1. The transect is modeled as range-independent, whose environment coincides with a priori assumptions as represented in Fig. 5.2. This is the “baseline” environment.
2. The transect is modeled as range-independent, whose environment coincides with the inversion outcome at 5 km;
3. Same as in point 2, except that the inversion outcome is obtained at 10 km;
4. The transect is modeled as range-dependent, according to Fig. 5.10 (a).
5. For each range in which to estimate the field, a range-independent transect is defined, according to Fig. 5.10 (b).

The approaches 4 and 5 are described in detail in the following. In approach 4, the ocean transect was modeled as composed of two range-independent sectors, each one 5 km in length. In the first sector, defined between 0.5 and 5 km from the acoustic source, the environmental model was made coincident with the acoustic inversion outcome at 5 km. In the second sector, defined between 5 and 10 km from the acoustic source, the environment was made coincident with the acoustic inversion outcome at 10 km. Refer to Fig. 5.10 (a), for an illustration. In parameterization 5, the ocean transect was not fixed to any particular environmental structure. For each range from the acoustic source at which it is intended to estimate the field (in a vertical set of receiver depths), a particular range-independent environment was defined between the acoustic source and the required receiver range. For receiver ranges in the interval $[0.5, 5]$ km, the range-independent environment coincides with the inversion outcome at 5 km. For a receiver range of 10 km, the range-independent

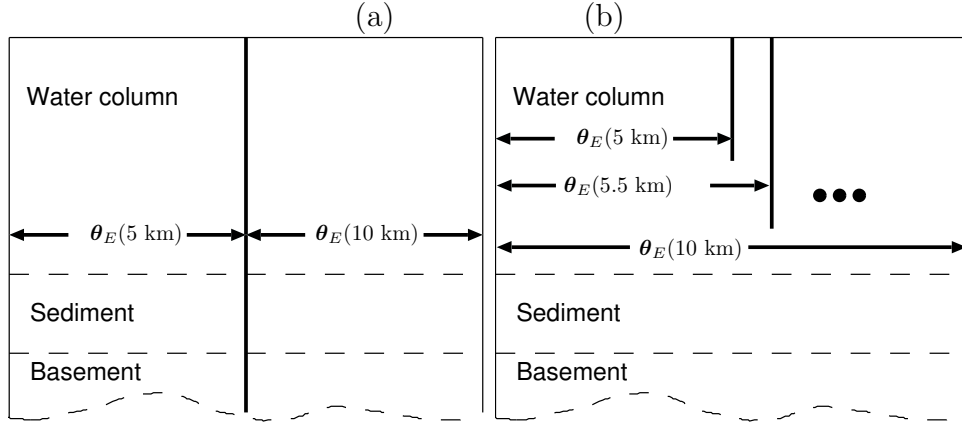


Figure 5.10: Approaches 4 (a) and 5 (b) for estimating the equivalent model for acoustic nowcast, in the 10-km transect. The approaches differ only for ranges in the $]5, 10]$ -km interval. In approach 4, the equivalent model is defined as a two-sector range-dependent environment, bounded at 5 km. The sectors coincide with the acoustic inversion outcomes at 5 and 10 km, respectively. In parameterization 5 (see list above), a range-independent environment is defined for each range in which to estimate the field. For ranges in the interval $]5, 10]$ km, the equivalent model is computed from spline-interpolation of the 5- and 10-km inversion outcomes.

environment coincides with the inversion outcome at 10 km. For each receiver range in the interval $]5, 10[$ km, a spline interpolator determined the parameter values of each range-independent environment to be used. The spline passes through the inversion outcomes at 5 and 10 km, and has zero first-order derivative at these ranges. Figure 5.11 shows an example of interpolation, for sediment upper compressional speed.

The above five equivalent model structures were provided as input to the propagation model SNAP (it is required that the propagation model used for forward modeling is the same as the one used for acoustic inversion), in order to compute the acoustic nowcast for every time sample. The acoustic estimates are characterized by two error functions. These are the complementary Bartlett misfit as defined in Eq. (4.3), and a transmission loss (TL) (with importance in several sonar applications) error measure:

$$\mathcal{C}_B(\boldsymbol{\theta}_E, r, t) = 1 - \frac{1}{N_f} \sum_{f=1}^{N_f} \frac{\mathbf{w}^H(\boldsymbol{\theta}_E, r, f, t) \mathbf{C}_{RR}(\boldsymbol{\theta}_0, r, f, t) \mathbf{w}(\boldsymbol{\theta}_E, r, f, t)}{\|\mathbf{w}(\boldsymbol{\theta}_E, r, f, t)\|^2 \text{tr}(\mathbf{C}_{RR}(\boldsymbol{\theta}_0, r, f, t))}, \quad (5.4)$$

$$\mathcal{C}_T(r, z, f, t) = \left| TL(r, z, f, t) - \hat{TL}(r, z, f, t) \right|, \quad (5.5)$$

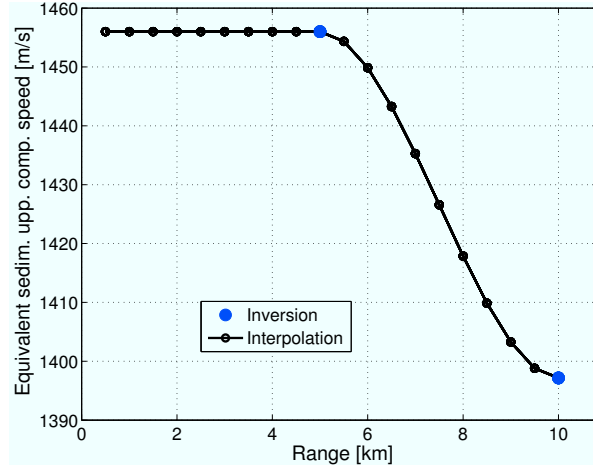


Figure 5.11: Interpolation of the acoustic inversion results to estimate an equivalent model component, using the sediment upper compressional speed as an example. For a range in the interval 0 to 5 km, the equivalent speed estimate coincides with the inversion outcome at 5 km. For a range between 5 and 10 km, the estimate is the result from a Hermite polynomial-spline interpolation, using the inversion outcomes at 5 and 10 km. The spline has zero derivative at 5 and 10 km.

respectively, where $\text{tr}()$ is the trace operator, and TL and \hat{TL} represent true and estimated TL, respectively, defined by:

$$TL(r, z, f, t) = -20 \log_{10} |u(r, z, f, t)|, \quad (5.6)$$

$$\hat{TL}(r, z, f, t) = -20 \log_{10} |\hat{u}(r, z, f, t)|, \quad (5.7)$$

where $u(r, z, f, t)$ and $\hat{u}(r, z, f, t)$ represent the true and the estimated acoustic field, respectively, defined as the ratio between the actual acoustic pressure at a given point and the acoustic pressure at 1-m distance from the acoustic source. Due to the difficulty in analyzing the multidimensional errors in Eqs. (5.4) and (5.5), ‘marginal’ range- and frequency-dependent error average and standard deviation measures were defined from Eqs. (5.4) and

(5.5), to easily characterize the acoustic estimates. The average values were defined as:

$$\mu_{Br}(r) = \frac{1}{N_t} \sum_{t=1}^{N_t} \mathcal{C}_B(r, t), \quad (5.8)$$

$$\mu_{Tr}(r) = \frac{1}{N_z N_f N_t} \sum_{z=1}^{N_z} \sum_{f=1}^{N_f} \sum_{t=1}^{N_t} \mathcal{C}_B(r, z, f, t), \quad (5.9)$$

$$\mu_{Tf}(f) = \frac{1}{N_r N_z N_t} \sum_{r=1}^{N_r} \sum_{z=1}^{N_z} \sum_{t=1}^{N_t} \mathcal{C}_T(r, z, f, t), \quad (5.10)$$

A frequency-dependent Bartlett-based acoustic error is not considered, since the elementary error in Eq. (5.4) already considers an average over frequency. The standard deviation values were defined as:

$$\sigma_{Br}(r) = \sqrt{\frac{1}{N_t - 1} \sum_{t=1}^{N_t} (\mathcal{C}_B(r, t) - \mu_{Br}(r))^2}, \quad (5.11)$$

$$\sigma_{Tr}(r) = \sqrt{\frac{1}{N_z N_f N_t - 1} \sum_{z=1}^{N_z} \sum_{f=1}^{N_f} \sum_{t=1}^{N_t} (\mathcal{C}_T(r, z, f, t) - \mu_{Tr}(r))^2}, \quad (5.12)$$

$$\sigma_{Tf}(f) = \sqrt{\frac{1}{N_r N_z N_t - 1} \sum_{r=1}^{N_r} \sum_{z=1}^{N_z} \sum_{t=1}^{N_t} (\mathcal{C}_T(r, z, f, t) - \mu_{Tf}(f))^2}. \quad (5.13)$$

Figure 5.12 shows the Bartlett-based acoustic error computed with Eqs. (5.8) and (5.11), corresponding to the five environmental parameterizations described in p. 95. Figure 5.12 (a) shows the error corresponding to all the parameterizations computed from acoustic inversion, while Fig. 5.12 (b) shows the error corresponding to parameterizations 1 (baseline environment) and 5 (the one corresponding to the minimum error). All the parameterizations lead to errors which increase with range, in principle due to the range-accumulated effect of environmental mismatch. As expected, the baseline parameterization (index 1, as in p. 95 —Fig. 5.12 (b)) corresponds to the highest error, since the baseline environment is not optimized to minimize any acoustic cost. The effect of acoustic inversion is significant, in terms of minimizing the Bartlett-based error, as seen in the error corresponding to all the other

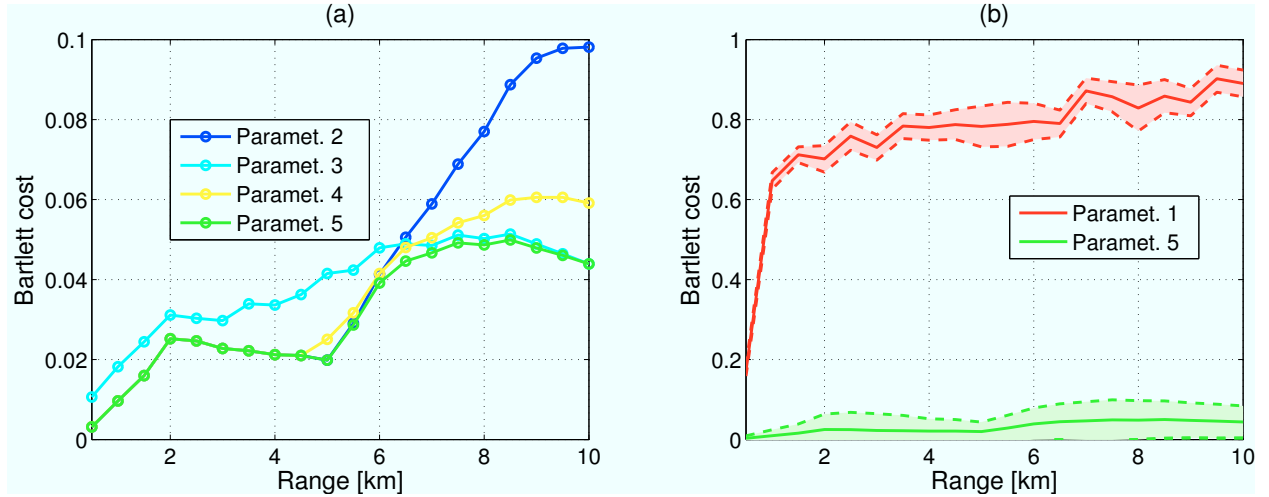


Figure 5.12: Bartlett-based acoustic estimation error as a function of range, when using each of the five environmental parameterizations described in p. 95. Those parameterizations, from 1 to 5, correspond to the colors pink, blue, cyan, yellow and green, respectively. In (a), all the parameterizations using equivalent models (indices 2 to 5) are compared, in terms of the corresponding average acoustic error, defined in Eq. (5.8). In (b), the parameterization 5 is compared with the parameterization 1 (baseline environment). In this case, the acoustic error is shown as an error band bounded by the average \pm one standard deviation (see Eq. (5.11)) (negative values clipped to zero).

parameterizations. Though the acoustic inversion outcome is in mismatch, this mismatch is optimized to minimize an acoustic cost, adapted to the mismatch in the parameters that are fixed during the inversion process. Regarding the equivalent models defined with information originating from a single receiver array (indices 2 and 3, as in p. 95), by referring to Fig. 5.12 (a), it is observed that the equivalent model obtained at each array drives the acoustic error to a low value at the corresponding array position, but not necessarily elsewhere. Nevertheless, when using the equivalent model found at 10 km (parameterization 3, as in p. 95), the Bartlett-based error at ranges < 5 km is acceptably low. This can be explained by the fact that the acoustic inversion outcome at 10 km constrains the modeled propagation features to be similar to true propagation, simultaneously reducing the error at ranges < 5 km. Regarding the equivalent models defined with information originating from the two receiver arrays (parameterizations 4 and 5, as in p. 95), the range-independent-based equivalent model (parameterization 5) leads to a lower acoustic error than the range-dependent

model (parameterization 4), as seen in Fig. 5.12 (a) (green and yellow curves, respectively). In fact, the range-independent-based equivalent model provides a lower bound on the error, over all the equivalent models tested. To be precise, only at the measuring receiver array ranges it is guaranteed that a lower bound is given by this equivalent model, since those are the positions at which the acoustic inversion exercise minimized the Bartlett-based acoustic cost, constrained on a range-independent environment. Any other environmental parameterization, including the range-dependent model, will not be ‘naturally’ suitable for forward modeling. This explains the deviation between the yellow and the green curves in Fig. 5.12 (a), for ranges greater than 5 km.

The error in TL, computed with Eqs. (5.9) and (5.12), is shown in Fig. 5.13, color-coded as in Fig. 5.12. In terms of relative average error, the pattern is similar to the

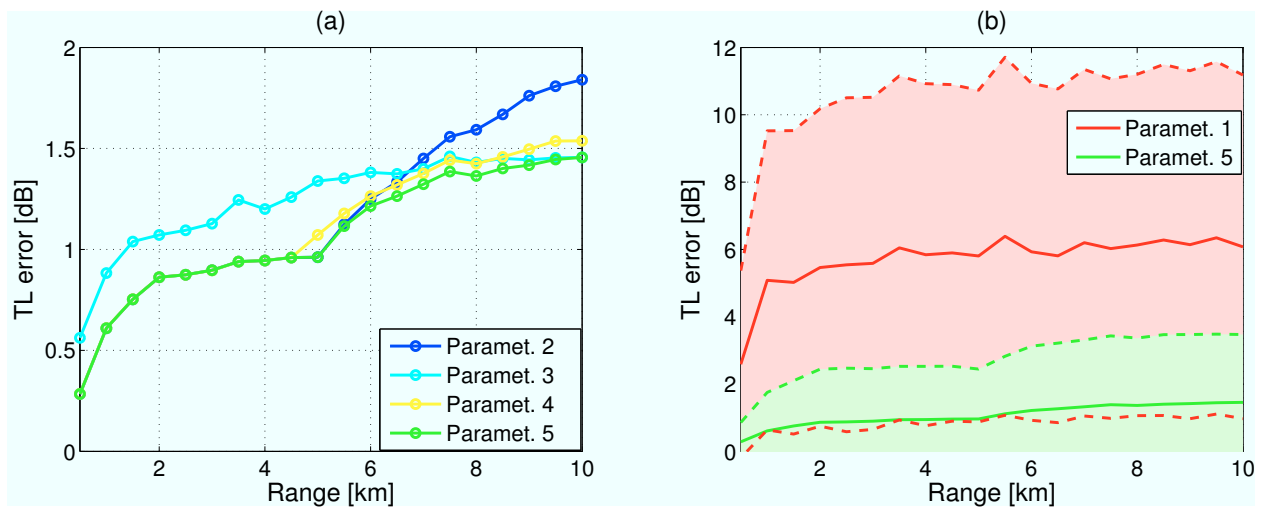


Figure 5.13: Transmission loss estimation error as a function of range, when using each of the five environmental parameterizations explained in p. 95. Those parameterizations, from 1 to 5, correspond to the colors pink, blue, cyan, yellow and green, respectively. In (a), all the parameterizations using equivalent models (indices 2 to 5) are compared, in terms of the corresponding average acoustic error, defined in Eq. (5.8). In (b), the parameterization 5 is compared with the parameterization 1 (baseline environment). In this case, the acoustic error is shown as an error band bounded by the average \pm one standard deviation (see Eq. (5.11)) (negative values clipped to zero).

one corresponding to the Bartlett-based error in Fig. 5.12. Care should be taken when

interpreting these results. As mentioned previously, the equivalent model that minimizes the cost function used in the acoustic inversion might not minimize the error that interests the user. The particular scenario will determine if the Bartlett-derived equivalent model is suitable to minimize that error. For instance, if the interest is on TL, then a TL cost function should be used in the acoustic inversion. However, the presence of noise in the acoustic data might prevent obtaining a meaningful equivalent model from acoustic inversion with a cost function based on TL. The present case is an example of a favorable behavior of TL error obtained with the Bartlett-based equivalent model, though it is not shown (outside the scope of the present work) if the TL error could be further reduced. Fig. 5.13 (b) shows acoustic error bands defined as average error \pm one standard deviation (negative values clipped to zero), corresponding to the baseline (parameterization 1, as in p. 95) and the range-independent-based equivalent model derived with data from the two acoustic arrays (parameterization 5, as in p. 95). Two interesting facts are observed. First, the standard deviation of the error is rather large, as compared to its average. This can be explained by the definition in Eq. (5.5), which requires computing the ratio between the estimated and the true field, which can become unstable, for large values of the former and small values of the latter. Second, it is observed that the error bands intersect. This is probably a combined effect of the above-mentioned instability and the fact that it is not guaranteed that the equivalent model obtained by acoustic inversion (using the Bartlett error as the cost function) also minimizes the TL error. In a situation of no environmental mismatch, the inversion of noiseless acoustic data would produce an environmental outcome which would drive any acoustic estimation error to zero. In that case, both the Bartlett error and the TL error would vanish. In the presence of environmental mismatch, there is no guarantee of the

equivalent model minimizing simultaneously both acoustic errors, because the definition of the errors is fundamentally different. For example, since the TL error is insensitive to signal phase, the TL error might exhibit low values for acoustic estimates which correspond to high Bartlett errors, or vice-versa. Figure 5.14 shows the ‘marginal’ TL error as a function of frequency. In terms of the average value, for the equivalent models obtained from acoustic measurements, it is seen in Fig. 5.14 (b) that there is a general trend for the error to increase with frequency. This can be explained by a residual environmental mismatch which could not be compensated by acoustic inversion at any of the receiver array locations. The consequence of this mismatch is more pronounced at shorter wavelengths (higher frequencies), due to a greater extent of accumulation of acoustic propagation errors. This is expressed also in terms of the standard-deviation of the error corresponding to the range-independent-based equivalent model (see Fig. 5.14 (a)). Though the average acoustic errors corresponding to the equivalent models differ only by a fraction of a decibel, their relative values are ordered in a similar way as compared to the range-dependent errors shown in Fig. 5.13 (d). The equivalent model obtained from the acoustic data at 10 km produces the highest acoustic errors, followed by the one corresponding to 5 km, then the range-dependent model, and finally the range-independent-based model. The high standard deviation and the intersection of the error bands in Fig. 5.14 (a) may have a similar explanation to the one in Fig. 5.13 (c) for the range-dependent error.

In summary, the inversion of acoustic data at particular array locations allows to obtain environmental parameterizations which, besides leading to a low acoustic error at the array locations, force the propagation of acoustic energy to be similar to the true propagation phenomenon, between the acoustic source and the array. The residual mismatch that cannot

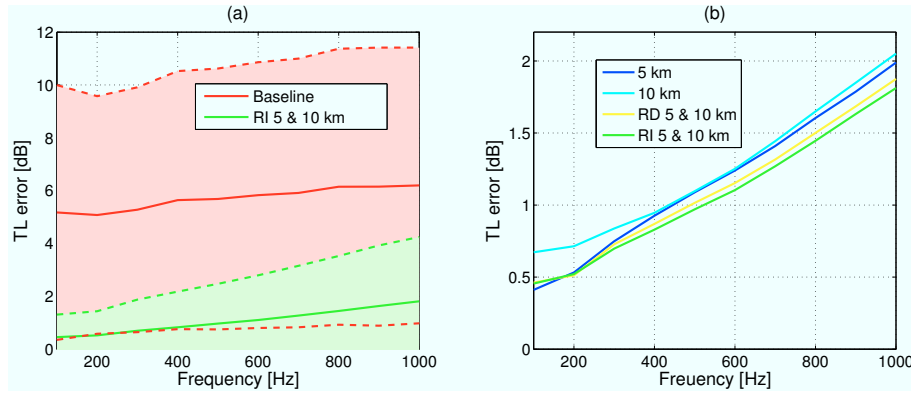


Figure 5.14: Transmission loss error corresponding to the baseline and the equivalent models, as a function of frequency. (a) Comparison for the usage of the baseline or the equivalent model defined as in “Approach 5” of Fig. 5.10; (b) comparison for the usage only of equivalent models.

be canceled out by acoustic inversion will be visible mainly at larger frequencies and ranges. If no use is made of acoustic observations to define/estimate an equivalent model, then the particular baseline environment will only by coincidence lead to small acoustic errors, making the difference between the true and estimated propagation patterns to have an irregular and unpredictable structure, conditioned on the environmental mismatch. Finally, one difficulty in estimating the acoustic field via equivalent environmental modeling is to know a priori which ocean locations are optimal to deploy the ‘calibrating’ receiver arrays. This is a non-trivial question. Only after deploying a high number of receiver arrays, it would be possible to invert the array data for the respective equivalent models, the latter used to solve the forward modeling problem. The final acoustic error would reveal which arrays could be discarded, for providing redundant information regarding the equivalent model. A less strict, more feasible approach is to deploy a single acoustic receiver array at the farthest range of interest. This is supported by the above results, which show that the array data at mid-range leads to an acoustic error which is more unstable with distance (varying between 0.3 and 1.8 dB) than the one corresponding to the array at the farthest range (with error varying between 0.6 and 1.5 dB). In terms of frequency dependence for the acoustic error,

there is no significant difference between the arrays. Thus, a single array deployed at the farthest range is likely to be able to ‘calibrate’ the propagation model at hand, for estimation of the acoustic field at all transect points, with small variance.

5.2 Acoustic Forecast

This section presents the approach adopted for acoustic forecast, i.e., the estimation of the acoustic field in an idealized ocean transect at any time sample posterior to the period of acoustic-oceanographic observation (recall Figs. 2.2 and 5.2). The estimation of the future acoustic field is treated here by fusing the time evolution of a suitable ocean circulation model with synthetic acoustic data received at a single vertical array, a baseline environmental description of the target oceanic area, and water column measurements (when applicable). In practice, the approach uses the acoustic inversion estimates and the oceanographic forecast of the water column at all times in the interval $[t_0, t_P]$ (past data), in a training phase. A functional mapping from oceanographic forecast to equivalent model —acoustic inversion estimate— is then determined. This mapping is fed a posteriori with the oceanographic forecast for the required future time t_F (or a SSP estimated from the forecast and the water column measurement), giving an equivalent model estimate. This estimate, in conjunction with the baseline assumptions and the oceanographic forecast, defines the full environmental parameterization for future time t_F , to be used in acoustic forward modeling. In order to discern the influence of the sources of estimation error, two cases of oceanographic forecast quality are analyzed: one in which the forecast simply coincides with the CTD measurement (an ideal oceanographic forecast), and one in which the forecast is computed with the Navy Coastal Ocean Model (NCOM), as used in the MREA’03 sea trial. In the latter case,

the sound speed forecasts to be used were defined as the result of linear interpolation of NCOM-computed SSPs to the space-time points of CTD measurement. Though in reality the NCOM model provided forecasts for a 48-h prediction window, it is considered here that the forecasts are available a priori for every future time sample in the full period (\approx one month) underlying the estimation exercise. The intention is to find an upper bound on the accuracy of the acoustic field estimate, independent of the oceanographic prediction window (which will likely increase in the future generations of ocean prediction systems). The problem of acoustic forecast is solved as a three-step process. In the first step, the equivalent model corresponding to present time is computed from acoustic inversion. In the second step, the equivalent model at the particular future time for which to compute the forecast, is estimated. In the third step, this estimate serves as input to an ocean acoustic propagation model whose output constitutes the acoustic forecast.

5.2.1 Acoustic Forecast Test Case

This section describes the test case that supports the numerical results of acoustic forecast. The synthetic acoustic field to be predicted is produced by an acoustic source in an ocean transect as shown in Fig. 5.15 (a). Similarly to what was considered for the example that supported the nowcast exercise in Sec. 5.1, it is assumed that some of the environmental parameters are taken with incorrect values, when modeling the acoustic field. This is the case exclusively of the water column depth and the geoacoustic parameters (see Fig. 5.15 (b)). The assumed known geoacoustic parameters describe an ocean bottom which absorbs more acoustic energy than the true one (in Fig. 5.15 (a)). This can be seen on the baseline underestimated sound speed and density, and overestimated attenuation.

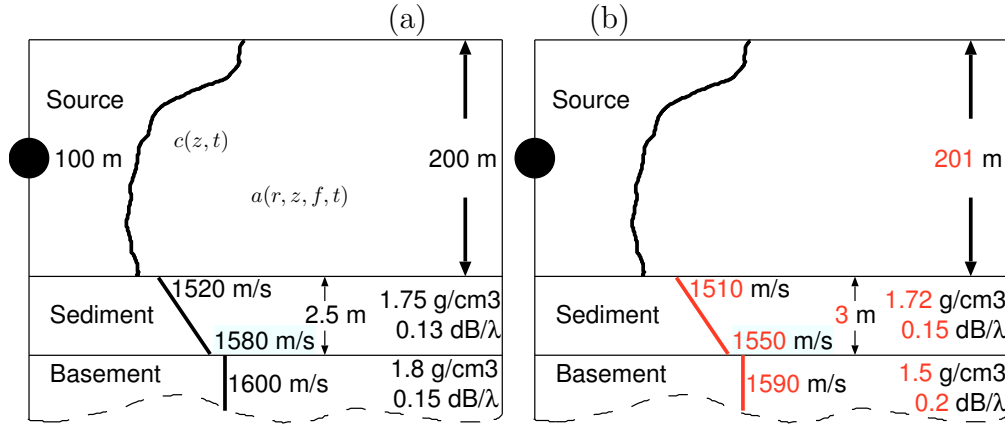


Figure 5.15: Idealized ocean transect in which the acoustic field forecast is to be computed. (a) True and (b) baseline environment. The red values express the parameters that are in mismatch.

5.2.2 Solution to the Acoustic Forecast

In order to forecast the acoustic field, the acoustic inversion outcomes obtained up to present time t_P , together with the oceanographic forecasts and baseline environmental information, enter an estimation block whose output is the estimate of the future equivalent model, $\hat{\theta}_E(t_F)$. This estimate is given as input to the acoustic propagation model, whose output constitutes the acoustic forecast $\hat{u}(r, z, f, t_F)$. The estimator of the future equivalent model is defined in Rem. 5.2.

Remark 5.2: The depth-frequency-independent equivalent model $\theta_E(r, t)$ as defined in Rem. 5.1 is a function \mathcal{M} of the true environment $\theta_T(r, t)$, due to its definition as the value that minimizes a cost function involving the measured acoustic field, which is a function of the true environment. Given an estimate $\hat{\mathcal{M}}$ of \mathcal{M} , then $\hat{\theta}_E(r, t_F) = \hat{\mathcal{M}}(\theta_T(r, t_F))$ or $\hat{\theta}_E(r, t_F) = \hat{\mathcal{M}}(\hat{\theta}_T(r, t_F))$ is an estimator of $\theta_E(r, t_F)$, where $\theta_T(r, t_F)$ and $\hat{\theta}_T(r, t_F)$ designate the future true and estimated true environment, respectively.

Remark 5.2, supported by Fig. 5.16, expresses that if an estimate of the mapping between the true environmental properties and the equivalent model is available, then the application of the estimated mapping to a future true environmental vector (or an estimate of it) will give an estimate of the corresponding future equivalent model. Here, an assumption of stationarity is made, supposing that \mathcal{M} is time-invariant. This assumption allows to estimate \mathcal{M} with past environmental data, and then use this estimate with data representing the

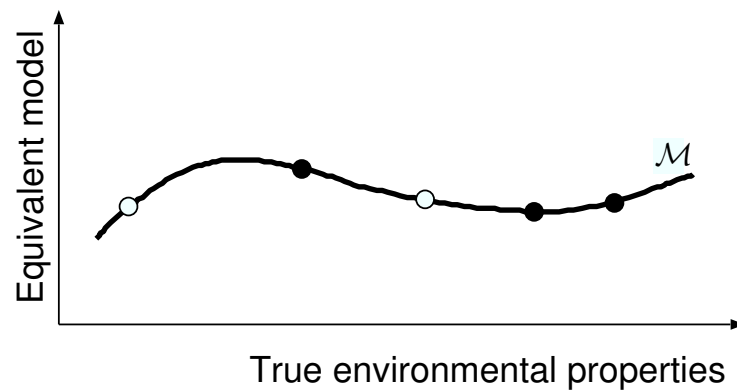


Figure 5.16: Hypothesis used for equivalent model forecast: the equivalent model is a function \mathcal{M} of the true environmental properties. The dots represent imaginary up-to-present-time (black) and future-time (white) data.

future environmental properties. The estimator described in Rem. 5.2 was applied in the present work, and is the main component of the acoustic forecast algorithm. Thus, the forecast of the equivalent model is not treated as a conventional forecast problem in the sense of modeling the time evolution of the quantity of interest. Instead, it is treated as a curve fitting problem, in which the equivalent model is interpreted as a function (mapping) \mathcal{M} of environmental data. The quality of the estimate of this “function” as well as of the future environmental data (object of the function) are the main factors determining the quality of the equivalent model estimate, hence of the acoustic forecast. The next sections elaborate on the estimation of \mathcal{M} .

Function Approximation

The estimation of the future equivalent model is based on determining a mapping \mathcal{M} between environmental properties —the predictors— and acoustic inversion outcomes —the response. The predictors consist of the oceanographic forecast sound speed values of each profile, and the response is the equivalent sediment upper compressional speed, in the illustrative example presented in the next sections. The estimation of the mapping \mathcal{M} was treated as a function

approximation problem, resorting to a support vector machine (SVM), whose concept is summarized in the next section. Function approximation was executed with training data relative to the time samples t_0, t_1, \dots, t_P , where t_P is the present time, the last instant of acoustic-oceanographic observation. Machine learning techniques have been used in the past, to predict acoustic inversion outcomes, using the acoustic field as input (predictor) to a radial basis function network, to predict the inversion results for seafloor parameters[CJ96]. In the present work, the predictors are environmental properties, and the learning tool is an SVM.

Support Vector Machine Function approximation was here tackled with support vector machines (SVMs). These are tools used in data mining, with documented reliable results. The next paragraphs resume the most important topics concerning SVMs, for their use as regressors in the problem of equivalent model forecast.

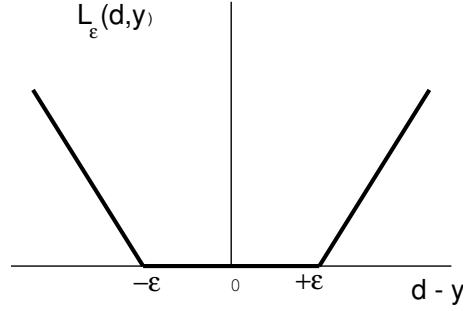
Generalities The SVM is an approach for supervised learning that takes as input an annotated training data set, and outputs a model which can then be used to predict the outcomes of future events[VGN92, Vap98]. Support vector machines have been used for solving classification, regression and linear operator inversion problems. Applications in classification include object and optical character recognition[SBV95, SSM98], speaker identification[SG96], face detection[OFG97], and text categorization[Joa98]. In regression, important examples are time series prediction[DBK⁺97, SGV99], image compression[GPCVGM05], financial applications[CT03], mass detection systems[SJ09], estimation of target-to-interferer ratio[HW11], and the positron emission tomography operator inversion problem[VSA97]. Support vector machines are attractive by a number of

features: they extract a subset of the training data which represents a stable characteristic of the data, they include mechanisms to minimize overfitting, they use kernel functions to model non-linearity, and can be trained relatively quickly on large data sets. The SVM can be interpreted as a method for the design of a feedforward neural network with a single hidden layer of nonlinear units. However, the underlying theory of an SVM avoids the need for heuristics often used in the design of neural networks. The number of hidden units is determined automatically, and the SVM training always finds a global minimum, which leads to a wider applicability[Gun98].

Application in Regression Consider a nonlinear regressive model in which the dependence of a random scalar d on a random vector \mathbf{x} is described by:

$$d = f(\mathbf{x}) + \nu. \quad (5.14)$$

The additive noise term ν is statistically independent from the input vector \mathbf{x} . The only available information is a set of training data $\{(\mathbf{x}_i, d_i)\}_{i=1}^N$, where \mathbf{x}_i is a sample of the input vector \mathbf{x} , and d_i is the corresponding value of the model output d . The problem is to provide an estimate of the dependence of d on \mathbf{x} . To construct an SVM for approximating a desired response d —performing “SVM regression”, or “support vector regression”—, a loss function $L_\epsilon(d, y)$ was originally proposed in Refs. [Vap95, Vap98], and illustrated in Fig. 5.17. The loss function $L_\epsilon(d, y)$, where ϵ is an user-defined parameter, expresses the goal of finding a function that has at most ϵ deviation from the actually obtained targets. The idea of support vector regression is based on the computation of a linear regression function in a high-dimensional feature space where the input data are mapped to via a nonlinear function. An estimate of d , denoted by y , is postulated as an expansion in terms of a set of nonlinear

Figure 5.17: ϵ -insensitive loss function.

basis functions $\{\varphi_j(\mathbf{x})\}_{j=0}^{m_1}$, as follows:

$$y = \sum_{j=0}^{m_1} w_j \varphi_j(\mathbf{x}). \quad (5.15)$$

The issue to be resolved is to minimize the cost functional

$$\Phi = C \left(\sum_{i=1}^N (\xi_i + \xi'_i) \right) + \frac{1}{2} \mathbf{w}^T \mathbf{w}, \quad (5.16)$$

subject to appropriate constraints, where ξ_i and ξ'_i are so-called “slack variables” [Hay99].

The optimization problem seeks the flattest function in feature space, which corresponds to a small \mathbf{w} . The user-specified constant $C > 0$ determines the trade-off between the flatness of f and the amount up to which deviations larger than ϵ are tolerated. A Lagrangian function is then defined, whose optimization can be stated as: given the training sample $\{(\mathbf{x}_i, d_i)\}_{i=1}^N$, find the Lagrange multipliers $\{\alpha_i\}_{i=1}^N$ and $\{\alpha'_i\}_{i=1}^N$ that maximize the convex functional

$$Q(\alpha_i, \alpha'_i) = \sum_{i=1}^N d_i (\alpha_i - \alpha'_i) - \epsilon \sum_{i=1}^N (\alpha_i + \alpha'_i) - \frac{1}{2} \sum_{i=1}^N \sum_{j=1}^N (\alpha_i - \alpha'_i) (\alpha_j - \alpha'_j) K(\mathbf{x}_i, \mathbf{x}_j), \quad (5.17)$$

where $K(\mathbf{x}_i, \mathbf{x}_j)$ is an inner-product kernel:

$$K(\mathbf{x}_i, \mathbf{x}_j) = \varphi^T(\mathbf{x}_i) \varphi(\mathbf{x}_j), \quad (5.18)$$

subject to appropriate constraints. The data points for which $\alpha_i \neq \alpha'_i$ define the support vectors for the machine. A well-grounded approach for the selection of the parameters ϵ

and C is still an open research area. An SVM for nonlinear regression may be implemented in the form of a polynomial learning machine, radial-basis function network, or two-layer perceptron. As an example, for a polynomial learning machine, we have the following inner-product kernel:

$$K(\mathbf{x}_i, \mathbf{x}_j) = (\mathbf{x}^T \mathbf{x}_i + 1)^p, \quad (5.19)$$

where the power p is specified a priori by the user.

5.2.3 Numerical Results

As discussed in previous sections, the necessary steps to compute the acoustic forecast consist of computing the equivalent model forecast, and posteriorly running an acoustic propagation model taking this forecast as input. This section shows the results of these steps, in which support vector regression was applied to compute the equivalent model used for acoustic forecast. Three estimation scenarios are described. The first one is an ideal situation of oceanographic forecasting: the forecast outcomes coincide with the water column measurements. In the second one, the oceanographic forecast is computed with the NCOM model. In the third one, in addition to using the NCOM forecasts, the CTD measurements enter the estimation scheme for the future SSP, prior to computing the acoustic forecast.

Acoustic Inversion

Acoustic inversion results for the sediment upper compressional speed were obtained, by running SAGA, performing an exhaustive search to minimize the cost function in Eq. (5.3)[Ger07]. The search space was bounded by 1510 and 1740 m/s, with a discretization of 0.25 m/s. The acoustic inversion results are shown in Fig. 5.18 (a). The equivalent sediment

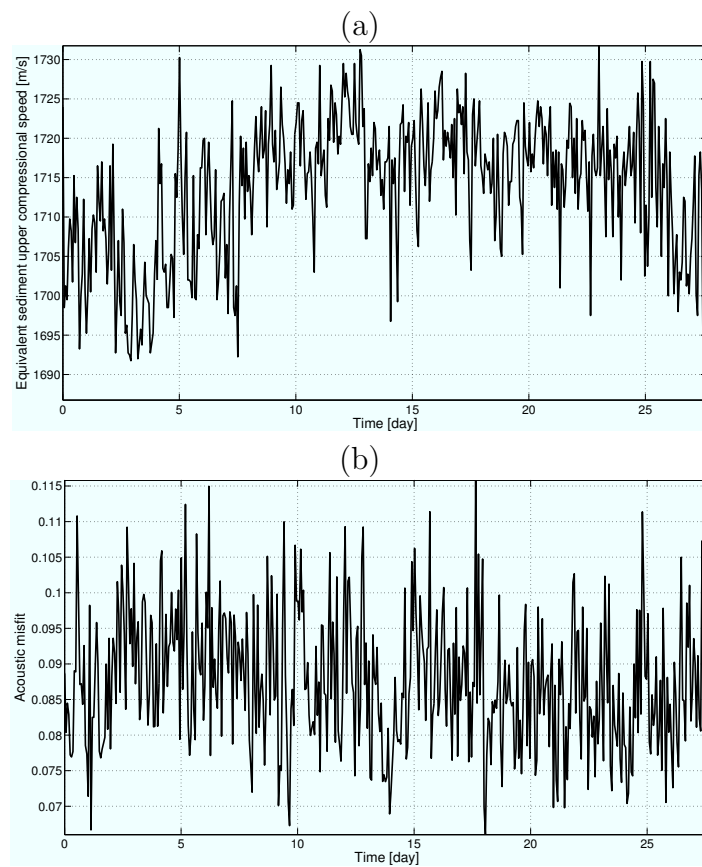


Figure 5.18: Acoustic inversion results for the forecast exercise. (a) Sediment upper compressional speed parameter estimate; (b) acoustic misfit corresponding to the previous estimate.

upper compressional speed is always superior to the true value of 1520 m/s, with differences ranging from 167 to 212 m/s. This can be explained by the mismatch existent in the ocean bottom properties, which represent a more absorbent bottom than in reality. The smaller density and sound speed, and larger compressional attenuation as assumed in the baseline environment, are here compensated by a larger equivalent sediment upper compressional speed. As seen in Fig. 5.18 (b), the acoustic misfit corresponding to the equivalent sediment upper compressional speed is acceptably low, with most of the values inferior to 0.1. This represents the potential to obtain an accurate acoustic prediction, as long as the equivalent values in Fig. 5.18 (a) can be predicted with low error with the SVM model.

Support Vector Machine Parameter Tuning

One of the important issues regarding SVMs is that they are designed for the estimation of a generic mapping between the predictors and the response. This mapping should be applicable to any value of a predictor in the input data domain. Another issue is that the estimation of this mapping requires the user to define the parameters ϵ (see Fig. (5.17)) and C (see Eq. (5.16)). In the present work, these parameters were tuned in such a way that the SVM is optimized for the input values that matter for the acoustic forecast problem. In other words, it is sufficient that the SVM produces accurate equivalent model outputs when presented with the future SSPs (oceanographic forecasts) as inputs. This principle was used as a criterion to tune the SVM, as follows. Let us consider a particular value of present time t_P , which represents the instant of the most recent acoustic measurement. The time window from initial time t_0 (the time of the first acoustic measurement) to t_P contains the training data for the SVM. Let us denote by $t_p, p = 0, 1, \dots, P$ the time sample corresponding to an

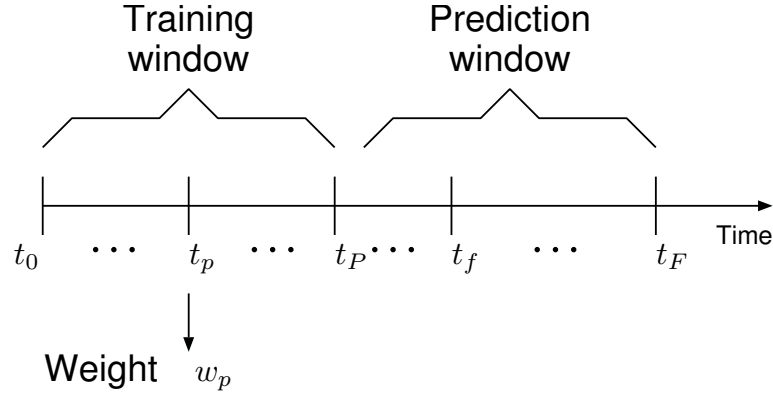


Figure 5.19: Timeline for acoustic forecast, using a support vector machine to estimate the mapping between oceanographic forecast and equivalent model. The support vector machine is trained with data acquired/produced during a “training window” (bounded by t_0 and t_P (present time)), with a time step of Δt , to estimate the future equivalent model corresponding to any time sample in the “prediction window”. The superior bound for the prediction window is t_F (farthest future time). The notation t_p and t_f designates any time sample in the training or prediction window, respectively. The time sample t_P runs from t_0 to $t_F - \Delta t$.

instantaneous sample from the training data. Similarly, let us denote by t_f , $f = P + 1, \dots, F$ a future time sample, and F the index of the farthest future time sample —refer to Fig. 5.19. Each training sample corresponding to time t_p was assigned a normalized weight w_p according to its similarity to the future SSPs:

$$w_p = 1 - \frac{\nu_p - \nu_{min}}{\nu_{max} - \nu_{min}}, \quad (5.20)$$

in which the “dissimilarity” ν_p is defined as:

$$\nu_p = \frac{1}{(F - P)N_z} \sum_{f=P+1}^F \sum_{z=1}^{N_z} |c(z, t_p) - c(z, t_f)|, \quad (5.21)$$

in which F and P are the indices of the farthest future and the present time, respectively, N_z is the number of SSP depths, t_f is the time sample of a future SSP, and ν_{min} and ν_{max} designate the minimum and the maximum of ν_p over p . The quantity ν_p indicates the average difference between each training SSP and the future SSPs. A small average difference for a particular present SSP will lead to a high weight w_p in Eq. (5.20), indicating that the particular SSP is very similar to the future SSPs. In this case, the corresponding equivalent

model value should be given a high weight for estimating the future equivalent model. These weights were used in defining a cost function ϕ which compares the training targets with their corresponding SVM-estimated values. This cost function depends on C and ϵ :

$$\phi(C, \epsilon) = \frac{1}{P+1} \sum_{p=0}^P ((\theta_E(t_p) - \hat{\theta}_E(t_p, C, \epsilon))w_p)^2, \quad (5.22)$$

and its minimum gives the values of ϵ and C to use in the training of the SVM to predict the equivalent model. This optimization was performed for every present time t_P , which runs from initial time t_0 to $t_F - \Delta t$ (Δt is the prescribed time step in the time axis).

Ideal Circulation Model

This section presents the acoustic forecast results in the context of ideal oceanographic modeling, i.e., an idealized situation in which the oceanographic forecast is forced to coincide with the actual water column SSP, at every time sample. First, the equivalent model forecast is described. Second, the acoustic forecast results are presented.

Equivalent Model Forecast This paragraph describes the results of equivalent model forecast. The equivalent model is composed solely of the sediment upper compressional speed. This is the free parameter, whose optimal values shown in Fig. 5.18 compensate for the mismatch in the parameters shown in Fig. 5.15. Such a simplified equivalent model serves the purpose of illustration, where the focus is on the method of acoustic forecast, in which the relationship between the water column sound speed and the equivalent model is the core functional to be estimated. Nonetheless, the low acoustic misfit observed in Fig. 5.18 shows that low acoustic errors can be obtained with this simplified equivalent model. Should more parameters be required to enter the equivalent model vector, then either an equivalent model

forecast procedure as described below could be applied to each parameter independently, or the full equivalent model could be predicted simultaneously for the future times of interest. As explained in the previous sections, the forecast was tackled as a regression exercise, performed by an SVM. The kernel was chosen as a first-order polynomial ($p = 1$, in Eq. (5.19)), and the implementation is attributed to Chan and Lin, who developed the LIBSVM library[CL11]. The true water column SSP is the only environmental property that changes over time, and explains the features of the equivalent model time series. Hence, only water column properties were taken as predictors. Ideally, the true water column properties should be considered to both: 1) train the regression model and 2) be used as future properties to be given as input to this model. This situation is feasible in the present context, since the synthetic oceanographic model outputs coincide with the true SSP. As an example, let us consider the problem of predicting the equivalent sediment upper compressional speed at times posterior to 8.6 h (referred to the beginning of the estimation timeline). In this case, 8.6 h defines the present time, and all the past data was acquired between time 0 and 8.6 h, which corresponds to seven SSP vectors (with 1-m discretization) and seven values of equivalent sediment upper compressional speed. The obtained prediction (regression) results are illustrated in Fig. 5.20. It can be seen that most of the features of the future equivalent sediment speed are followed by the estimate given by the SVM, till the end of the exercise time window (> 25 days after). This shows the adequacy of SVMs for the problem at hand, supported by Fig. 5.21, where we can see the range of variation of the SSPs used for training the SVM. The latter is able to extract the main features of the mapping from SSP to equivalent sediment speed, with only seven samples of SSP inside the gray area in Fig. 5.21, and the corresponding equivalent sediment speed values (shown in Fig. 5.20, in the

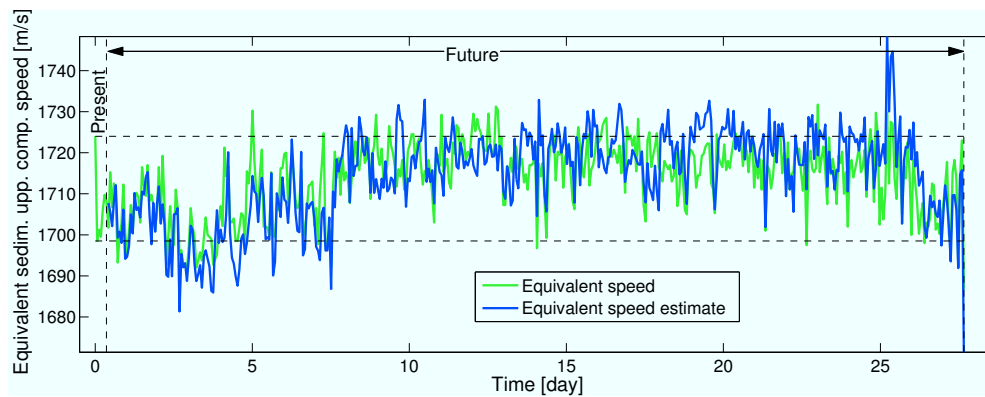


Figure 5.20: Prediction of the equivalent sediment upper compressional speed. (Green): equivalent speed for all times; (blue): estimated equivalent speed by SVM regression. The bounds of the observed response during the training period are represented by horizontal dashed lines. Prediction made with data observed during a 8.6-h time window, with a sampling period of 1.4 h.

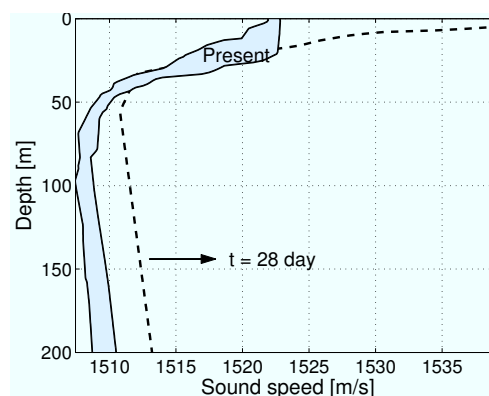


Figure 5.21: Sound speed profile information used in the training phase of the SVM, for regression, with a training time window of 8.6 h (7 data samples). The shaded area represents the minimum and maximum values of the sound speed, at each depth, of the profiles used to train the SVM. For reference, the sound speed profile at the farthest future time (day 28) is shown (dashed line).

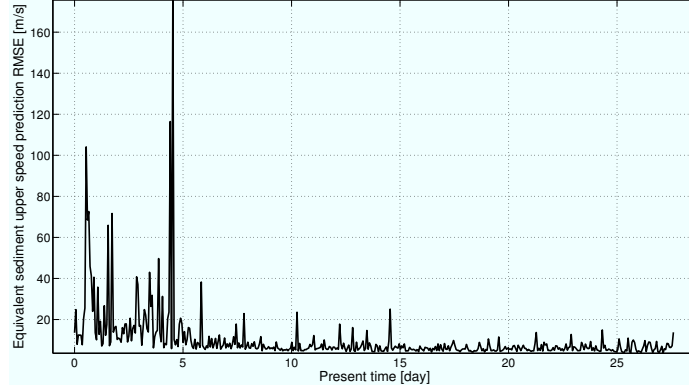


Figure 5.22: Error (defined in Eq. (5.23)) of the prediction of the equivalent sediment upper compressional speed given by the SVM, for the case of ideal oceanographic modeling. For each present time $0 \leq t_P < 28$ [day] at which the forecast is issued, the error quantifies the quality of the estimates for times greater than t_P .

“Present” section). The root mean square error (RMSE) of the fit for the future equivalent sediment upper compressional speed, for all future times > 8.6 h, is 7.7 m/s.

An equivalent model forecast (regression) exercise was then performed for every possible present time t_P running from day 0 to day 28. For each present time, the corresponding trained SVM was used to forecast the equivalent model at all future times posterior to the present time. A forecast error measure was defined for each fixed present time $0 \leq t_P < 28$, as the RMSE of the estimates for all the corresponding future times:

$$g_{RMSE}(t_P) = \sqrt{\frac{1}{E - P} \sum_{k=P+1}^E [\theta_E(t_k) - \hat{\theta}_E(t_k)]^2}, \quad (5.23)$$

where E is the index of the farthest future time, P is the index of the present time, $\theta_E(t_k)$ is the true value of the equivalent model at future time t_k (as shown in Fig. 5.18), and $\hat{\theta}_E(t_k)$ is the estimate given by the SVM. This error is shown in Fig. 5.22. It is seen that, as the present time increases and thus more information is used regarding the SSP-sediment speed mapping, the prediction error decreases.

Acoustic Field Forecast The predicted equivalent sediment upper compressional speed was given as input to the acoustic propagation model, to obtain the acoustic forecast. The quality of this forecast was assessed with error measures in a similar way to what was done for the acoustic nowcast exercise. Both Bartlett-based and TL-based estimation errors were computed, based on Eqs. (5.4) and (5.5). For the present case, further averaging was performed over the forecast instance:

$$\begin{aligned}\mu_{nr}(r) &= \frac{1}{N_z N_f N_t N_p} \sum_{p=1}^{N_p} \sum_{z=1}^{N_z} \sum_{f=1}^{N_f} \sum_{t=1}^{N_t} \mathcal{C}_n(r, z, f, t, p), \\ \sigma_{nr}(r) &= \sqrt{\frac{1}{N_z N_f N_t N_p - 1} \sum_{p=1}^{N_p} \sum_{z=1}^{N_z} \sum_{f=1}^{N_f} \sum_{t=1}^{N_t} (\mathcal{C}_n(r, z, f, t, p) - \mu_{nr}(r))^2}, \\ \sigma_{Tf}(f) &= \sqrt{\frac{1}{N_r N_z N_t N_p - 1} \sum_{p=1}^{N_p} \sum_{r=1}^{N_r} \sum_{z=1}^{N_z} \sum_{t=1}^{N_t} (\mathcal{C}_n(r, z, f, t, p) - \mu_{nf}(f))^2},\end{aligned}$$

where p is the index of the time at which the forecast was issued, N_p is the total number of forecast exercises, and $\mathcal{C}_n(r, z, f, t, p)$ is the cost in Eq. (5.4) evaluated upon the forecast issued at time t_p . The comparison of this error measure for the case in which the full baseline environment in Fig. 5.15 was used, without executing acoustic inversion, is compared to the case in which the predicted equivalent sediment upper compressional speed was used (together with the other baseline parameters), in Figs. 5.23 and 5.24. In Fig. 5.23, the Bartlett-type error is shown to be smaller for the case in which the predicted equivalent model was used, with values essentially below 0.2. The average error increases with range, due to the accumulation of residual modeling errors originating from two possible causes: 1) the environmental mismatch cannot be fully compensated by any value of sediment compressional speed; 2) the regression step for the estimation of the future equivalent sediment speed is susceptible to errors. The measures of TL error as a function of frequency or time

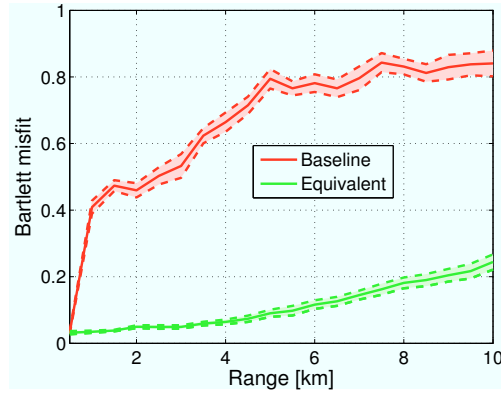


Figure 5.23: Bartlett misfit as a function of range, in the problem of acoustic forecast, for the case of ideal oceanographic modeling, when using the baseline (pink) or the equivalent (green) environments.

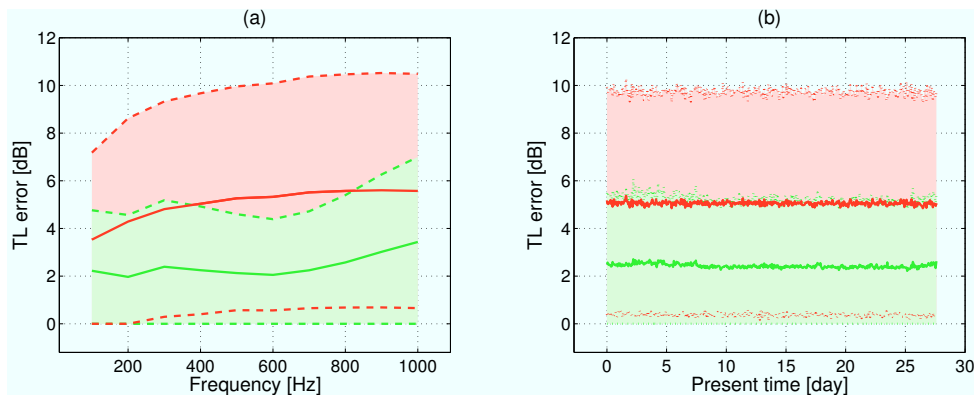


Figure 5.24: Transmission loss error as a function of range, in the problem of acoustic forecast, for the case of ideal oceanographic modeling, when using the baseline (red and pink) or the equivalent (green) environments, as a function of frequency (a) and time (b). The errors are shown as average value \pm one standard deviation.

are shown in Fig. 5.24. In terms of average, it is seen that the use of the predicted equivalent model leads to lower errors, both seen as a function of frequency or time. The standard deviation of the error corresponding to the equivalent model is approximately half of the one corresponding to the full baseline environment. One explanation for that standard deviation to not be smaller is the fact that the equivalent model was determined in such a way that it minimizes the joint acoustic error at different frequencies and depths, for a single range, according to the approximation in Rems. 5.1 and 5.2. The results shown in Fig. 5.24 consider averages over ranges at which acoustic arrays are not available, hence for which the equivalent model determined at 5 km might not be appropriate. In reality, both error

average and standard deviation would decrease, if any of these exemplifying modifications was introduced in the experimental setup: 1) to define a different equivalent model for each frequency, performing several single-frequency acoustic inversion exercises; 2) to observe the acoustic field at several ranges, positioning vertical receivers, at least, at farther ranges from the acoustic source (refer to the case of acoustic nowcast, in Fig. 5.13, where two acoustic receiver arrays were employed). Since the equivalent model is a function of frequency and space (see Eq. (2.4)), only by positioning receivers at all space points of interest and determining equivalent model outcomes for every point and frequency, the final acoustic error will be close to zero, with small variance.

Real Circulation Model: NCOM

The acoustic forecast results in the context of real oceanographic modeling as performed by the NCOM model are presented in this section. The equivalent model forecast is described, followed by a presentation of the acoustic forecast results.

Equivalent Model Forecast This paragraph describes the equivalent model forecast results for the case in which the oceanographic forecasts were obtained with the NCOM model. As an example, let us consider the problem of predicting the equivalent sediment upper compressional speed at day > 5.2 , using the data available from day 3.4 to day 5.2 (the NCOM model was run for day ≥ 3.4 , during the MREA'03 sea trial). The estimate obtained with the SVM for the future equivalent sediment upper compressional speed is illustrated in Fig. 5.25. The RMSE of the estimate is 10 m/s.

The prediction of the equivalent sediment upper compressional speed was then done for every possible present time (the time sample at which the forecast was issued) in the interval

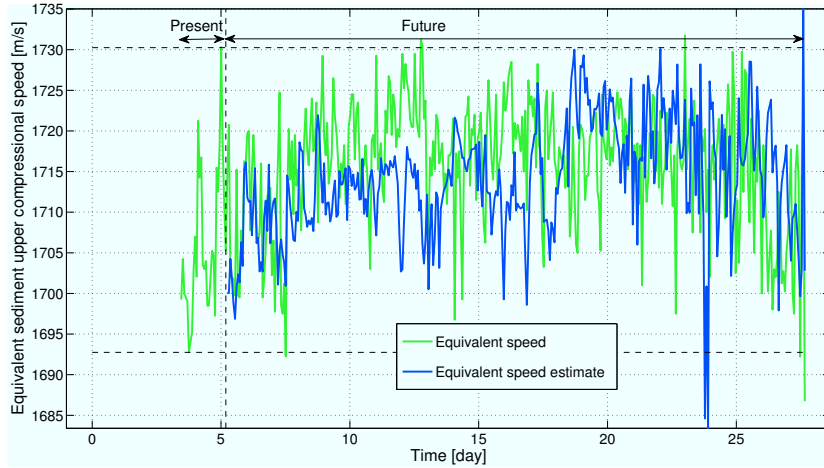


Figure 5.25: Prediction of the equivalent sediment upper compressional speed, in the problem of acoustic forecast, for the case of real oceanographic modeling.

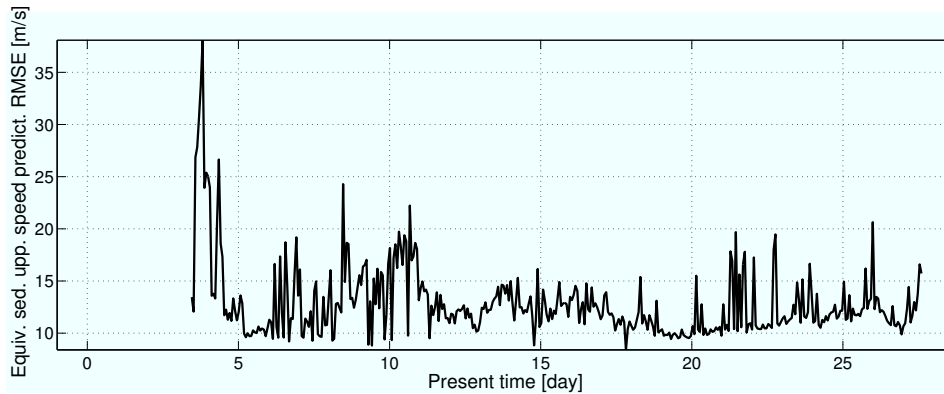


Figure 5.26: Error (defined in Eq. (5.23)) of the prediction of the equivalent sediment upper compressional speed given by the SVM, for the case of real oceanographic modeling (with NCOM). For each present time $3.4 \leq t_P < 28$ [day] at which the forecast is issued, the error quantifies the quality of the estimates for times greater than t_P .

$3.4 \leq t_P < 28$ [day] (limited by the availability of the NCOM forecasts). The forecast error as defined in Eq. (5.23) was computed for the predicted values, and is represented in Fig. 5.26. Differently from what is verified for the case of ideal oceanographic modeling in the previous section —see Fig. 5.22—, the equivalent model estimation error exhibits larger variations, which reflect the contribution of the oceanographic forecast time-variant error.

Acoustic Field Forecast The predicted equivalent sediment upper compressional speed was given as input to the acoustic propagation model, to obtain the acoustic forecast.

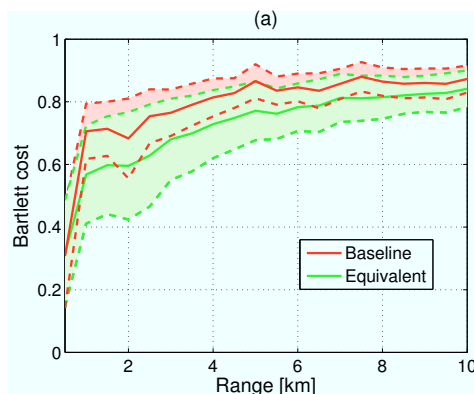


Figure 5.27: Bartlett misfit as a function of range, when using the baseline (pink) or the equivalent (green) environments. These errors correspond to acoustic forecast, in the case that the oceanographic model is the NCOM.

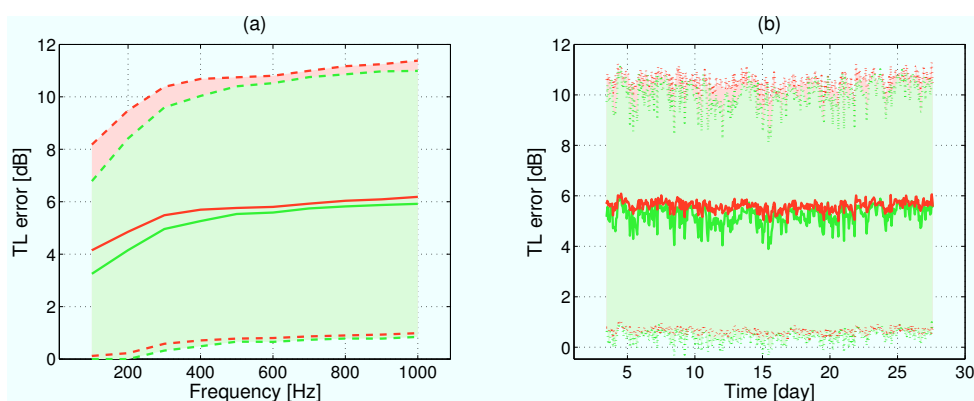


Figure 5.28: Transmission loss error as a function of frequency (a) and time (b), when using the baseline (red and pink) or the equivalent (green) environments. These errors correspond to acoustic forecast, in the case that the oceanographic model is the NCOM.

Similarly to the previous case of ideal oceanographic modeling, three types of acoustic forecast error are shown here: range-, frequency- and time-dependent error. For the range-dependent case, the Bartlett-based error is shown in Fig. 5.27. For the frequency- and time-dependent cases, the acoustic error is shown in Fig. 5.28 (a) and (b), respectively. These results show that there is no significant difference between using the equivalent model or the full baseline model to predict the acoustic field. By comparing Figs. 5.27 and 5.28 with Figs. 5.23 and 5.24, it can be concluded that the oceanographic error has a major influence on the acoustic forecast results. The fact that the water column has a significant impact on acoustic propagation, added to the inevitable errors of the particular operational

circulation model at hand, mask the effect of the equivalent model in compensating for the mismatch on the ocean bottom parameters.

Sensitivity to Oceanographic Error The high sensitivity of the acoustic forecast to the oceanographic forecast error was studied with a simple analysis as follows. An estimation timeline was defined as comprising a training time window from day 3.5 to day 4.0 (10 samples), and a forecast time window defined from day 4.1 to day 4.6 (10 samples). The purpose is to use the information obtained from the 10 training samples, to issue an acoustic forecast for the 10 next time samples. The information obtained from the 10 training samples is the equivalent sediment upper compressional speed and an SVM model of the relationship between the true water column properties and the equivalent sound speed. The estimation of the future acoustic field follows exactly the same procedure as presented above, for the cases of ideal and real oceanographic forecast modeling. Nevertheless, here several estimation exercises are executed (50 in total), each of them characterized by different synthetic oceanographic forecasts. In each estimation exercise, the instantaneous oceanographic forecast is defined as a weighted average of the true water column SSP and the NCOM-computed forecast:

$$c_{syn}(t) = \rho c_{NCOM}(t) + (1 - \rho) c_{true}(t), \quad (5.24)$$

with ρ running from 0 to 1 over the exercises. Each value of ρ corresponds to a particular value of oceanographic error, here quantified as an RMSE value:

$$\begin{aligned} e_{RMSE}(\rho) &= \sqrt{\frac{1}{N_z N_t} \sum_{z=1}^{N_z} \sum_{t=1}^{N_t} (c_{true}(z, t) - c_{syn}(z, t))^2} \\ &= \rho \sqrt{\frac{1}{N_z N_t} \sum_{z=1}^{N_z} \sum_{t=1}^{N_t} (c_{true}(z, t) - c_{NCOM}(z, t))^2}, \end{aligned} \quad (5.25)$$

where N_z and N_t are the number of SSP depths and time samples (here, $N_t = 20$ time samples), respectively, $c_{true}(z, t)$ designates a true SSP at depth z and time t , and $c_{syn}(z, t)$ is a synthetic oceanographic forecast defined as in Eq. (5.24). The extremes $\rho = 0$ and $\rho = 1$ lead to the results associated (not exactly equal, because the time windows are much smaller in the present case) to the ideal circulation model and the real circulation model (NCOM), respectively. The RMSE of the synthetic oceanographic forecast as a function of ρ , defined in Eq. (5.25), is shown in Fig. 5.29. For each estimation exercise, the acoustic forecast

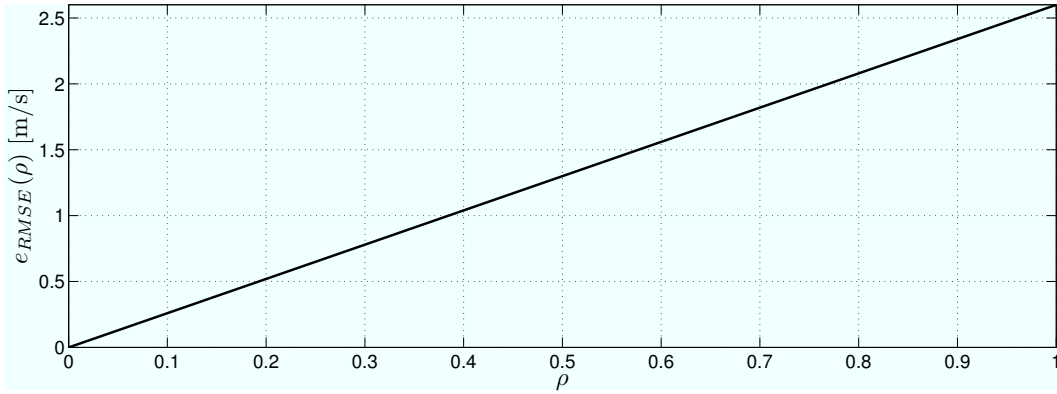


Figure 5.29: Root-mean-square-error of the synthetic oceanographic forecast as a function of the weighted average parameter ρ , as defined in Eq. (5.25).

was computed in two different ways, as in the previous sections. In the first approach, the acoustic propagation model takes as input the water column SSP given by Eq. (5.24), and the baseline environmental model shown in Fig. 5.15. In the second approach, the difference in the input environmental parameters for the acoustic propagation model consists in the sediment upper compressional speed, which is estimated with an SVM, as described in the previous sections. For each approach, average acoustic forecast errors were computed as:

$$\mu_{baseline} = \frac{1}{N_r N_z N_f N_t} \sum_{r=1}^{N_r} \sum_{z=1}^{N_z} \sum_{f=1}^{N_f} \sum_{t=1}^{N_t} |TL(r, z, f, t) - \hat{T}L_{baseline}(r, z, f, t)|, \quad (5.26)$$

$$\mu_{equivalent} = \frac{1}{N_r N_z N_f N_t} \sum_{r=1}^{N_r} \sum_{z=1}^{N_z} \sum_{f=1}^{N_f} \sum_{t=1}^{N_t} |TL(r, z, f, t) - \hat{T}L_{equivalent}(r, z, f, t)|, \quad (5.27)$$

where $\mu_{baseline}$ and $\mu_{equivalent}$ correspond to the first and second approaches, respectively. The approaches were compared through their forecast errors, and a measure I of increase in quality of the acoustic forecast was defined as a difference of the acoustic errors:

$$I = \mu_{baseline} - \mu_{equivalent}. \quad (5.28)$$

With this measure, a high value for I represents the situation in which the use of the equivalent model leads to a high improvement in the final acoustic estimate, over the baseline model. The value of I as a function of e_{RMSE} , for all the estimation exercises, is shown in Fig. 5.30. It is seen that, for average oceanographic forecast errors smaller than 1.7 m/s,

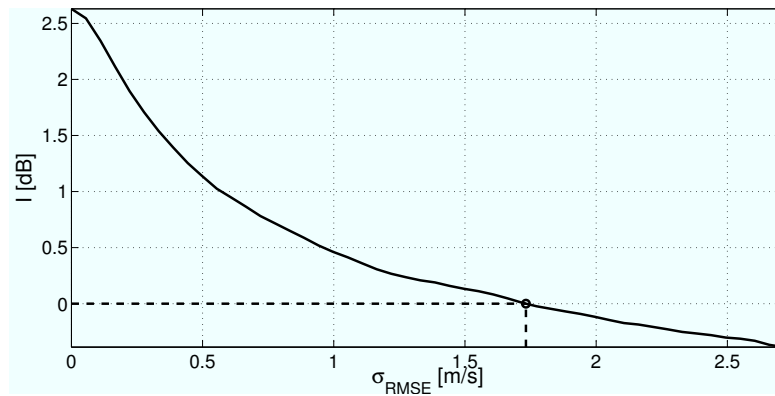


Figure 5.30: Measure of improvement of equivalent modeling over baseline modeling, in terms of acoustic forecast error. The improvement is computed as the difference between the acoustic errors corresponding to the baseline and the equivalent model, respectively, and shown as a function of the synthetic oceanographic forecast RMSE —see Fig. 5.29.

the equivalent model always outperforms the baseline model.

Real Circulation Model and Water Column Measurements

This section presents acoustic forecast results computed with the forecasts given by NCOM, and a scheme to take into account the oceanographic forecast error. The information from the oceanographic forecasts and the CTD measurements is fused, in order to be consistent with the following principles:

1. The value of the equivalent model is a function of the true environment, and not directly of an oceanographic prediction of that environment;
2. The only information available regarding the future true environment is contained in the oceanographic forecast (future measurements are never available).

The points above express that, since the outcome of the equivalent model is a function of the true environment (which applies to present and future times), and this “function” can be estimated with a function approximator, ideally the true environment should be used as input to the approximated function, to estimate the future equivalent model. If the future true environment is replaced by a circulation model-estimate, then the quality of the equivalent model estimate becomes highly dependent on the accuracy of the circulation model-estimate, as seen in previous sections. Here, an algorithm is proposed which intends to alleviate the dependence of the equivalent model estimate on the oceanographic forecast accuracy, as follows: first, the mapping from the true environment to the equivalent model is estimated (in the same way as for the case of an ideal circulation model, as described in p. 115), resorting to an SVM; second, an estimate of the future true environmental measurement is produced from the oceanographic prediction; third, the mapping estimated on the first step is fed with the estimate of the future environmental measurement. The idea is to capture the oceanographic forecast estimation bias from past data consisting of synchronous measurements and forecasts, and then trying to ‘unbias’ future estimates.

An oceanographic forecast error measure was defined as:

$$\epsilon_{SSP}(t) = \frac{1}{(F - P)N_z} \sum_{z=1}^{N_z} \sum_{f=P+1}^F [c_{CTD}(z, t_f) - \hat{c}(z, t_f)], \quad (5.29)$$

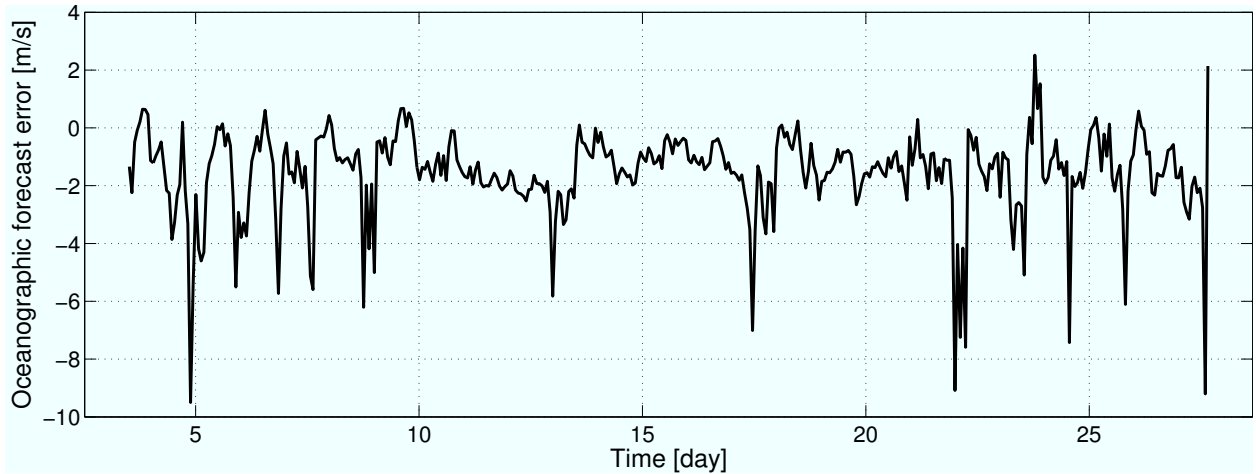


Figure 5.31: Sound speed estimation error of the forecast given by NCOM. Each point in the curve is the average absolute value of the difference between the true and the forecast sound speed, over depth.

in which t is the time for which the forecast was issued. The error, as a function of time, is shown in Fig. 5.31. The error is negative for most of the time samples, because at most depths, the forecast sound speed is larger than the true one, as summarized in the average measured and forecast profiles in Fig. 5.32. The error in Fig. 5.31 is rather unstable, as seen in Fig. 5.31. Nevertheless, periods of relative stability can be found for example between day 9 and 13. Thus, it is expected that, if only data from this period was used to estimate the oceanographic forecast bias, to be used on a prediction of the true SSP for e.g. day 20, the forecast bias could in principle be highly minimized. In the present section, similarly to previous sections, it is assumed that the true SSP coincides with the measured SSP.

The future true SSP is estimated from the oceanographic prediction, by using Bayesian estimators, which start by estimating the probability of the CTD measurement conditioned on the forecast. Each depth is treated independently. By designating the CTD measurement at depth z by $c_{CTD}(z)$ and the corresponding forecast by $c_{NCOM}(z)$, the starting point for the Bayesian estimators is to estimate $p(c_{CTD}(z)|c_{NCOM}(z))$, in which p is a probability density function. From the estimate of the probability density function, $\hat{p}(c_{CTD}(z)|c_{NCOM}(z))$, three

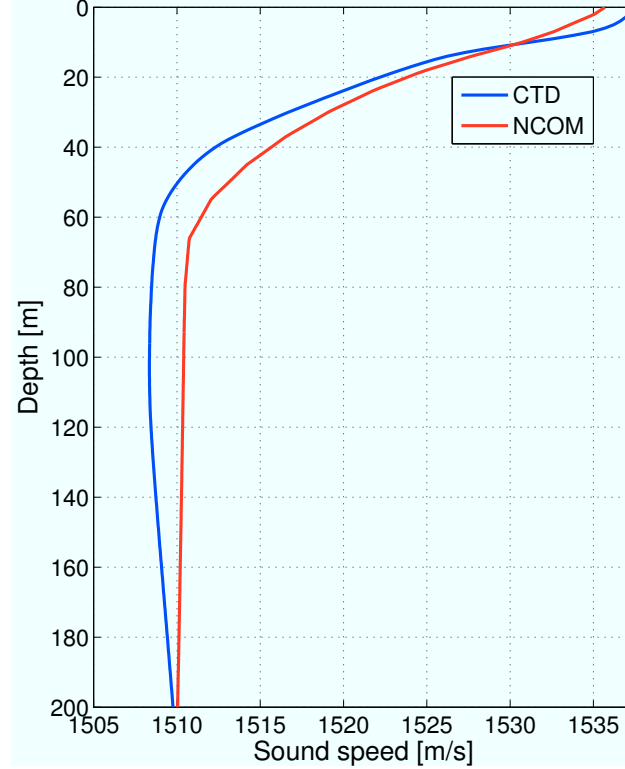


Figure 5.32: Average measured (CTD) and forecast (NCOM) sound speed profiles.

Bayesian estimates are readily obtained, for the realization of $c_{CTD}(z)$:

$$\hat{c}_{MAP}(z) = \arg \max_{c_{CTD}(z)} \hat{p}(c_{CTD}(z)|c_{NCOM}(z)); \quad (5.30)$$

$$\hat{c}_{MMSE}(z) = \int c_{CTD}(z) \hat{p}(c_{CTD}(z)|c_{NCOM}(z)) dc_{CTD}(z); \quad (5.31)$$

$$\hat{c}_{MED}(z) = \text{median of } \hat{p}(c_{CTD}(z)|c_{NCOM}(z)), \quad (5.32)$$

designated as maximum a posteriori, minimum-mean-square-error (MMSE) and median estimates, respectively[Kay93]. In practice, the posterior probability density $p(c_{CTD}(z)|c_{NCOM}(z))$ was estimated from the joint density of $c_{CTD}(z)$ and $c_{NCOM}(z)$, the latter estimated with a kernel density estimator, using a Gaussian kernel. The joint density was then normalized by the marginal density of $c_{NCOM}(z)$. For each present time t_P , an estimate of the future values of sound speed was obtained, at each depth. For each type of estimate in Eqs. (5.30),(5.31) and (5.32), an estimation error was defined as a function of

present time, as follows:

$$e_{SSP}(P) = \frac{1}{(F-P)N_z} \sum_{z=1}^{N_z} \sum_{f=P+1}^F |c_{CTD}(z, t_f) - \hat{c}(z, t_f)|, \quad (5.33)$$

in which P is the index of present time t_P , f is an index of a future time sample, and $\hat{c}(z, t_f)$ is any of the three estimates in Eqs. (5.30), (5.31) and (5.32). The idea is to quantify the predictability characteristics of the estimators, as a function of the available information. If the joint statistics between the measurement and the forecast are stationary, it is expected that the estimation error decreases as present time moves forward. The error defined in Eq. (5.33) is shown in Fig. 5.33. One can find a reasonable correlation between the results and

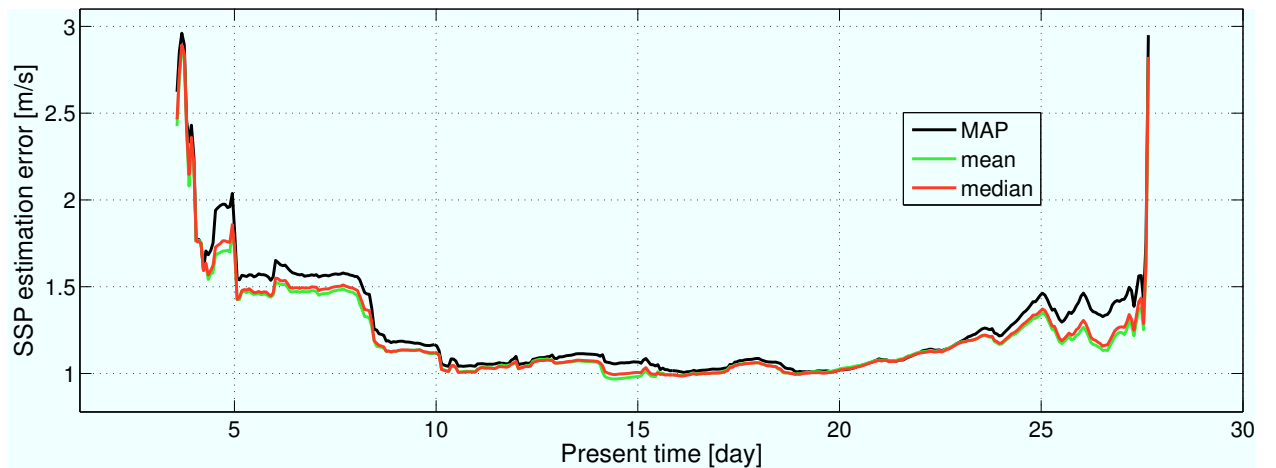


Figure 5.33: Sound speed estimation error, for each present time with index P , t_P . The estimate is any of the Bayesian estimates which take the oceanographic forecast as the observation, to infer the CTD measurement at a future time.

the oceanographic error presented in Fig. 5.31. For $t_P < \text{day } 10$, the forecast error is quite unstable, which leads to estimates of the conditional probability of $c_{CTD}(z)$ which deviate very likely from the true density for future times. For present time in the period from day 10 to day 20, the Bayesian estimates exhibit low error, which is correlated with a more stable forecast error seen in Fig. 5.31. For a present time $> \text{day } 20$, the Bayesian estimates deviate from the true values in a significant extent, possibly because the behavior of the forecast

error is different from the one at past values (see 5.31). Though some of the fluctuations in this period were already observed before day 10, their importance is smaller than the more stable characteristics of the forecast error, which remain approximately valid for a total of 10 days (from day 10 to day 20). In general, the error corresponding to the MMSE estimate is the lowest, hence only MMSE estimates are considered in the following.

As mentioned above, an SVM is previously trained with the CTD profiles as predictors, and the acoustic inversion results as response, exactly as for the case of an ideal oceanographic model. The trained SVM is then fed with the MMSE estimate defined in the above paragraph, and gives as output the estimate of the future equivalent model. The latter is used in an acoustic forward modeling exercise, which provides the acoustic forecast. For each possible present time sample, a different series of acoustic forecasts for all the possible future time samples is obtained. An error measure was defined accordingly, fixing the present time, and varying the future time, with the mean and standard deviation defined as follows:

$$\mu(r) = \frac{1}{N_z N_f N_{t_f}} \sum_{z=1}^{N_z} \sum_{f=1}^{N_f} \sum_{t_f=1}^{N_{t_f}} \mathcal{C}_n(r, z, f, t_f), \quad (5.34)$$

$$\sigma(r) = \sqrt{\frac{1}{N_z N_f N_{t_f} - 1} \sum_{z=1}^{N_z} \sum_{f=1}^{N_f} \sum_{t_f=1}^{N_{t_f}} (\mathcal{C}_n(r, z, f, t_f) - \mu_{nr}(r))^2}, \quad (5.35)$$

in which $\mathcal{C}_n(r, z, f, t_f)$ is the Bartlett-type cost defined in Eq. (5.4), and t_f is a future time sample. For a selected value of present time $t_P = \text{day } 14$, this error is shown in Fig. 5.34, for both cases of the SSP given either directly by the NCOM model, or given by the MMSE estimate above. It is seen that both errors increase with distance, due to range-accumulated effects of mismatch. Additionally, the average error corresponding to the Bayesian estimate of the SSP and the equivalent model estimate is lower than the one corresponding to the baseline. A simple comparison with the result in Fig. 5.27 (method

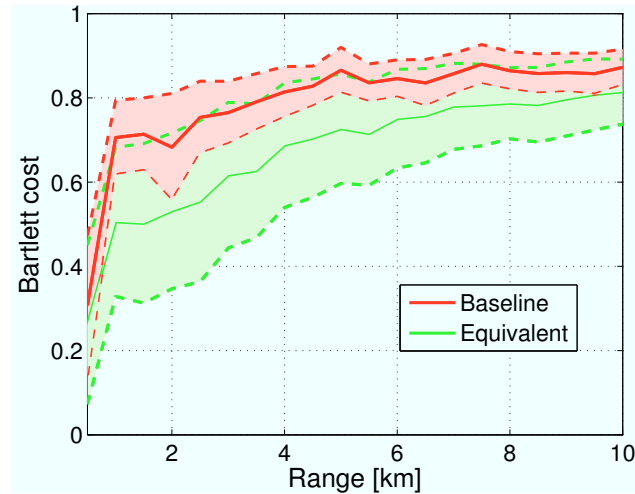


Figure 5.34: Bartlett misfit as a function of range, when using the baseline (red and pink) or the equivalent (green) environments. These errors correspond to acoustic forecast, in the case that the water column is determined by Bayesian estimation using NCOM and CTD data, and the equivalent model is determined by an SVM trained with the CTD data and the acoustic inversion results up to present time, and responding to the Bayesian estimate as input.

using the real oceanographic forecast as a water column realization for the future time sample) can be done. For the present case, the error corresponding to the equivalent model and the Bayesian-estimated SSP is lower than the one shown in Fig. 5.27 (green curve), showing the advantage of using information from both the oceanographic forecast and the CTD measurements. A comparative study of the different methods of acoustic forecast presented in this work was done, in which the RMSE in TL was computed as a function of present time t_P , for each method. The results are shown in Fig. 5.35, and described below according to decreasing error. It is seen that, if no optimization for acoustics is done, the largest error is obtained (red curve in Fig. 5.35). A lower error is obtained in the case in which acoustic measurements are taken into account to estimate the equivalent model. The latter is combined with the NCOM-derived forecasts, as mentioned previously, for the case of the real oceanographic forecast (see, for example, Fig. 5.27, showing the corresponding overall error, as a function of range). Below this error, we find the error corresponding

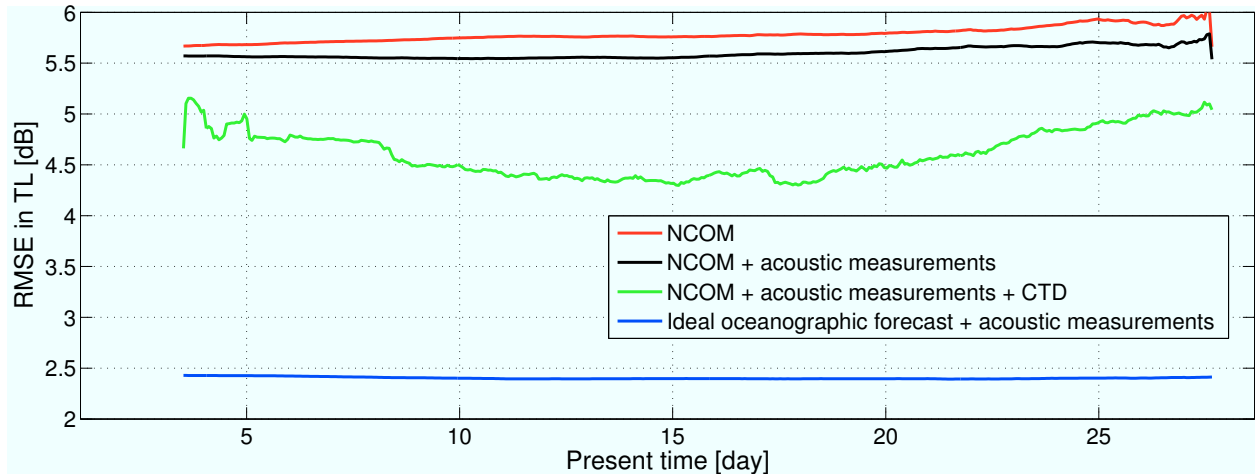


Figure 5.35: Root-mean-square of transmission loss estimation error, as a function of present time. The curves represent four types of acoustic estimation: (red) water column fixed to the NCOM forecast, and remaining environmental parameters set to baseline values; (black) water column fixed to the NCOM forecast, and equivalent model determined by an SVM trained with the NCOM forecast and the equivalent model up to present time; (green) water column determined by Bayesian estimation using NCOM and CTD data, and equivalent model determined by an SVM trained with the CTD data and the equivalent model up to present time, and responding to the Bayesian estimate as input; (blue) SSP fixed to the ideal oceanographic forecast (coincident with the true SSP), and equivalent model computed as the response of the SVM to that SSP.

to the forecast-measurement data fusion proposed in the present section. The error curve reflects the characteristic of the sound speed estimation error shown in Fig. 5.33 (which is a consequence of the oceanographic forecast error features in Fig. 5.31). The lowest values of acoustic error appear for values of present time $10 < t_P < 20$ [day]. Contrarily to what could be expected, in terms of the consequences of accumulating oceanographic information, for the acoustical application, this error curve does not decrease over time. This can be explained by the irregularity of the oceanographic forecast (see Fig. 5.31). The joint statistics of measurement and forecast are non-stationary, and hence it is not guaranteed that: 1) the Bayesian estimate of the future SSP is sufficiently close to the true value (for acoustical estimation); 2) the estimate of the joint density of the measurement and the forecast is consistent (tending to the true density, as the number of samples tends to infinity). In this scenario of acoustic forecast, in which several types of information are

fused (oceanographic measurements and forecasts, and acoustic measurements), it is seen the advantage of: 1) using acoustic measurements to minimize the impact of geoacoustic mismatch; 2) using CTD measurements to infer the origin of the equivalent model pattern; 3) combining the oceanographic forecast with the CTD (in situ) measurement, to refine the highly operational (relying on very few in situ measurements) oceanographic forecast for the fine scale necessary for the acoustical application. In Fig. 5.35, the lowest error (blue curve) is obviously the one corresponding to the ideal oceanographic forecast (procedure explained in p. 115).

5.3 Summary

The present chapter presents approaches to acoustic nowcast and forecast, using the concept of equivalent model. Acoustic nowcast is solved using data from a past period of oceanographic sampling, and an acoustic measurement at the time of nowcast. The acoustic data is inverted, to obtain the equivalent model. The latter, in a strict definition, is the set of environmental parameter values best suited to be used as propagation model inputs, to model the field received at a single spatial point and a single frequency. Impracticability of implementing this definition motivated an approximation consisting of a range-dependent, frequency-depth-independent model, which is determined by acoustic inversion with a vertical array. By using two vertical arrays, two instances of equivalent model are determined, which are interpolated/extrapolated to model the acoustic field at inter- and outer-array ranges. The tests showed an improvement of ≈ 5 dB in the estimate of transmission loss, as compared to a standard estimation procedure which does not consider acoustic measurements. Summarily, the following aspects are to be retained: 1) the use of the equivalent

model shows an improvement on the acoustic estimate, as compared to a baseline parameterization; 2) acceptable results are obtained by interpolating the equivalent model between the receiver array ranges; 3) there is a residual acoustic error at the end of acoustic inversion, which cannot be removed with the structure considered for the equivalent model; 4) this error leads to a degradation of the acoustic nowcast, increasing with range and frequency.

In its elementary form, acoustic forecast is solved for a time sample posterior to a period of acoustic-oceanographic measurement. In the proposed method, the addition with respect to acoustic nowcast is that the equivalent model outcome is seen as a function of the true environment. This functional relationship is estimated with a support vector machine. According to the present rationale, the future true environment contains relevant information concerning the future equivalent model. On its turn, the latter contains the full information concerning the future acoustic pressure. Running the acoustic propagation model parameterized with the future equivalent model produces directly the future acoustic estimate. Thus, the forecast process starts by estimating the future true environment. A valuable estimate can be obtained with a circulation model, such as NCOM. However, the circulation model estimate per se did not allow to obtain an accurate estimate of the future equivalent model, and also could not be used directly in the propagation model, without leading to significant acoustic error. To overcome this difficulty, a scheme is proposed in which NCOM forecasts and water column measurements are fused, capturing and minimizing forecast uncertainties. Interestingly, this proved to reduce the final acoustic forecast error, as compared to the estimation scenario which did not take the oceanographic forecast error into account. In numerical terms, the transmission loss estimation error decreased from 5.5 to 4.3 dB, in the simple illustrative tests with a single equivalent model parameter.

Chapter 6

Conclusion

“What happens when the future has come and gone?”

Robert Half

“**T**HROUGHOUT the book, wherever we can, we perform the trick of Janus, the mythological Roman God, who simultaneously faces in opposite directions. One view, called ‘the forward problem of ocean acoustics’, is in the traditional direction where the knowledge of ocean parameters allows one to predict the propagation of sound. The opposite view, called ‘the inverse problem’, uses the distinctive details of the propagation at a time and place to deduce the parameters and processes of the particular ocean through which the sound has traveled”. The above text, opening Ref. [MC98], reflects how acoustic propagation models can be applied in ocean acoustics. In any of these applications, apart from the accuracy in modeling the fine details of the propagation process, it is fundamental that the model is framed by accurate oceanographic information. In the “forward problem”, incorrect values of some environmental parameters may lead to an incorrect acoustic prediction[WLH⁺06, WLH⁺09]. In the “inverse problem”, the accuracy of environmental knowledge (often more important than the signal-to-noise ratio) will determine the ability of the estimation process to pin-

point the unknown property (e.g. source location or geoacoustic stratification)[Del88, Sha88, Gin89, Tol89, Byr92, Pre92, BKM93, Smi93, GG94, GH98, JPS⁺00, LL05]. In applications of the inverse problem, variants of the original techniques were proposed, which are able to cope with environmental uncertainty. For example, in source localization, both the source location and some properties of the ocean environment are estimated. Though the source position fortunately appears at the correct location, the environmental parameter estimates have incorrect values[CK91, GG94, ZDF96, BC05]. This type of approaches deals with what is called an “equivalent model” in the present work, and has its definition attached to a particular acoustic effect, in a certain oceanic scenario of interest. In the present work, in which the forward problem is the focus, inevitable environmental mismatch is not seen as a tremendous gap in the available information. Instead, it is treated and used ‘as it is’. This apparent simplicity of terms and procedures comes at the cost of adding independent (acoustic) measurements to the estimation process. In reality, this is not necessarily a cost, since the emphasis on environmental measurement can be transferred to acoustical measurement, because the latter is the minimum necessary to calibrate the acoustic modeling tool at hand. Acoustic measurements can alleviate the need to do in situ measurements of some environmental properties, whose true value is even not required in exact terms, for the acoustical application. The forward problem appears here as less sensitive to environmental mismatch than in classical simple forward problems, due to the addition of an inverse problem as a pre-processing step, which finds an equivalent model appropriate for acoustic prediction.

It is expected that the ideas developed in the present work can be applied in several problems of acoustic estimation, such as ocean ambient noise monitoring or sonar performance prediction. In the first application, a network of acoustic arrays can be deployed at sea,

continuously acquiring man-made/biological/environmental noise. The acoustic array data, when inverted, provides equivalent model outcomes for the respective arrays. The spatial interpolation/extrapolation of the equivalent models can then be used in a forward problem, to estimate the acoustic field in between the arrays, and outside the array perimeter area. At the end, an oceanic noise map can be built from the individual forward model runs. In a problem of sonar performance prediction for target detection, the main difference from the above is the requirement to have at hand oceanographic estimates of the ocean state at a future time. A hypothetical scenario could consider a training phase in which an acoustic source is positioned at possible target locations. In that phase, acoustic inversion would be performed to determine the equivalent model representative of the static properties of the area. In a second phase, the water column sound speed would be fixed to the oceanographic forecast, and used together with an estimate of the future equivalent model, to estimate the acoustic field produced by a hypothetical underwater target, and hence the sonar detection capability. With a highly accurate oceanographic model, minimal environmental measurements would be sufficient. In the case of a highly operational model, water column sound speed measurements would be required to be fused with the oceanographic forecast and the equivalent model, in order to maximize the accuracy of the future equivalent model estimate.

The present framework is limited by several factors: 1) degree of mismatch; 2) stability/regularity of the equivalent model; 3) composition of the equivalent model. First, the degree of mismatch is a function of prior knowledge about the environment, and the environmental structure imposed by the propagation model. Higher mismatch, if not almost completely removed by acoustic inversion, implies less reliability of the equivalent model to represent the acoustic field. Second, the equivalent model is a function of the true environ-

ment, of the mismatch, of the propagation features and of the acoustic signal characteristics. In case the equivalent model is a smooth function of some of these quantities, it can be interpolated with respect to those quantities. For instance, if it does not change significantly with space, two acoustic arrays may be enough to estimate the inter-array equivalent model, in a distance of several kilometers, as seen in the present work, for the problem of nowcast. In the opposite case, interpolation will produce equivalent model estimates which are inappropriate for the targeted local area/signal frequencies. Third, the composition of the equivalent model has to be chosen as a tradeoff. In the one hand, an equivalent model with many parameters has at least two advantages: 1) to allow a priori a very high acoustic fit in acoustic inversion; 2) to alleviate the need to do expensive and time-consuming environmental measurements, since acoustic inversion is able to provide estimates of the environment. In the other hand, an equivalent model with a high number of parameters might lead to overfitting, which renders the equivalent model less stable over space, frequency, etc. Equivalent model instability might also exist when ‘sub-equivalent models’ appear inside the equivalent model vector, defined by sets of correlated parameters.

Whether the targeted application is the “forward problem” or the “inverse problem”, or a complex interdisciplinary data assimilation problem[RL03], the intended message of the present work is: 1) to acknowledge that it is virtually impossible to use a propagation model parameterized with the full detail of the real environment, and obtain the full detail of the real acoustic pressure at the output; 2) the previous point is not a dead end, as long as the model parameters, potentially different from real counterparts, are optimized for the model output to be sufficiently close to the real/measured acoustic field. Among the various inputs/outputs of the model, only some of them will match real counterparts. The remaining

ones have to be optimized according to that match, and the particular application of the model. In summary, a model has to be treated as a model, and the reality has to be treated as reality.

Bibliography

- [Ack12] Steven G. Ackleson, *Ocean Observatories: Evolution and Future Directions*, Ocean Sciences Meeting (Washington, DC), 2012.
- [Aka08] Tuncay Akal, *Rapid environmental assessment at NURC*, *Oceanography* **21** (2008), no. 2, 44–51.
- [AL04] R.P. P Angliss and K.L. L Lodge, *Alaska marine mammal stock assessments, 2003*, Tech. Report NMFS-AFSC-144, U.S. Dep. Commer., NOAA Tech. Memo, 2004.
- [APM05] Ian F. Akyildiz, Dario Pompili, and Tommaso Melodia, *Underwater acoustic sensor networks: research challenges*, *Ad Hoc Networks* **3** (2005), no. 3, 257–279.
- [AUfU09] D.R. Arcas, B. Uslu, NOAA Center for Tsunami Research, and Pacific Marine Environmental Laboratory (U.S.), *A tsunami forecast model for Crescent City, California*, NOAA OAR special report, U.S. Department of Commerce, National Oceanic and Atmospheric Administration, Pacific Marine Environmental Laboratory, 2009.

- [AvdSZ⁺11] M. André, M. van der Schaar, S. Zaugg, L. Houégnigan, A.M. Sánchez, and J.V. Castell, *Listening to the deep: live monitoring of ocean noise and cetacean acoustic signals*, Mar Pollut Bull **63** (2011), no. 1-4, 18–26.
- [BBC⁺11] Sarah Betz, Karen Bohnsack, A. Renee Callahan, Lauren E. Campbell, Sarah E. Green, and Kate M. Labrum, *Reducing the risk of vessel strikes to endangered whales in the Santa Barbara Channel: an economic analysis and risk assessment of potential management scenarios*, Master's thesis, UC Santa Barbara, 2011.
- [BC03] Andrew Bass and Christopher Clark, *The Physical Acoustics of Underwater Sound Communication*, Acoustic Communication (Andrea Simmons, Richard Fay, and Arthur Popper, eds.), Springer Handbook of Auditory Research, vol. 16, Springer New York, 2003, pp. 15–64.
- [BC05] Ralph N. Baer and Michael D. Collins, *Source localization in the presence of internal waves*, J. Acoust. Soc. America **118** (2005), no. 5, 3117.
- [BKM93] A.B. Baggeroer, W.A. Kuperman, and P.N. Mikhalevsky, *An Overview Of Matched-field Methods In Ocean Acoustics*, IEEE J. Ocean. Eng. **18** (1993), 401–424.
- [BLK87] G. Botseas, D. Lee, and D. King, *FOR3D: A computer model for solving the LSS three-dimensional, wide angle wave equation*, NUSC Technical Report 7993, Naval Underwater Systems Center, New London, CT, 1987.

- [BM87] A.F. Blumberg and G.L. Mellor, *A description of a three-dimensional coastal ocean circulation model*, AGU Coastal and Estuarine Ser., vol. 4, ch. 1, pp. 1–16, American Geophysical Union, Washington D.C., 1987.
- [BM92] Arthur A.B. Baggeroer and W.H. Walter Munk, *The Heard Island feasibility test*, *Physics Today* **45** (1992), no. 9, 22–30.
- [BSRB08] Brian Borowski, Alexander Sutin, Heui-Seol Roh, and Barry Bunin, *Passive acoustic threat detection in estuarine environments*, *Optics and Photonics in Global Homeland Security IV* **6945** (2008), no. 13, 694513.
- [Buc83] Homer P. Bucker, *An equivalent bottom for use with the split-step algorithm*, *J. Acoust. Soc. America* **73** (1983), no. 2, 486–491.
- [Buc92] Michael J. Buckingham, *Ocean-acoustic propagation models*, *J. Acoustique Juin* (1992), 223–287.
- [Bur87] David S. Burnett, *Finite Element Analysis: From Concepts to Applications*, Addison Wesley Publishing Company, 1987.
- [BV11] J.W. Bradbury and S.L. Vehrencamp, *Principles of Animal Communication*, Sinauer Associates, 2011.
- [BvVV12] Guus Beckers, Robbert van Vossen, and Gert Vlaming, *Low-frequency synthetic aperture sonar for detecting explosives in harbors*, *Sea Technology March* (2012), 15–18.

- [Byr92] Charles L. Byrne, *Effects of modal phase errors on eigenvector and nonlinear methods for source localization in matched-field processing*, The Journal of the Acoustical Society of America **92** (1992), no. 4, 2159.
- [CBGE⁺86] S.A. Chin-Bing, K.E. Gilbert, R.B. Evans, M.F. Werby, and G.J. Tango, *Research and development of acoustic models at NORDA*, pp. 39–44, Stennis Space Center, USA, 1986.
- [CCM⁺12] Gabriel Codato, Leandro Calado, Néelson E. Martins, Wandrey D. Watanabe, Ricardo M. Domingues, and S. M. Jesus, *Acoustic prediction using a feature-oriented regional modeling system and acoustic inversion*, ... Meetings on Acoustics **17** (2012), 1–8.
- [CEB86] C. Clark, W. Ellison, and K. Beeman, *Acoustic tracking of migrating bowhead whales*, 1986.
- [CJ96] A. Caiti and S.M. Jesus, *Acoustic estimation of seafloor parameters: a radial basis functions approach*, J. Acoust. Soc. Am. **100** (1996), no. 3, 1473–1490.
- [CK91] M.D. Michael D. Collins and W.A. Kuperman, *Focalization: Environmental focusing and source localization*, J. Acoust. Soc. America **90** (1991), no. 3, 1410–1422.
- [CL11] Chih-Chung Chang and Chih-Jen Lin, *LIBSVM: A Library for Support Vector Machines*, ACM Transactions on Intelligent Systems and Technology **2** (2011), 27:1—27:27.

- [Col89] Michael D Collins, *A higher-order parabolic equation for wave propagation in an ocean overlying an elastic bottom*, J. Acoust. Soc. America **86** (1989), no. 4, 1459–1464.
- [Com01] National Research Council Committee for Mine Warfare Assessment, Naval Studies Board, *Naval mine warfare: operational and technical challenges for naval forces*, The National Academies Press, 2001.
- [Con98] The ATOC Consortium, *Ocean climate change: comparison of acoustic tomography, satellite altimetry, and modeling*, Science **281** (1998), no. 5381, 1327–1332.
- [Cou09] Arctic Council, *Arctic marine shipping assessment 2009 report*, Arctic **1** (2009), 39–55.
- [CR87] E.F. Carter and A.R. Robinson, *Analysis models for the estimation of oceanic fields*, J. Atmos. Oceanic Tech. **4**(1) (1987), 49–74.
- [CT03] L J Cao and Francis H E H Tay, *Support vector machine with adaptive parameters in financial time series forecasting.*, IEEE transactions on neural networks / a publication of the IEEE Neural Networks Council **14** (2003), 1506–18.
- [CWC⁺11] G.A.S. Codato, W.B. Watanabe, L. Calado, N. Martins, and A.E.A. Ramos, *A Influência da Frente Térmica da Ressurgência Costeira de Cabo Frio na Perda do Sinal Acústico: um Estudo Numérico*, X Encontro de Tecnologia Acústica Submarina - ETAS (Rio de Janeiro (Brasil)), 2011.

- [CWH06] C.P. Chang, Z. Wang, and H. Hendon, *The Asian winter monsoon*, Praxis, Berlin, 2006.
- [DAH⁺07] Brian Dushaw, R. Andrew, B. Howe, J. Mercer, R. Spindel, P. Worcester, B. Cornuelle, M. Dzieciuch, T. Birdsall, K. Metzger, and D. Menemenlis, *A Decade of Acoustic Thermometry in the North Pacific Ocean: Using Long-range Acoustic Travel Times to Test Gyre-scale Temperature Variability Derived From Other Observations and Ocean Models*, *J. Acoust. Soc. America* **121** (2007), no. 5, 3054–3054.
- [DBK⁺97] Harris Drucker, Chris J C Burges, Linda Kaufman, Alex Smola, and Vladimir Vapnik, *Support vector regression machines*, *Advances in Neural Information Processing Systems* **9** **1** (1997), 155–161.
- [dCM11] Universitat Politècnica de Catalunya and Sciencedaily Mar, *Sounds of Japan earthquake and aftershocks from underwater observatories*, *ScienceDaily* **Mar.** (2011), 1–5.
- [Del88] Donald R. Del Balzo, *Effects of water-depth mismatch on matched-field localization in shallow water*, *The Journal of the Acoustical Society of America* **83** (1988), no. 6, 2180.
- [DMD⁺07] Ciaran O Donnell, Gavin Macaulay, Ian Doonan, Anthony Grehan, Nils Roar N.R. Haride, Jenny Ullgren, Mick Mackey, Fabio Sachetti, Sam Sheppard, and C. O'Donnell, *An Acoustic Survey of Orange Roughy Aggregations to the West and North of the Porcupine Bank*, Tech. Report 18, Marine Institute, 2007.

- [DMH⁺99] G.L. D'Spain, J.J. Murray, W.S. Hodgkiss, N.O. Booth, and P.W. Schey, *Mirages in shallow water matched field processing*, J. Acoust. Soc. America **105** (1999), 3245–3265.
- [DMHB95] G. L. D'Spain, J. J. Murray, W. S. Hodgkiss, and N. O. Booth, *Mirages in shallow water matched-field processing*, J. Acoust. Soc. America **97** (1995), no. 5, 3291 (en).
- [Dos93] S.E. Dosso, *Matched-field inversion for source localization with uncertain bathymetry*, J. Acoust. Soc. America **94** (1993), 1160–1163.
- [DPSS00] Xavier Démoulin, Laurent Péliissero, Yann Stephan, and Yann Stéphan, *Faisabilité opérationnelle de l'inversion géoacoustique par milieux équivalents: principe et application aux données INTIMATE96*, Rapport d'étude 003 / 00, S.H.O.M., BREST, France, July 2000.
- [DWCH94] B.D. Dushaw, P.F. Worcester, B.D. Cornuelle, and B.M. Howe, *Barotropic currents and vorticity in the central North Pacific Ocean during summer 1987 determined from long-range reciprocal acoustic transmissions*, J. Geophys. Res. **99** (1994), 3263–3272.
- [DZD95] S E Dosso, Pierre Zakarauskas, and Pierre Dosso, S.E. and Zakarauskas, *Matched-Field Inversion for Source Location and Equivalent Bathymetry*, Full Field Inversion Methods in Ocean and Seismo-Acoustics (H. Diachok, O. and Caiti, A. and Gerstoft, P. and Schmidt, ed.), Modern approaches in geophysics, vol. 12, Springer Netherlands, 1995, pp. 279–284.

- [Ear90] F.C.F. Earney, *Marine Mineral Resources*, Routledge, New York, 1990.
- [EFM⁺10] Frank Ehlers, Warren Fox, Dirk Maiwald, Martin Ulmke, and Gary Wood, *Advances in signal processing for maritime applications*, EURASIP J. Adv. Sig. Proc. **2010** (2010), 1–5.
- [ER12] Emanuel Ey and Orlando C. Rodríguez, *cTraceo - User Manual*, Tech. report, CINTAL, Faro, Portugal, 2012.
- [Ett12] Paul C. Etter, *Advanced applications for underwater acoustic modeling*, Advances in Acoustics and Vibration **2012** (2012), no. January, 1–28.
- [Ett13] ———, *Underwater Acoustic Modeling and Simulation*, fourth ed. ed., CRC Press, Boca Raton, 2013.
- [FBC⁺02] Daniel N. Fox, Charlie N. Barron, Michael R. Carnes, Martin Booda, Germana Peggion, and John Van Gurley, *The Modular Ocean Data Assimilation System*, Oceanography **15** (2002), no. 1, 22–28.
- [FCPR⁺09] Emanuel Ferreira-Coelho, Germana Peggion, Clark Rowley, Gregg Jacobs, Richard Allard, and Elaina Rodriguez, *A note on NCOM temperature forecast error calibration using the ensemble transform*, Journal of Marine Systems **78** (2009), no. Supplement 1, S272–S281.
- [FES02] Steven Finette, Thomas Evans, and Colin Shen, *Sub-mesoscale modeling of environmental variability in a shelf-slope region and the effect on acoustic fluctuations, ... Littoral Environmental Variability on Acoustic ...* (2002), 401–408.

- [FOT⁺00] S. Finette, M.H. Orr, A. Turgut, J. Apel, M. Badiey, C.-S. Chiu, R.H. Headrick, J.N. Kemp, J.F. Lynch, A.E. Newhall, K. von der Heydt, B. Pasewark, S.N. Wolf, and D. Tielbuerger, *Acoustic Field Variability Induced by Time-evolving Internal Wave Fields*, *J. Acoust. Soc. Am.* **108** (2000), 957–972.
- [Fri93] J. Robert Fricke, *Acoustic scattering from elemental Arctic ice features: Numerical modeling results*, *The Journal of the Acoustical Society of America* **93** (1993), no. 4, 1784.
- [FTB⁺02] D.N. N. Fox, W.J. J. Teague, C.N. N. Barron, M.R. R. Carnes, and C.M. M. Lee, *The modular ocean data assimilation system (MODAS)*, *J. Atmos. Ocean. Technol.* **19** (2002), no. 2, 240–252 (EN).
- [Ger07] Peter Gerstoft, *SAGA User Manual 5.4: An inversion software package*, Tech. report, SACLANTCEN and MARINE PHYSICAL LABORATORY, September 2007.
- [GG94] D.F. Gingras and P. Gerstoft, *Inversion for geometric and geoacoustic parameters in shallow water: Experimental results*, Tech. report, SACLANT Undersea Research Centre, San Bartolomeo (SP), Italy, 1994.
- [GGA08] Manel Gazo, Joan Gonzalvo, and Alex Aguilar, *Pingers as deterrents of bottlenose dolphins interacting with trammel nets*, *Fisheries Research* **92** (2008), no. 1, 70–75.

- [GH98] AJ De Groot and DB Harris, *Computationally efficient, robust algorithm for matched field processing*, Circuits, Systems and Signal Processing **17** (1998), 165–193.
- [Gin89] Donald F. D.F. Gingras, *Methods for predicting the sensitivity of matched-field processors to mismatch*, J. Acoust. Soc. America **86** (1989), no. 5, 1940–1949.
- [Gin94] D.F. Gingras, *North Elba sea trial summary*, Tech. rep. Aug., report and acoustic dataset are published at the Signal Processing Information Base at Rice University on the world wide web, <http://spib.rice.edu>, NATO SACLANTCEN, La Spezia, 1994.
- [GPCVGM05] Gabriel Gómez-Pérez, Gustavo Camps-Valls, Juan Gutiérrez, and Jesús Malo, *Perceptual adaptive insensitivity for support vector machine image coding.*, IEEE transactions on neural networks / a publication of the IEEE Neural Networks Council **16** (2005), 1574–1581.
- [Gri12] Stephen M. Griffies, *Elements of the Modular Ocean Model (MOM) - GFDL Ocean Group Technical Report No. 7*, Tech. report, NOAA/Geophysical Fluid Dynamics Laboratory, 2012.
- [Gun98] Steve R. Gunn, *Support vector machines for classification and regression*, Tech. report, UNIVERSITY OF SOUTHAMPTON, SOUTHAMPTON, 1998.

- [Hay99] Simon Haykin, *Neural networks - a comprehensive foundation*, second ed., Prentice Hall, Upper Saddle River, New Jersey 07458, 1999.
- [Her65] J.B. B. Hersey, *Sound reflections in and under oceans*, *Physics Today* **18** (1965), no. 11, 17–24.
- [HHD⁺13] Richard M. Hodur, Xiaodong Hong, James D. Doyle, Julie Pullen, James Cummings, Paul Martin, and Mary Alice Rennick, *The Coupled Ocean/Atmosphere Mesoscale Prediction System (COAMPS)*, Coastal Ocean Prediction (C. N. K. Mooers, ed.), 9781118665527, 2013, pp. 125–155.
- [HO00] C.W. Holland and J. Osler, *High-resolution geoacoustic inversion in shallow water: a joint time- and frequency-domain technique*, *J. Acoust. Soc. America* **107** (2000), 1263–1279.
- [Hod97] Richard M. Hodur, *The Naval Research Laboratory's Coupled Ocean/Atmosphere Mesoscale Prediction System (COAMPS)*, *Monthly Weather Review* **125** (1997), no. 7, 1414–1430 (EN).
- [HSM91] A.D. Heathershaw, C.E.E.E. Stretch, and S.J. Maskell, *Coupled ocean-acoustic model studies of sound propagation through a front*, *J. Acoust. Soc. America* **89** (1991), no. January, 145–155.
- [HT73] R.H. Hardin and F.D. Tappert, *Applications of the split-step Fourier method to the numerical solution of nonlinear and variable coefficient wave equations*, *SIAM Rev.* **15** (1973), 423.

- [Hua88] Dehua Huang, *Finite element solution to the parabolic wave equation*, The Journal of the Acoustical Society of America **84** (1988), no. 4, 1405.
- [Hua12] Xiaopeng Huang, *Shallow water acoustic channel modeling with adaptive communications*, The Journal of the Acoustical Society of America **132** (2012), no. 3, 2016.
- [HW07] Leila T. Hatch and Andrew J. Wright, *A Brief Review of Anthropogenic Sound in the Oceans*, International Journal of Comparative Psychology **20** (2007), 121–133.
- [HW11] Kun Han and DeLiang Wang, *An SVM based classification approach to speech separation*, 2011 IEEE International Conference on Acoustics, Speech and Signal Processing (ICASSP) (2011), 4632–4635.
- [JBS⁺09] Srinivasan Jagannathan, Ioannis Bertsatos, Deanelle Symonds, Tianrun Chen, Hadi Tavakoli Nia, Ankita Deepak Jain, Mark Andrews, Zheng Gong, Redwood Nero, Lena Ngor, Mike Jech, Olav Rune Godø, Sunwoong Lee, Purnima Ratilal, and Nicholas Makris, *Ocean Acoustic Waveguide Remote Sensing (OAWRS) of marine ecosystems*, Marine Ecology Progress Series **395** (2009), 137–160.
- [JF79] F.B. Jensen and M.C. Ferla, *SNAP: The SACLANTCEN Normal-Mode Acoustic Propagation Model*, SACLANTCEN memorandum, SACLANT ASW Research Centre, La Spezia, 1979.

- [JKPS93] F.B. B Jensen, W.A. A Kuperman, M.B. B Porter, and H. Schmidt, *Computational Ocean Acoustics*, American Institute of Physics, New York, 1993.
- [JKPS11] Finn B. Jensen, William A. Kuperman, Michael B. Porter, and Henrik Schmidt, *Computational Ocean Acoustics*, second edi ed., Modern Acoustics and Signal Processing, Springer, New York, Dordrecht, Heidelberg, London, 2011.
- [Joa98] Thorsten Joachims, *Text categorization with Support Vector Machines: Learning with many relevant features*, Machine Learning: ECML-98 **1398** (1998), 137–142.
- [JPS+00] S.M. Jesus, M.B. Porter, Y. Stéphan, X. Démoulin, O.C. Rodríguez, and E.M.M.F. Coelho, *Single hydrophone source localization*, IEEE J. Ocean. Eng. **25** (2000), no. 3, 337 – 346.
- [JRG87] R.M. Jones, J.P. Riley, and T.M. Georges, *HARPO—a versatile three-dimensional Hamiltonian ray tracing program for acoustic waves in an ocean with irregular bottom*, Noaa wave propagation laboratory report, NOAA, 1987.
- [JSSC04] S.M. Jesus, Cristiano Soares, A.J. Silva, and E. Coelho, *Acoustic Oceanographic Buoy testing during the Maritime Rapid Environmental Assessment 2003 sea trial*, Proceedings of the 7th European Conference on Underwater Acoustics, ECUA 2004 (Delft, The Netherlands), no. 04/03, SiPLAB, University of Algarve, 2004, pp. 271–279.

- [Kah99] V.A. Kaharl, *Sounding Out the Ocean's Secrets*, National Academy of Sciences, 1999.
- [Kay93] SM Kay, *Fundamentals of Statistical Signal Processing, volume I: Estimation theory (v. 1)*, Prentice Hall PTR, 1993.
- [KP60] F.I. Kriazhev and N.A. Petrov, *a*, Soviet Phys. Acoust. **6** (1960), 60—70.
- [KTNK10] T. Kato, Y. Terada, T. Nagai, and S. Koshimura, *Development of a GPS buoy system for monitoring tsunami, sea waves, ocean bottom crustal deformation and atmospheric water vapor*, EGU General Assembly Conference Abstracts, EGU General Assembly Conference Abstracts, vol. 12, May 2010, p. 7377.
- [LAL00] P.F.J. Lermusiaux, D.G.M. Anderson, and C.J. Lozano, *On the mapping of multivariate geophysical fields: Error and variability subspace estimates*, Q.J.R. Meteorol. Soc. **126** (2000), 1387–1429.
- [LB98] D. Lee and G. Botseas, *IFD: an implicit finite-difference computer model for solving the parabolic equation*, Tech. Report 6659, Naval Underwater Systems Technical Report, New London, CT, 1998.
- [LBS92] D. Lee, G. Botseas, and W.L. Siegmann, *Examination of three-dimensional effects using a propagation model with azimuth-coupling capability (FOR3D)*, J. Acoust. Soc. Am. **91** (1992), no. 6, 3192–3202.
- [LC02] P.F.J. F J Lermusiaux and C.-S. S Chiu, *Four-dimensional data assimilation for coupled physical-acoustical fields*, Acoustic Variability, 2002 (N.G. Pace Jensen and F.B., eds.), Kluwer Academic Press, 2002, pp. 417–424.

- [LCR02] P.F.J. Lermusiaux, C.-S. Chiu, and A.R. R. Robinson, *Modeling Uncertainties in the Prediction of the Acoustic Wavefield in a Shelfbeak Environment*, Proceedings of the 5th ICTCA, May 21–25, 2001 (E.-C. Shang, Qihu Li, and T F Gao, eds.), World Scientific Publishing Co., May 2002, pp. 191–200.
- [Ler99] P.F.J. Lermusiaux, *Estimation and Study of Mesoscale Variability in the Strait of Sicily*, *Dynamics of Atmospheres and Oceans* **29** (1999), no. 2-4, 255–303.
- [Ler06] Pierre F.J. Lermusiaux, *Uncertainty Estimation and Prediction for Interdisciplinary Ocean Dynamics*, *Journal of Computational Physics* **217** (2006), no. 1, 176–199.
- [LFMN04] G. Lauriano, C.M. Fortuna, G. Moltedo, and G. Notarbartolo di Sciara, *Interactions between common bottlenose dolphins (*Tursiops truncatus*) and the artisanal fishery in Asinara Island National Park (Sardinia): assessment of catch damage and economic loss*, *Journal of Cetacean Resource Management* **6** (2004), no. 2, 165–173.
- [LH97] Jing-Fang Li and M. Hodgson, *Evaluation of equivalent-fluid geoacoustic seabed models*, *Oceans '97. MTS/IEEE Conference Proceedings*, vol. 1, IEEE, 1997, pp. 666–671.
- [LHJ⁺09] Frans-Peter a. Lam, Patrick J. Haley, Jeroen Janmaat, Pierre F.J. J Lermusiaux, Wayne G. Leslie, Mathijs W. Schouten, Lianke a. te Raa, Michel Rixen, and Patrick J Haley Jr., *At-sea real-time coupled four-dimensional oceano-*

- graphic and acoustic forecasts during Battlespace Preparation 2007*, Journal of Marine Systems **78** (2009), S306–S320.
- [LHZ⁺09] Baosheng Li, Jie Huang, Shengli Zhou, K. Ball, M. Stojanovic, L. Freitag, and P. Willett, *MIMO-OFDM for High-Rate Underwater Acoustic Communications*, 2009, pp. 634–644.
- [Lic19] H. Lichte, *On the influence of horizontal temperature layers in seawater on the range of underwater sound signals*, Physikalische Zeitschrift **17** (1919), no. (translated by A.F. Wittenborn), 385–389.
- [LL05] Ying-Tsong Lin and James F. Lynch, *Uncertainty bounds for geoacoustic inversions due to sound speed variations in water column*, The Journal of the Acoustical Society of America **117** (2005), no. 4, 2442.
- [LM88] D Lee and S T McDaniel, *a*, Pergamon Press, New York, 1988.
- [Lor56] E Lorenz, *Empirical orthogonal functions and statis*, Scientific report 1, Air Force Cambridge Research Center, Air Research and Development Command, Cambridge Mass., 1956.
- [LPA⁺94] C.J. Lozano, Jr. P.J. Haley, H.G. Arango, N.Q. Sloan, and A.R. Robinson, *Harvard coastal*, Harvard Open Ocean Model reports 52, Department of Earth and Planetary Sciences, Harvard University, MA, July 1994.
- [LRA⁺96a] Carlos J. Lozano, Allan R. Robinson, Hernan G. Arango, Avijit Gangopadhyay, Quinn Sloan, Patrick J. Haley, Laurence Anderson, and Wayne

- Leslie, *Modern Approaches to Data Assimilation in Ocean Modeling*, Elsevier Oceanography Series, vol. 61, Elsevier, 1996.
- [LRA⁺96b] C.J. Lozano, A.R. Robinson, H.G. Arango, A. Gangopadhyay, N.Q. Sloan, P.J. Haley, W.G. Leslie, Gary D. Egbert, and Andrew F. Bennett, *An interdisciplinary ocean prediction system: Assimilation strategies and structured data models*, Modern Approaches to Data Assimilation in Ocean Modelling, P. Malanotte-Rizzoli (Ed.), Elsevier Oceanography Series, vol. 61, Elsevier Science, 1996, pp. 413–452.
- [Man00] J. Mann, *Cetacean societies: field studies of dolphins and whales*, Cetacean societies, University of Chicago Press, 2000.
- [Mar97] John; A. Adcroft; C. Hill; L. Perelman; C. Heisey Marshall, *A finite-volume, incompressible Navier Stokes model for studies of the ocean on parallel computers*, J. Geograph. Res. **102** (1997), no. C3, 5753–5766.
- [Mar00] P.J. Martin, *Description of the Navy Coastal Ocean Model version 1.0*, report NRL/FR/7322-00-9962, Naval Research Laboratory, 2000.
- [Mar13] Sheri Martinelli, *Computational modeling of acoustic wavefronts propagating in an underwater environment with uncertain parameters*, The Journal of the Acoustical Society of America **134** (2013), no. 5, 4114–4114.
- [Mar14] Nelson Martins, *Acoustic-oceanographic Data Fusion for Prediction of Oceanic Acoustic Fields*, Phd (in preparation), University of Algarve, 2014, p. 203.

- [MB99] Christoph F Mecklenbra and Johann F Bo, *Hypothesis testing for geoacoustic environmental models*, J. Acoust. Soc. Am. **105** (1999), no. 3, 1738–1748.
- [MC98] Herman Medwin and Clarence S. Clay, *Fundamentals of Acoustical Oceanography*, APPLICATIONS OF MODERN ACOUSTICS Series, AP, San Diego, 1998.
- [McC04] Elena McCarthy, *International Regulation of Underwater Sound: Establishing Rules and Standards to Address Ocean Noise Pollution*, Kluwer Academic Publishers, 2004.
- [Med05] Herman Medwin (ed.), *Sounds in the Sea: From Ocean Acoustics to Acoustical Oceanography*, Cambridge University Press, New York, USA, July 2005.
- [MFJ11] Nelson Martins, Paulo Felisberto, and Sérgio M. Jesus, *Acoustic Field Calibration for Noise Prediction: the CALCOM'10 Data Set*, OCEANS 2011 IEEE - Spain **1** (2011), 1–6.
- [MH04] S.A. Macklin and G.L. Hunt Jr. (eds.), *The southeast Bering Sea ecosystem: implications for marine resource management*, Contribution (Pacific Marine Environmental Laboratory (U.S.)), U.S. Department of Commerce, National Oceanic and Atmospheric Administration, National Ocean Service, Centers for Sponsored Coastal Ocean Research, Coastal Ocean Program, Seattle, WA, 2004.

- [MHCO10] Karyn Morrissey, Stephen Hynes, Michael Cuddy, and Cathal O'Donoghue, *Ireland's Ocean Economy*, Tech. report, Socio-Economic Marine Research Unit, Galway, Ireland, December 2010.
- [MJ09] N.E. Martins and S.M. Jesus, *Bayesian Acoustic Prediction Assimilating Oceanographic and Acoustically Inverted Data*, *Journal of Marine Systems* **78** (2009), S349–S358.
- [MJ10] N. Martins and S.M. Jesus, *From oceanographic to acoustic forecasting: acoustic model calibration using in situ acoustic measures*, IX Encontro de Tecnologia Acustica Submarina - IX ETAS (Rio de Janeiro, Brasil), 2010.
- [MMS⁺99] A.J. Miller, J.C. McWilliams, N. Schneider, J.S. Allen, J.A. Barth, R.C. Beardsley, F.P. Chavez, T.K. Chereskin, C.A. Edwards, R.L. Haney, K.A. Kelly, J.C. Kindle, L.N. Ly, J.R. Moisan, M.A. Noble, P.P. Niiler, L.Y. Oey, F.B. Schwing, R.K. Shearman, and M.S. Swenson, *Observing and modeling the California Current System*, *Eos, Transactions American Geophysical Union* **80** (1999), no. 45, 533–539.
- [MRS⁺10] Franciscus Colijn Moritz Bollmann, Thomas Bosch, Kerstin Güssow Ralf Ebinghaus, Rainer Froese, Arne Körtzinger Setareh Khalilian, Sebastian Krastel, Birte Matthiessen Martina Langenbuch, Mojib Latif, Sven Petersen Frank Melzner, Andreas Oschlies, Johanna Reichenbach Alexander Proelß, Martin Quaas, Philip Rosenstiel Till Requate, Thorsten Reusch, Henning Sichel Schmidt Jörn O. Schmidt, Kerstin Schrottke, Ulrich Sommer Ursula Siebert, Rüdiger Soltwedel, Tina Treude Karl Statteger, Horst Sterr,

- Renate Sturm, Carlo van Bernem Athanasios Vafeidis, Martin Visbeck Justus van Beusekom, Rüdiger Voss, and Florian Weinberger Martin Wahl, Klaus Wallmann, *World Ocean Review: Living with the Oceans*, Mareverlag, 2010.
- [MSJ08] N. Martins, C. Soares, and S. Jesus, *Environmental and acoustic assessment: The AOB concept*, *Journal of Marine Systems* **69** (2008), no. 1-2, 114–125.
- [MSMH06] Sue E. Moore, Kathleen M. Stafford, David K. Mellinger, and John A. Hildebrand, *Listening for large whales in the offshore waters of Alaska*, *BioScience* **56** (2006), no. 1, 49–55.
- [MW79] W.H. Munk and C. Wunsch, *Ocean acoustic tomography: A scheme for large scale monitoring*, *Deep-Sea Research* **26 A** (1979), 123–161.
- [MW82] W. Munk and C. Wunsch, *Observing the ocean in the 1990s*, *Phil. Trans. Roy. Soc.* **A307** (1982), 439–464.
- [MW08] Marine Mammals and Andrew J. Wright, *Shipping Noise and Marine Mammals*, *International Workshop On Shipping Noise And Marine Mammals* (2008), no. April, 1–9.
- [MWW95] W Munk, P F Worcester, and C Wunsch, *Ocean acoustic*, *Cambridge Monographs on Mechanics*, Cambridge University Press, Cambridge, 1995.
- [OFG97] E. Osuna, R. Freund, and F. Girosit, *Training support vector machines: an application to face detection*, *Proceedings of IEEE Computer Society Conference on Computer Vision and Pattern Recognition* (1997), 130 – 136.

- [OLR92] E Özsoy, C J Lozano, and A R Robinson, *A consistent baroclinic quasi-geostrophic ocean model in multiply connected ocean domains*, Math. Comput. Simul. **34**(1) (1992), 51–79.
- [ONSF02] Peter F. Olesiuk, Linda M. Nichol, Margaret J. Sowden, and John K.B. Ford, *Effect of the sound generated by an acoustic harassment device on the relative abundance and distribution of harbor porpoises (*Phocoena Phocoena*) in Retreat Passage, British Columbia*, Marine Mammal Science **18** (2002), no. 4, 843–862.
- [Pag12] Susanne S. Pagano, *Deepwater Operations Show Growth In US Gulf, International Regions*, Sea Technology **April** (2012), 31–33.
- [Pap94] J.S. Papadakis, P.J. and Taroudakis, M.I. and Papadakis, *Recovery of the properties of an elastic bottom using reflection coefficient measurements*, Proceedings of the 2nd European Conference on Underwater Acoustics, volume II (Copenhagen, Denmark), 1994, pp. 943–948.
- [PB87] Michael B. Porter and Homer P. Bucker, *Gaussian beam tracing for computing ocean acoustic fields*, J. Acoust. Soc. America **82** (1987), no. 4, 1349–1359.
- [Pek48a] C.L. Pekeris, *Propagation of Sound in the Ocean*, Geol. Soc. Am. Mem., vol. 27, Geological Society of Amer, 1948.
- [Pek48b] ———, *Theory of Propagation of Explosive Sound in Shallow Water*, Geological Society of America Memoir **27** (1948), 1–117.

- [PFB01] G. Peggion, D.N. Fox, and C. Barron, *Validation of a Rapidly Relocatable Prediction System*, Proceeding of the 7th International Conference on Estuarine and Coastal Modeling (Tampa, FL), 2001, pp. 1061–1074.
- [PFB02] G. Peggion, D. Fox, and C. Barron, *A rapidly relocatable prediction system: operational implementation and validation*, Oceans '02 MTS/IEEE **2** (2002), 841–846.
- [PJ10] N. MARTINS P. FELISBERTO and S.M. JESUS, *Field Calibration a Tool for Acoustic Noise Prediction: the CALCOM'10 data set*, IX Encontro de Tecnologia Acustica Submarina - IX ETAS (Arraial do Cabo (Brasil)), 2010.
- [POC63] T. E. POCHAPSKY, *Measurement of small-scale oceanic motions with neutrally-buoyant floats*, Tellus **15** (1963), no. 4, 352–362.
- [Por91] M.B. Porter, *The Kraken Normal Mode Program*, Saclant Undersea Research Centre, 1991.
- [Pre92] James C. Preisig, *Adaptive matched field processing in an uncertain propagation environment*, Ph.d. thesis, Massachusetts Inst. of Technology Woods Hole Oceanographic Inst. Joint Program, 1992.
- [RBSR02] C. Rowley, C. Barron, L. Smedstad, and R. Rhodes, *Real-time ocean data assimilation and prediction with global NCOM*, Oceans '02 MTS/IEEE **2** (2002), 775–780.
- [RCG94] A.R. Robinson, J.C. Carman, and S.M. Glenn, *A dynamical system for acoustic applications*, Oceanography and acoustics: Prediction and Propagation

- Models, Allan R. Robinson and Ding Lee (Eds.), *Modern Acoustics and Signal Processing*, vol. 3, American Institute of Physics, New York, 1994, pp. 80–117.
- [RGH⁺09] Michel Rixen, Jean-Claude Le Gac, Jean-Pierre Hermand, Germana Peggion, and Emanuel Coelho, *Super-ensemble Forecasts And Resulting Acoustic Sensitivities In Shallow Waters*, *Journal of Marine Systems* **78** (2009), no. Supplement 1, S290–S305.
- [RHT⁺12] P.H. H Ressler, T. Honkalehto, R.H. H Towler, S.C. C Stienessen, D.R. R McKelvey, and A.L. L Mccarthy, *Acoustic Vessel-of-Opportunity (AVO) index for midwater Bering Sea walleye pollock*, Tech. Report 2012-04, Alaska Fish. Sci. Cent., NOAA, Natl. Mar. Fish. Serv., 7600 Sand Point Way NE, Seattle WA 98115, 2012.
- [RIC05] Jake C. RICE, *Implementation of the ecosystem approach to fisheries management—asynchronous co-evolution at the interface between science and policy*, *Marine Ecology Progress Series* **300** (2005), 265–270 (eng).
- [RL94] A R Robinson and D Lee, *Oceanography and Acoustics: Prediction and Propagation Models*, AIP Series in Modern Acoustics and Signal Processing, American Inst. of Physics Press, New York, 1994.
- [RL03] A.R. R Robinson and P.F.J. F J Lermusiaux, *Prediction Systems with Data Assimilation for Coupled Ocean Science and Ocean Acoustics*, Sixth International Conference on Theoretical and Computational Acoustics (ICTCA)

- (Honolulu, HI, 11 August) (et al. A. Tolstoy, ed.), World Scientific Publishing, 2003, pp. 325–342.
- [RL04] A.R. Robinson and P.F.J. Lermusiaux, *Prediction Systems with Data Assimilation for Coupled Ocean Science and Ocean Acoustics*, Proceedings of the Sixth International Conference on Theoretical and Computational Acoustics (ICTCA) (Honolulu, HI, 11 August) (Ed. A. Tolstoy et al., ed.), World Scientific Publishing, 2004, pp. 325–342.
- [RNS⁺07] S. Rankin, T.F. Norris, M.A. Smultea, C. Oedekoven, A.M. Zoidis, E. Silva, and J. Rivers, *A visual sighting and acoustic detections of minke whales, *Balaenoptera acutorostrata* (Cetacea: Balaenopteridae), in nearshore Hawaiian waters*, Pacific Science **61** (2007), 395–398.
- [Rob87] A.R. Robinson, *Dynamical forecasting of mesoscale fronts and eddies for acoustical applications*, J. Acoust. Soc. America **82**, **Supp.** (1987), S43.
- [Rob97] Allan R AR Robinson, *Forecasting and simulating coastal ocean processes and variabilities with the Harvard Ocean Prediction System, . . .*, Saclantcen Conference Proceedings Series CP-44, . . . (1997), 1–14.
- [Rod02] O.C. Rodríguez, *Basin scale simulations of ocean acoustic tomography in the Portuguese Exclusive Economic Zone*, Tech. Report 03/02, SiPLAB, University of Algarve, Faro, Portugal, November 2002.

- [Ros99] Allan P. Rosenberg, *A new rough surface parabolic equation program for computing low-frequency acoustic forward scattering from the ocean surface*, The Journal of the Acoustical Society of America **105** (1999), no. 1, 144.
- [RR02] Karl W. Rehn and Penny K. Riggs, *Non-lethal swimmer neutralization study*, Tech. Report 3138, The University of Texas at Austin, 2002.
- [RW87] A R Robinson and L J Walstad, *a*, J. Appl. Numer. Math. **3(1–2)** (1987), 89–131.
- [RY79] F. Rowe and J. Young, *An ocean current profiler using Doppler sonar*, Oceans '79, 1979, pp. 292–297.
- [SB06] S. Sun and R. Bleck, *Multi-century simulations with the coupled GISS-HYCOM climate model: control experiments*, Climate Dynamics **26** (2006), 407–428.
- [SB12] Gregory K. Silber and Shannon Bettridge, *An assessment of the final rule to implement vessel speed restrictions to reduce the threat of vessel collisions with North Atlantic right whales*, Tech. Report Technical Memorandum NMFS-OPR-48, NOAA, Silver Spring, MD 20910, February 2012.
- [SBE⁺07] B.L. Southall, A.E. Bowles, W.T. Ellison, J.J. Finneran, R.L. Gentry, C.R. Greene Jr., D. Kastak, D.R. Ketten, J.H. Miller, P.E. Nachtigall, W.J. Richardson, J.A. Thomas, and P.L. Tyack, *Marine mammal noise exposure criteria: initial scientific recommendations (2007)*, Aquatic Mammals **33** (2007), no. 4, 411–521.

- [SBV95] Bernhard Scholkopf, Chris Burges, and Vladimir Vapnik, *Extracting Support Data for a Given Task*, first international conference on knowledge discovery and data mining, 1995, pp. 252–257.
- [Sch95] P Schippers, *The ALMOST PC model for propagation and reverberation in range dependent environments*, Proceedings of UDT Europe, vol. The ALMOST, 1995.
- [Sch00] Rs Schick, *Spatial components of bowhead whale (*Balaena mysticetus*) distribution in the Alaskan Beaufort Sea*, Canadian Journal of Fisheries and Aquatic Sciences **2200** (2000), 2193–2200.
- [Sch02] H. Schmidt, *AREA: Adaptive Rapid Environmental Assessment*, Impact of littoral environmental variability on acoustic predictions and sonar performance (N G Pace and F B Jensen, eds.), Kluwer Acad. Pub., 2002, pp. 587–594.
- [SDW03] Mark Simmonds, Sarah Dolman, and Lindy Weilgart (eds.), *Oceans of noise: A WDCS science report*, A WDCS science report, Whale and Dolphin Conservation Society, 2003.
- [SG96] M. Schmidt and H. Gish, *Speaker identification via support vector classifiers*, 1996 IEEE International Conference on Acoustics, Speech, and Signal Processing Conference Proceedings **1** (1996), 105 – 108.
- [SGV99] M. Stitson, Alex Gammerman, and Vladimir Vapnik, *Support Vector regression with ANOVA Decomposition Kernels*, Support vector (1999), 1–22.

- [SH94] Y.T. Song and D.B. Haidvogel, *A semi-implicit ocean circulation model using a generalized topography-following coordinate system*, Journal of Computational Physics **115** (1994), 228–244.
- [SH11] Richard C.J. J. Somerville and Susan Joy Hassol, *Communicating the science of climate change*, Physics Today **64** (2011), no. 10, 48–53.
- [Sha88] E. C. Shang, *Waveguide characterization and source localization in shallow water waveguides using the Prony method*, The Journal of the Acoustical Society of America **83** (1988), no. 1, 103.
- [SJ09] Xiong Si Xiong Si and Lu Jing Lu Jing, *Mass Detection in Digital Mammograms Using Twin Support Vector Machine-Based CAD System*, 2009 WASE International Conference on Information Engineering **1** (2009), 240 – 243.
- [Sku63] E.J. Skudrzyk, *Underwater Acoustics*, Plenum Press, New York, 1963.
- [Smi93] G. B. Smith, *Performance stability of high-resolution matched-field processors to sound-speed mismatch in a shallow-water environment*, The Journal of the Acoustical Society of America **93** (1993), no. 5, 2617.
- [Sou05] Brandon L. Southall, *Final report of the National Oceanic and Atmospheric Administration (NOAA) international symposium: “Shipping noise and marine mammals: a forum for science, management, and technology”*, April 2005.
- [SSM98] Bernhard Schölkopf, Alexander Smola, and Klaus-Robert Müller, *Nonlinear Component Analysis as a Kernel Eigenvalue Problem*, 1998, pp. 1299–1319.

- [Ste88] Ralph A. Stephen, *A review of finite difference methods for seismo-acoustics problems at the seafloor*, *Reviews of Geophysics* **26** (1988), no. 3, 445.
- [Sto03] Michael Stocker, *Ocean bio-acoustics and noise pollution*, *Soundscape* **Spring** (2003), 16–29.
- [Stu05] Frédéric Sturm, *Numerical study of broadband sound pulse propagation in three-dimensional oceanic waveguides*, *The Journal of the Acoustical Society of America* **117** (2005), no. 3, 1058–1079.
- [SZM06] A. Silva, F. Zabel, and C. Martins, *Acoustic Oceanographic Buoy: a telemetry system that meets rapid environmental assessment requirements*, *Sea Technology* **47** (2006), no. 9, 15–20.
- [TC87] I. Tolstoy and C.S.S. Clay, *Ocean Acoustics - Theory and Experiment in Underwater Sound*, 2 ed., American Institute of Physics, New York, 1987.
- [TC00] P.L. Tyack and C.W. Clark, *Communication and acoustic behavior of dolphins and whales*, *Hearing in Whales and Dolphins* (W Au, A N Popper, and R R Fay, eds.), Springer-Verlag, New York, 2000, pp. 156–224.
- [TdSGG00] R. Tyce, F. de Strobel, V. Grandi, and L. Gualdesi, *Trawl-safe profiler development at SACLANT Centre for shallow water environmental assessment and real time modeling*, *Oceans 2000 MTS/IEEE*, 2000.
- [Tol89] A. Tolstoy, *Sensitivity of matched field processing to sound-speed profile mismatch for vertical arrays in a deep water Pacific environment*, *The Journal of the Acoustical Society of America* **85** (1989), no. 6, 2394.

- [Tol92] ———, *Review of matched field processing for environmental inverse problems*, *Int. J. Modern Physics* **3** (1992), no. 4, 691–708.
- [Tol96] ———, *3-D propagation issues and models*, *J. Comput. Acoust* **4** (1996), 243–271.
- [Vap95] V.N. Vapnik, *The nature of statistical learning theory*, *Statistics for Engineering and Information Science*, no. 6, Springer, 1995.
- [Vap98] Vladimir N Vapnik, *Statistical Learning Theory*, *Wiley Series on Adaptive and Learning Systems for Signal Processing, Communications and Control*, no. 4, Wiley & Sons-Interscience, 1998.
- [VGN92] Bernhard E. Boser Vapnik, Isabelle M. Guyon, and Vladimir N., *A Training Algorithm for Optimal Margin Classifiers*, *Proceedings of the 5th Annual ACM Workshop on Computational Learning Theory*, ACM Press, 1992, pp. 144—152.
- [VSA97] V. Vapnik, S. Golowich, and A. Smola, *Support Vector Method for Function Approximation, Regression Estimation, and Signal Processing*, *Advances in Neural Information Processing Systems* **9**, 1997, pp. 281–287.
- [VSJ11] U. Vilaipornsawai, A.J. Silva, and S.M. Jesus, *Underwater Communications for Moving Source Using Geometry-adapted Time Reversal and DFE: UAN10 Data*, *Oceans, 2011 IEEE - Spain*, June 2011, pp. 1–7.

- [vVBvdS11] Robbert van Vossen, Peter Beerens, and Ernest van der Spek, *Anti-submarine warfare with continuously active sonar*, Sea Technology **November** (2011), 33–35.
- [WLH⁺06] Ding Wang, P.F.J. PFJ Lermusiaux, PJ P.J. Haley, W.G. Leslie, and H. Schmidt, *Adaptive acoustical-environmental assessment for the Focused Acoustic Field-05 at-sea exercise*, Oceans (2006), 175–187.
- [WLH⁺09] Ding Wang, Pierre F J Lermusiaux, Patrick J Haley, Donald Eickstedt, Wayne G Leslie, and Henrik Schmidt, *Acoustically focused adaptive sampling and on-board routing for marine rapid environmental assessment*, J. Mar. Sys. **78** (2009), no. Supplement 1, S393 – S407.
- [WX06] Yong Wang and Hong-jie Xing, *Knowledge Discovery and Integration Based on A Novel Neural Network Ensemble Model*, Semantics, Knowledge and Grid, 2006. SKG '06. Second International Conference on, 2006.
- [Yak08] Alexander Yakubovskiy, *Bistatic sonar, explained*, Journal of Empirical Research on Human Research Ethics **3** (2008), no. 1, 8 pp.
- [Zak10] Manell Zakharia, *The evolution of underwater acoustics viewed through the ECUA mirror*, Proceedings of the 10th European Conference on Acoustics, vol. 1, 2010.
- [ZDF96] Pierre Zakarauskas, Stanley E. Dosso, and John A. Fawcett, *Matched-field inversion for source location and optimal equivalent bathymetry*, J. Acoust. Soc. Am. **100** (1996), no. 3, 1493–1500 (en).

- [Zim11] W.M.X. Zimmer, *Passive acoustic monitoring of cetaceans*, Cambridge University Press, 2011.

